Phenotypic Characterization of the Male *Tafazzin*-Knockout Mouse Model of Barth Syndrome at 3-, 6-, and 12-Months of Age

by

Michelle Victoria Tomczewski

A thesis
presented to the University of Waterloo
in fulfillment of the
thesis requirement for the degree of
Master of Science
in
Kinesiology

Waterloo, Ontario, Canada, 2022

Author's Declaration

I hereby declare that I am the sole author of this thesis. This is a true copy of the thesis, including any required final revisions, as accepted by my examiners.

I understand that my thesis may be made electronically available to the public.

Abstract

Barth Syndrome (BTHS) is a devastating disorder caused by mutations in the gene encoding for Tafazzin (TAZ), a key enzyme involved in the biosynthesis of the phospholipid cardiolipin, which is vital for maintaining the structural integrity of the inner mitochondrial membrane. A deficiency of TAZ in BTHS results in mitochondrial dysfunction. This compromises the function of highly energetic tissues, and as a result, cardioskeletal myopathy is one of the most defining and incapacitating manifestations of BTHS. Metabolic abnormalities are a natural secondary complication of mitochondrial dysfunction, and altered metabolism has been reported at multiple levels in BTHS, from mitochondrial to whole-body, and may play an important role in the pathogenesis of BTHS. Currently, there is no cure for this disease. As with all diseases, the development of novel therapeutics is aided by availability of a model that successfully recapitulates the major symptoms and outcomes of the human disease. In this regard, a novel mouse model of BTHS has recently been generated, the *Taz*-KO model. The cardiac phenotype of these mice has been studied in young animals, but other physiological and metabolic aspects have not yet been reported. Additionally, little is known about the phenotype of mice at older ages. In this thesis, I sought to characterize the physiological and functional phenotype of the *Taz*-KO mouse model pertaining to birth rate, growth, lifespan, gross anatomy, whole-body energy and substrate metabolism, exercise capacity and glucose homeostasis across aging in 3-, 6-, and 12-month-old male *Taz*-KO mice. This work demonstrates that the *Taz*-KO mouse model faithfully recapitulates important aspects of BTHS, including fetal and perinatal lethality, lean body mass deficiency, preference for glucose as a metabolic substrate, and progressive exercise intolerance. Additional findings that may yield mechanistic insight into the pathology of BTHS include increased whole-body energy expenditure, low adiposity, splenic atrophy with age and a shortened lifespan due to progression of disease. Therefore, the *Taz*-KO mouse model fulfills the critical need for a genetic model of BTHS that closely parallels the human syndrome.

Acknowledgements

First, I would like to sincerely thank my supervisor, Dr. Robin Duncan, for allowing me to be part of the Lipid Enzyme Discovery Lab and for being the most understanding, intelligent, and fantastic mentor I could have asked for. I've learned so much from you and I'm grateful for all the opportunities you provided me; I would've lived a smaller life if it weren't for your guidance and encouragement to pursue research!

I would also like to thank my committee members, Dr. Michaela Devries-Aboud and Dr. Ken Stark, for reviewing my thesis and for providing insightful feedback.

A special thank you to all my lab members whom have been great colleagues that I can now call my friends: Dr. Maria Fernanda Fernandes, your expertise was invaluable and your passion for science is inspiring; John Chan, for always being willing to help with my experiments despite your busy schedule and for many conversations about life and science; Kalsha De Silva, for reminding me to have fun and for being a joyful presence in the lab; Joey Hung, for many, many laughs; Ashkan Hashemi, for helping me with experiments along the way.

Finally, I would like to express my immense gratitude to my family. Thank you to my parents for their sacrifice and hard work, especially to my mother for her unwavering care and love. Thank you, Rhonda Firmi and John Guy, for their generous support and for being great role models. Christian Firmi, thank you for your unconditional love and for believing in me the most.

Dedication

In loving memory of Aniela Izdebska

Table of Contents

List of Figures

List of Tables

List of Abbreviations

ANOVA – Analysis of covariance
ATP – Adenosine triphosphate
AUC – Area under the curve
BAT – Brown adipose tissue
BMI – Body mass index
BTHS – Barth Syndrome
BW – Body weight
Ca^{2+} – Calcium
CL – Cardiolipin
CLAMS – Comprehensive Lab Animal Monitoring System
DCM – Dilated cardiomyopathy
Dox - Doxycycline
ETC – Electron transport chain
FFA – Free fatty acid
FFM – Fat-free mass
GTT – Glucose tolerance test
HFD – High-fat diet
iAUC – Inverse area under the curve
IGF-1 – Insulin-like growth factor 1
IL-6 – Interleukin-6
IMM – Inner mitochondrial membrane
i.p. – Intraperitoneal
iPSC-CMs - Induced pluripotent stem cell-derived cardiomyocytes
ITT – Insulin tolerance test
LBM – Lean body mass
L4-LC – Tetra-linoleoyl cardiolipin
MCU – Mitochondrial calcium uniporter
MLCL – Monolysocardiolipin
mRNA – Messenger ribonucleic acid
OXPHOS – Oxidative phosphorylation
PCR – Polymerase chain reaction
RER – Respiratory exchange ratio
RNA – Rribonucleic acid
shRNA – Short hairpin ribonucleic acid
SR – Sarcoplasmic reticulum
Taz-cKO – Cardiomyocyte-specific tafazzin knockout
Taz-KD – Tafazzin knockdown
Taz-KO – Tafazzin knockout
TEE – Total energy expenditure
TEF – Thermic effect of food
VLCAD – Very long chain acyl CoA dehydrogenase
VCO_2 – Carbon dioxide production rate
VO_2 – Oxygen consumption rate
VO_{2max} – Maximum rate of oxygen consumption

VO_{2peak} – Peak rate of oxygen consumption
WAT – White adipose tissue
WT – Wildtype
6MWT – Six-minute walk test

Chapter 1: Introduction

Barth Syndrome (BTHS) is an X-linked recessive mitochondrial disorder characterized by cardiomyopathy, skeletal muscle myopathy, exercise intolerance, growth retardation and cyclic neutropenia. BTHS results from deleterious mutations in the gene encoding for tafazzin (TAZ), a phospholipid-lysophospholipid transacylase responsible for generating the mature form of cardiolipin (CL), a key phospholipid enriched in mitochondrial inner membranes [1]. Changes in the phospholipid composition, due to loss of TAZ, destabilize the mitochondrial membranes and interfere with mitochondrial function, and thus forms the biochemical basis for the BTHS disorder [2].

Historically, 70 – 80% of patients died in infancy and childhood due to heart failure and/or overwhelming bacterial infection [3, 4]. The fatal infantile nature of BTHS was reported in the initial 1983 description of the disease by Dr. Peter Barth, the namesake of the disorder [5]. Due to improvements in diagnosis and symptom management strategies, the survival rate of BTHS patients has increased substantially, with a prognosis of 10 – 20% mortality [1, 3, 4]. However, mortality still peaks in the first years of life, and BTHS remains a debilitating disorder that lacks a curative therapy.

The decrease in early mortality has allowed a new age-group of BTHS patients to emerge – middle-aged adults. In 2019, the Barth Syndrome Foundation estimated that in the next 5 years, there may be 19 BTHS patients that are 35 years of age and older; at the time, the oldest studied BTHS patient was 59 years old [6]. As the natural history of the disease has yet to be fully observed, understanding of disease progression is limited, although preliminary reports indicate progressive degenerative skeletal muscle disease in BTHS patients with older age [6-8].

Cardiomyopathy, skeletal muscle myopathy, and neutropenia are noted as the clinical triad of the disease and have been the subject of extensive research and more recently, therapeutic trials. However, altered whole-body energy metabolism is also observed in BTHS, but the causes and consequences of metabolic abnormalities are not well understood, and are the focus of only limited clinical monitoring. Development of a better understanding of physiological and metabolic characteristics in BTHS is important for the development of novel therapies, while understanding these differences across the lifespan will be important for the implementation of strategies to promote healthier aging in this genetic population.

Since 2011, the only mouse model available was the inducible TAZ knockdown model (*Taz*-KD mouse) that caused an incomplete enzyme ablation and did not fully recapitulate the cardiac phenotype of the disorder. Recently, a new mouse model was developed with systemic deletion of the *Taz* gene (*Taz*-KO mouse), and therefore complete loss of TAZ, successfully modeling the cardiomyopathy of BTHS [9]. Due to the novelty of the model, characterization has focused almost exclusively on the clinical triad of BTHS, being cardiomyopathy, skeletal myopathy, and immune dysfunction, although replication of the other symptoms of BTHS in the *Taz*-KO mouse model has not been confirmed yet. Furthermore, there has been little research to assess the impact of age on disease progression in the *Taz*-KD or *Taz*-KO model, although the mouse presents an excellent opportunity to study the natural disease progression and potentially predict the course of BTHS.

This thesis aims to further characterize the *Taz*-KO mouse model by investigating gross anatomy, whole-body energy and substrate metabolism, spontaneous physical activity levels, endurance exercise capacity, and systemic glucose metabolism at 3-, 6-, and 12-months of age. The examination of these functional and metabolic characteristics across aging will ascertain that the *Taz*-KO mouse biology is congruent with the human condition of BTHS, and may also facilitate the evaluation of disease progression through aging and identification of useful outcome measures for preclinical trials in the *Taz*-KO mouse.

Chapter 2: Literature Review

2.1. Barth Syndrome

2.1.1. Barth Syndrome Overview

BTHS is a rare, recessive, X-linked disorder caused by mutations in the tafazzin (*TAZ*) gene in region q28 on chromosome X, and which primarily affects males [5, 10]. The disease has variable presentation and severity of the following wide spectrum of clinical features, including cardiomyopathy, skeletal myopathy, exercise intolerance, neutropenia, growth delay, and 3-methylglutaconic aciduria [11]. TAZ is a phospholipid-lysophospholipid transacylase that catalyzes the final step in the biosynthesis of the mitochondrial phospholipid CL, and thus the loss of TAZ function in individuals leads to a deficiency in CL, accompanied by structural and functional defects in the mitochondria [1].

The incidence of BTHS is reported to be 1 case in 500,000 live births [3], but the identified prevalence has a much lower estimate of 1 BTHS case per 1,000,000 male population [12]. With only 230 – 250 cases known worldwide, this discrepancy between incidence and prevalence suggests early mortality resulting in underdiagnosis of BTHS [12]. Despite advances in symptomatic management, BTHS patients report a low quality of life, and the disease still carries a significant burden of morbidity and mortality [6, 13].

2.1.2. Cardiolipin Remodeling and Tafazzin Deficiency

BTHS is the only human disease that is known to be caused by a primary defect in CL remodeling [1], although abnormalities in CL have been implicated in many other major clinical pathologies, including heart failure, diabetes, and Alzheimer's disease [14-16]. As a structural component of the inner mitochondrial membrane (IMM), CL contributes to ATP production through the maintenance of mitochondrial cristae architecture, structural integrity of electron transport chain (ETC) complexes, and their assembly into higher-order supercomplexes [17, 18]. Beyond its role in bioenergetics, CL is also implicated in a diverse collection of mitochondria-related functions including generation and detoxification of reactive oxygen species, apoptosis, autophagy, and calcium (Ca^{2+}) homeostasis [19-21].

Unlike most phospholipids, which carry two fatty acyl chains, CL has four acyl chains, which suggests great potential for compositional complexity and a vast variety of CL species [22]. However, in highly oxidative tissues, the majority of CL acyl chains are linoleic acid

(18:2n6), and tetra-linoleoyl CL (L4-LC) is the predominant molecular species [23]. In mammalian cardiac and skeletal muscle, L4-CL constitutes up to 70 – 80% of total CL [24].

During CL biosynthesis, a fatty acyl chain of nascent CL is removed, generating a monolysocardiolipin (MLCL) molecule carrying three acyl chains, which is then reacylated into a mature CL molecule by remodeling enzymes such as TAZ (**Fig. 1A**) [25]. In cardiac and skeletal muscle, TAZ is an important regulator of the maturation of CL, achieving the linoleoyl enrichment that is characteristic of CL in these tissues [26]. Thus, the biochemical pathogenesis in BTHS, as a consequence of TAZ deficiency, is the accumulation of MLCL and a decrease in L4-CL as well as total CL [27-29]. As a result, the MLCL/CL ratio is one of the most reliable diagnostic indicators of BTHS [30, 31] and a significant clinical measure as the CL profile is a major determinant of mitochondrial function and energy metabolism [14-16].

The functional integrity of mitochondria is intricately linked to the phospholipid composition of the organelle's double membranes [32]. Notably, it is the abundance of CL that most distinguishes the phospholipid composition of the IMM (comprising ~15 – 20% of phospholipids) from the outer mitochondrial membrane (comprising ~5% of phospholipids) [33]. The enrichment of CL in the IMM is likely contributive to the formation of the cristae, the regions of highly folded membrane invaginations which hosts the oxidative phosphorylation (OXPHOS) system. The chemical structure of four acyl chains bound to one head group give CL its characteristic conical shape with a propensity to induce and stabilize membrane curvatures (**Fig. 1B,C**) [34]. As a result of CL and MLCL abnormalities, disorganized cristae structures are a prominent feature of TAZ-deficient cells [9, 35, 36], highlighting the important role of CL in maintaining mitochondrial morphology, and thereby function.

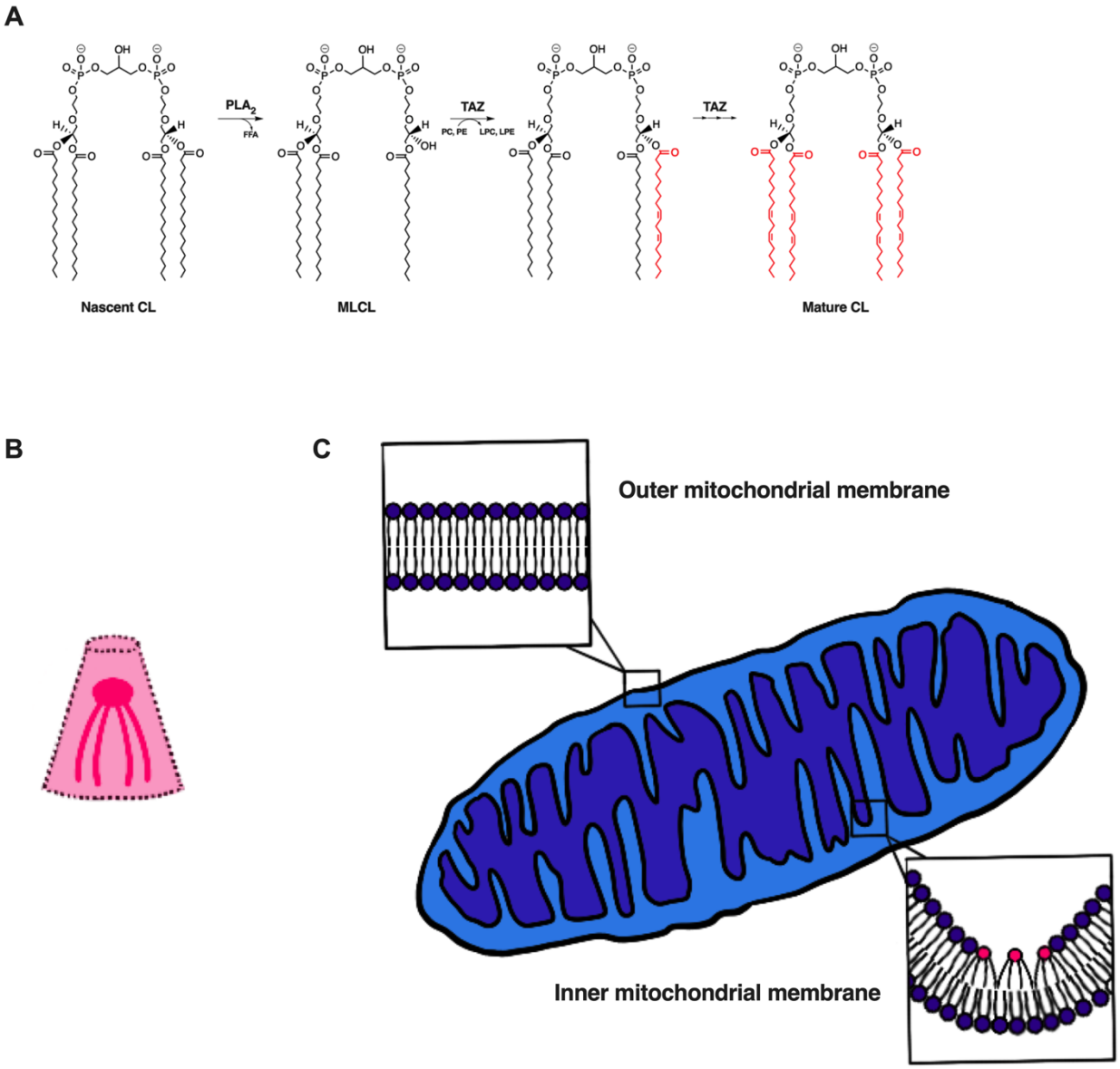

Figure 1: The role of CL in maintaining mitochondrial membrane integrity. Schematic representation of CL remodeling. Nascent CL undergoes remodeling to yield mature CL through sequential deacylation and reacylation reactions, in which saturated acyl chains are replaced with unsaturated acyl chains. Deacylation yields MLCL, and TAZ performs the reacylation to reconstitute the unique dimeric structure of CL. Figure adapted from Yadav and Rajasekharan (2016) [37]. (**B**) CL is a cone-shaped phospholipid which induces membrane curvature. (**C**) CL is concentrated at the apex of the cristae curvatures. Figures adapted from Falabella et al. (2021) [38].

2.2. Models of Barth Syndrome

The *TAZ* gene is evolutionarily conserved, and yeast, drosophila, and zebrafish have served as model organisms to study the function of TAZ and the consequences of its deficiency [39-42]. Approximately 10 years ago, the first mammalian mouse model of BTHS, with a short-hairpin RNA-mediated knockdown of *Taz* expression (*Taz*-KD), became available [43, 44]. The *Taz*-KD mouse has provided valuable insights into basic disease mechanisms of BTHS and allowed testing of multiple potential therapies [45-51]. However, a major limitation to the *Taz*-KD mice is the adult-onset cardiomyopathy, a stark incongruity to the infantile cardiomyopathy that devastates many BTHS patients [43, 52]. Thus, more recently, BTHS mouse models based on Cre-LoxP recombination have been developed, including a constitutive knockout (*Taz*-KO) and a cardiomyocyte-specific knockout (*Taz*-cKO) [9, 53].

2.2.1. The *Taz*-KD Mouse Model

The *Taz*-KD mouse model relies on a doxycycline (Dox)-inducible short hairpin RNA (shRNA) to knockdown systemic expression of *Taz* mRNA. Upon administration of Dox to the mice, shRNA is expressed, leading to the cleavage and degradation of the *Taz* mRNA through the RNA interference pathway, thereby blocking protein expression. In the most common knockdown strategy, *Taz* silencing is induced *in utero* and continuously maintained postnatally by placing dams and transgenic pups on Dox-containing diet (625 mg of Dox/kg of chow). Data show that *Taz* knockdown is highly efficient, with 85 – 95% knockdown of mRNA in the heart and skeletal muscle and to somewhat varying degrees in other organs, such as liver, kidneys, and brain. Despite the robust decrease in *Taz* mRNA, it has proven more difficult to verify TAZ knockdown at the protein level due to poor antibody specificity [43, 44]. Independent groups report different efficiencies of TAZ protein knockdown, despite analyzing *Taz*-KD mice induced with the same dosing regimen. For example, Cole et al. (2016) report more efficient knockdown of protein in skeletal muscle (~89% reduced) compared to heart (~58% reduced) [54], whereas Goncalves et al. (2021) report almost complete ablation of TAZ protein in the heart and an ~81% reduction in skeletal muscle [55]. Regardless of different reported knockdown efficiencies, a consistent finding is residual TAZ activity to some degree and thus the *Taz*-KD model displays a hypomorphic phenotype, incongruent with human BTHS patients that frequently have complete loss of functional TAZ [56]. Nonetheless, *Taz*-KD mice achieve a cardiac and skeletal muscle CL profile that is typical of BTHS, with a dramatic decrease of L4-CL and concomitant increase of

MLCL, and hence increased MLCL/CL ratio, even in mice as young as 2 months old [43, 44, 57, 58]. However, the continued use of antibiotic Dox may have some confounding effects, since it impairs mitochondrial function, although control mice are subjected to the same Dox regimen [59, 60].

2.2.2. The *Taz*-KO Mouse Model

The *Taz*-KO model was generated using a Cre-LoxP approach, and thus *Taz* is genomically excised in this model. Exons 5 – 10 of the *Taz* gene on the X chromosome are flanked by LoxP sequences in transgenic murine embryonic stem cells (ESCs), which undergo recombination, causing excision of flanked exons upon the transient expression of Cre recombinase enzyme and achieving targeted deletion of *Taz*. Thus, male *Taz*-KO mice derived from the transgenic ESCs have only one defective *Taz* gene present in cells throughout embryogenesis, consistent with human BTHS patients. Wang et al. (2020) conducted extensive cardiac phenotyping of the *Taz*-KO model, and confirmed the absence of TAZ protein along with a robust increase in MLCL/CL ratio in the hearts of mice [9]. The model has high neonatal mortality and cardiac dysfunction present at postnatal day 1, which recapitulates some aspects of BTHS in humans [9]. However, it is not yet known whether *Taz*-KO mice also model other physiological, pathophysiological, and metabolic characteristics of human BTHS.

2.3. Clinical Features of Barth Syndrome

BTHS is considered a multi-system disorder. This section will focus on the cardiac and skeletal muscle phenotypes, as these tissues contribute significantly to the burden of disease, and will also address aspects of whole-body metabolism, which is significantly dysregulated by mitochondrial dysfunction. The current state of knowledge on the extent to which these clinical features are recapitulated in the *Taz*-KD and *Taz*-KO mouse models will be discussed.

2.3.1. Cardiomyopathy

Cardiomyopathies are a heterogenous group of disorders in which the heart muscle is structurally and functionally abnormal. Cardiomyopathy is one of the most early and severe manifestations of BTHS, with an overwhelming majority (90%) of BTHS patients presenting with some form of cardiac dysfunction [3, 61]. BTHS-related cardiomyopathy typically manifests as dilated cardiomyopathy (DCM), which is often accompanied by left ventricular non-compaction.

More rarely than DCM, hypertrophic cardiomyopathy is also encountered in BTHS [62]. These cardiomyopathic phenotypes can lead to arrhythmia, congestive heart failure, and sudden cardiac death [1, 11, 62, 63].

Histological studies of BTHS cardiac tissue disclose myofiber disarray, interstitial fibrosis, and large aggregates of mitochondria [64]. Enlarged, malformed mitochondria with tightly packed cristae in a concentric array are frequently present [5, 64]. In healthy individuals, mitochondria normally occupy 25% of total myofiber area, whereas in BTHS cases the area occupied ranges from 34 – 44% [5]. Cardiac tissues have the most severe mitochondrial abnormalities, compared to other tissues such as skeletal muscle and liver [5].

Patients developing heart failure require appropriate treatment with anti-heart failure medications (e.g., angiotensin-converting enzyme inhibitors, beta-blockers, diuretics, etc.), which generally yield favourable outcomes and some recovery of cardiac function. However, in patients that are unresponsive to standard medical management, progressive heart failure necessitates heart transplantation [65]. While cardiomyopathy often emerges as a crisis in infancy and early childhood, cardiac function tends to improve and stabilize in children and adolescents, although a majority of patients are maintained on at least one anti-failure therapy [3, 6, 66]. It is unclear whether this developmental clinical improvement is due to cardiac medication or heart remodelling, or a combination of both [61].

In the *Taz*-KD model, an opposite prognosis is evident – mice have no cardiac dysfunction or mitochondrial abnormalities in early life (i.e., 2 months of age), and only manifest DCM at 7 – 8 months of age [5, 57]. At this later stage, the cardiac pathology observed in the *Taz*-KD mouse includes chamber dilation and thinning of ventricular walls, and a significant reduction in cardiac function, consistent with DCM [43, 44, 67]. Cardiac muscle also demonstrates abnormalities of both sarcomere organization and mitochondrial morphology. Mitochondria are frequently present in large aggregates between sarcomeres and contain circular bundles of cristae with onion-shaped morphology, similar to that observed in histopathological examination of hearts recovered from BTHS transplant patients [43, 68].

The *Taz-KO* mouse more closely models the relevant parameters of cardiomyopathy in BTHS. Cardiac dysfunction and dilation are present in neonatal mice and become progressively more severe as the mice aged to 5 months. Histological examinations show myocardial fibrosis, and ultrastructural studies revealed abnormal sarcomere structure and mitochondrial aggregates.

Cardiac mitochondria in *Taz*-KO mice are smaller compared to control mitochondria, and display sparse, disorganized cristae (**Fig. 2B**) [9].

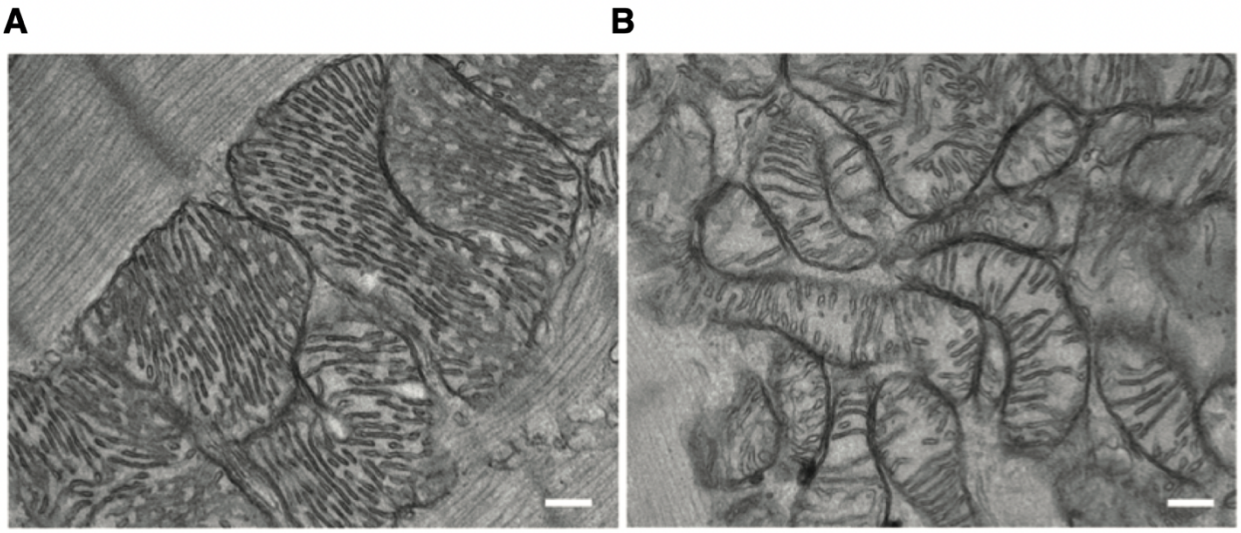

Figure 2: Electron microscopy images of cardiac mitochondria showing alterations in mitochondrial size and ultrastructure due to TAZ deficiency. Representative image of (**A**) WT and (**B**) *Taz*-KO cardiac mitochondria. Mitochondria from *Taz*-KO mice exhibit a drastic reduction in internal complexity and overall size. Bar = 200 nm. Figure adapted from Wang et al. (2020) [9].

2.3.2. Skeletal Myopathy and Exercise Capacity

Skeletal myopathy is an early feature of BTHS and continues to remain a functional limitation through the life course of patients. Myopathy in BTHS predominantly affects proximal limb muscles, leading to generalized muscle weakness, wasting, hypotonia, and exercise intolerance [46, 69, 70]. Histological and ultrastructural examination of skeletal muscle from BTHS patients shows an increased number of lipid droplets, muscle fiber degeneration, and normal and abnormal mitochondria [7, 71-74]. Related to skeletal myopathy but a separate phenomenon on its own, many individuals experience extreme tiredness and fatigue, which makes activities of daily living difficult to perform and drastically reduces quality of life [69].

The first description of progressive myopathy in BTHS was a 2012 case report of a 51-year-old male with muscle weakness since early childhood that remained stable until middle-age, although involvement of a *TAZ* deficiency was not initially diagnosed. At age 43, he began falling more frequently, had greater difficulty climbing stairs, and a decreased ability to perform his job on a farm. Eventually, a definitive BTHS diagnosis was reached, and he became recognized as the oldest surviving BTHS patient on record. At the most recent update at age 50, the man's

myopathy continued to progress, and he could no longer walk unassisted [7]. A 2016 study compared skeletomuscular parameters in pediatric versus adult BTHS patients and discovered several indicators of worsening muscle weakness with age, including decreasing functional exercise capacity. For example, pediatric BTHS patients achieved a higher average predicted value on the 6-minute walk test (6MWT) compared to adults, had greater lower limb muscle strength normalized to body weight, and reduced reported fatigue [8]. A 2019 qualitative study evaluating life quality by semi-structured interviews with BTHS individuals also revealed personal accounts of worsening muscle weakness and fatigue with age [6].

Exercise intolerance is thought to be a consequence of diminished skeletal muscle oxygen extraction and/or utilization, and impaired cardiac contractile reserve [69]. During a graded exercise test, oxygenated hemoglobin paradoxically increases in BTHS patients whereas deoxygenated hemoglobin slightly decreases, opposite to the hemodynamic responses observed in controls [69]. Peak respiratory exchange ratio (RER) during exercise is significantly higher in BTHS patients, suggesting lactic acidosis which would also impair endurance during exercise, and potentially signifying a greater reliance on glycolysis in BTHS [69].

Pathologic changes in skeletal muscle mitochondria of *Taz*-KD mice are apparent at 2 months of age, with a much earlier onset than cardiac mitochondrial abnormalities [43]. Skeletal muscle mitochondria are clustered in aggregates, and there is an abundance of giant mitochondria with whorled cristae [43, 44]. Skeletal myopathy is confirmed by a reduction in soleus contractile strength and increased muscle fatigability in *Taz*-KD mice [44, 49, 51]. When stressed with aerobic exercise on a forced treadmill test, *Taz*-KD mice have severely compromised exercise endurance and elevated blood lactate levels [45].

Skeletal muscle defects are present at the subcellular, cellular, and organ level in *Taz*-KO mice. Mitochondria are more abundant, smaller in size, and have disorganized cristae [9]. *Taz*-KO muscle fibers have reduced cross sectional area and are more fibrotic than controls. Not surprisingly, *Taz*-KO mice have drastically reduced endurance capacity during a forced treadmill exhaustive test [9].

2.3.3. Altered Whole-Body Energetics and Substrate Metabolism

BTHS is characterized by a prepubertal growth delay, and patients younger than 18 years of age are typically below average for weight and height [66]. A delayed growth spurt occurs between ages 15 – 21, and individuals then achieve average height, weight, and BMI [11]. However,

despite having similar weights as controls, there are significant differences in body composition. BTHS patients have lower fat-free mass (FFM) and greater fat mass than age-matched controls [75, 76]. Children with BTHS have lower relative fat mass than adults with BTHS [77]. On a whole-body level, the resting energy expenditure, expressed per kg FFM, is not different between BTHS adults and controls [75].

Substrate metabolism studies found that under resting conditions, BTHS patients do not demonstrate any impairments in fatty acid oxidation rate related to FFM [75]. However, moderate exercise uncovers a severely impaired ability to upregulate fatty acid oxidation in patients [78]. Evidently, in BTHS there is a drastic limitation in the capacity to utilize fatty acids as energy substrates during submaximal workloads, possibly compromising exercise performance. Conversely, BTHS patients appear to have higher glucose metabolism than controls during submaximal exercise, which may partially compensate for impaired fatty acid oxidation and insufficient ATP generation.

Even at rest, glucose metabolism in BTHS is significantly higher than controls, potentially signifying inappropriately high energy consumption [78]. Anecdotal reports indicate that younger BTHS children often consume a nightly dose of oral cornstarch to prevent nocturnal hypoglycemia [78]. An increased reliance on glucose utilization in BTHS patients is also demonstrated by a higher RER during exercise [69], a greater insulin-stimulated glucose disposal rate per kg FFM than controls [75] and, most strikingly, a basal myocardial glucose utilization rate that was double that of controls, even in BTHS patients without frank heart failure [79].

BTHS patients may also utilize amino acids as alternate substrates for energy production. The amino acid arginine, and its non-proteinogenic derivatives ornithine and citrulline, are significantly lower in serum of BTHS patients. It has been hypothesized that these amino acids are depleted due to their increased utilization as anapleurotic metabolites in the citric acid cycle [75, 80]. Furthermore, BTHS patients have an increased rate of appearance of the ketogenic amino acid leucine per kg FFM, suggesting whole-body proteolysis to supply amino acids for energy needs. Chronic proteolysis may promote skeletal muscle weakness and reduced cardiac function [75].

Overall, observed metabolic derangements in BTHS patients are typically associated with clinical symptoms, and may represent compensation for the energy deficit caused by CL-mediated mitochondrial dysfunction. No metabolic studies have yet been reported on *Taz*-KO mice, therefore all findings discussed on mice pertain to the *Taz*-KD mouse model.

The *Taz*-KD mouse is characterized by a lean phenotype, weighing ~56% less than their wildtype (WT) littermates at 7 months of age, with decreased lean mass (~1.4-fold reduction) and even greater decreases in fat mass (~3.5-fold reduction), despite consuming more food than controls [49, 81]. Energy expenditure normalized to FFM is elevated in *Taz*-KD mice, and thus hypermetabolism is postulated to be responsible for the lean phenotype [54]. RER analysis via indirect calorimetry on *Taz*-KD mice produces results that cover all possible outcomes of comparisons; no difference in RER between *Taz*-KD mice and controls [49]; lower RER in *Taz*-KD mice, indicating that proportionally more fat than carbohydrates is oxidized [54]; and higher RER in *Taz*-KD mice, suggesting carbohydrates are exclusively oxidized [81]. It is uncertain what accounts for these inconsistencies, as mice from all three studies were induced *in utero* with the 625 mg Dox/kg chow regimen, although differences in mouse age (thereby differences in disease severity), indirect calorimetry systems, and acclimatization protocols could contribute to the variability. Whole-body substrate utilization studies are therefore ambiguous, although there are multiple studies that examine mitochondrial-level substrate oxidation.

Mitochondrial respiration rates with fatty acid substrate were assayed in intact skeletal muscle fibers and hepatocyte mitochondria from *Taz*-KD mice. Decreased fatty acid oxidation was evident in skeletal muscle mitochondria, but increased respiration was observed in hepatocytes [54]. Multiple studies in isolated cardiac mitochondria show decreased fatty acid oxidation [49, 82], even when the subsarcolemmal and interfibrillar cardiac mitochondria populations are analyzed separately [68, 83]. Decreased mitochondrial fatty acid oxidation persisted with permeabilized cardiac fibers [83]. At the organ level, *ex vivo* isolated working hearts from *Taz-KD* mice exhibited similar fatty acid oxidation rates to WT hearts, but upon the addition of insulin, fatty acid oxidation rates significantly increased in *Taz*-KD mice [84]. The differences in cardiac fatty acid oxidation between molecular/cellular and organ findings may be reconciled by the workload of *in vitro* isolated mitochondria or cardiac myocytes versus *ex vivo* intact working heart, or may be due to the fact that high-resolution respirometry studies did not involve or examine insulin effects [84]. Of note, the intact hearts were isolated from 8- to 10-week-old *Taz-KD* mice, far earlier than the onset of cardiac dysfunction and possibly metabolic remodeling. On the whole-body level, the failure to upregulate fatty acid oxidation in response to increasing exercise intensity is mirrored in *Taz*-KD mice. With increased workload during treadmill exercise, the RER of WT mice suddenly drops, representing a “second wind” phenomenon, in which they dynamically shift their metabolic fuel preference from

predominantly glucose to mixed substrates, including fatty acids. This phenomenon was absolutely absent in *Taz*-KD mice, and glucose metabolism continuously rose alongside exercise intensity [45].

Metabolic perturbations of glucose metabolism demonstrate the greatest discrepancy between *Taz*-KD mice as a model, and BTHS patients. Energy metabolism analysis of *Taz*-KD *ex vivo* working hearts has revealed deficiencies in glucose oxidation compared with their WT littermates, which was only exacerbated in the presence of insulin – while glucose oxidation expectedly increased in WT hearts, it further decreased in *Taz*-KD hearts [84]. Glucose tolerance testing (GTT) in *Taz*-KD mice show that they are slightly, but significantly glucose intolerant compared to controls. Insulin tolerance tests (ITTs) conducted with *Taz*-KD mice demonstrate that they have no defects in insulin responsiveness, and thus insulin resistance does not mediate glucose intolerance [54]. However, lower fasting insulin levels are consistently found in *Taz*-KD mice [54, 84, 85], which are a consequence of a basal insulin secretory dysfunction [85]. Despite *Taz*-KD mice having normal glucose-stimulated insulin secretion, it is insufficient to restore reduced circulating insulin levels; therefore, a downward shift of insulin plasma levels is observed throughout the GTT, and glucose disposal is lower compared to control mice [85]. While individuals with BTHS seem to have a greater reliance on glucose, the same cannot be concluded for *Taz*-KD mice.

Evaluation of protein metabolism in *Taz*-KD mice consists of mitochondrial respirometry studies and genome-wide transcriptional profiling. Genes involved in the metabolism of proteins and amino acids are upregulated in *Taz*-KD hearts [50]. Experiments with intact cardiac cells and isolated mitochondria from these cells show that *Taz*-KD mice have the greatest OXPHOS capacity with the amino acid glutamate compared to other respiratory substrates, and glutamate oxidation is enhanced compared to controls [82, 83]. This suggests a shift toward the preference of amino acids as bioenergetic fuel for cardiac tissue, rather than the normally preferred fatty acids. Of note, there are three additional studies that either find no difference or decreased respiration with glutamate as the primary substrate, although these conflicting findings may be a result of a different *Taz* silencing induction protocols - two studies use a 625 mg Dox/kg chow dose, although it was administered to mice either after weaning [68] or adulthood [58] rather than *in utero*, and the other study used a much lower dose of 200 Dox mg/kg chow [51].

Although altered metabolism in the *Taz*-KD mouse is undeniable, certain findings are inconsistent across different mouse studies, and certain studies even offer contradictory findings

to the human condition. Although the technical variation in the induction of Taz silencing may be responsible for the inconsistent findings in the mouse studies, it is also important to acknowledge that it is difficult to ascertain whether the biology of BTHS is being examined in the *Taz*-KD mouse model due to chronic Dox exposure and delayed disease manifestation. A model such as the *Taz*-KO mouse circumvents these limitations, and with proper characterization, will facilitate studies that have previously been hindered by the lack of a mammalian model that faithfully and consistently recapitulates the disorder.

Chapter 3: Rationale and Purpose

3.1. Rationale

To date, there are few studies that have characterized the newly developed Cre-mediated knockout mouse models of BTHS. The cardinal symptom, being cardiomyopathy, has received priority in the study of pathophysiology, pathogenesis, and potential therapies in the *Taz*-KO [9] and *Taz*-cKO mice [86, 87]. To a lesser degree, investigations into skeletal muscle and immune function have been conducted in the *Taz*-KO mouse [9, 88, 89]. Thus, characterization efforts have largely addressed only the clinical triad of BTHS. However, other significant symptoms in patients such as growth delay, altered substrate metabolism and whole-body energetics, and impaired physical activity have not yet been investigated in the *Taz*-KO mouse, or have not yet been considered in the context of aging. The phenotypic characterization of the *Taz*-KO mouse model is incomplete without consideration of these aspects of the syndrome, especially since these features may have implications for the cardioskeletal pathology of BTHS across the lifespan.

A thorough and robust characterization is necessary to establish the validity of the *Taz*-KO mouse as a preclinical model for BTHS, especially if this model is to be used successfully for drug discovery and development. A valid disease model must capture the human condition pathophysiology and symptomology [90]; a model that does not is often inadequate for studying how a drug affects various aspects of a disease and may sabotage clinical extrapolation. Of the potential pharmaceuticals that are deemed safe and effective in rodent studies, a staggering 90% fail during human trials, resulting in huge investment losses of time, money, and effort, and a high sacrificial cost on behalf of the patients who are restricted from accessing other therapies during the trial. The translational failure cannot only be attributed to biological discrepancies between mouse models and human diseases, as suboptimal experimental design is also reported to contribute to the dismal success rate [91-93]. In order to improve the value of models used in comparative biology, it is crucial to know if an animal model only replicates certain aspects of disease symptomology, or if it is truer to the complete syndrome, since these limitations can define the fit-for-purpose use of the model. Thorough characterization of the *Taz*-KO mouse model can also help to elucidate mechanisms underlying the disease, uncover new therapeutic

targets, and set the stage to evaluate the efficacy of candidate drugs and therapeutic interventions.

3.2. Objective

The primary objective of this thesis was to characterize the physiological and functional phenotype of the *Taz*-KO mouse model pertaining to birth rate, growth, lifespan, organ morphometry, energy metabolism, exercise capacity and glucose homeostasis across aging from 3 month to 12 months, in order to establish the preclinical utility of the *Taz*-KO mouse model for use in studying the nature of the disease and potential avenues for treatment of BTHS. The characterization was intentionally directed at the organismal level to identify the 'net' effects of TAZ deficiency in the *Taz*-KO mouse that could be assessed with the facilities and equipment available at the University of Waterloo. The net effects that resemble the human condition may represent pathophysiological consequences whose improvements through various possible treatment modalities may yield meaningful benefits for patients with BTHS.

3.3. Study Design

Characterization was directed at male *Taz*-KO mice, since BTHS is a recessive X-linked disorder, and boys and men constitute the vast majority of the patient population. Mice were ear notched at 4 weeks of age and genotyped to determine birth rate, based on the total number of mice over 4 weeks of age. A growth curve was generated by taking weekly body weights of mice as they aged. A subset of mice were selected to age out to either their natural death or a humane endpoint, in order to measure the lifespan of *Taz*-KO mice; these mice did not undergo the test battery. For the phenotypic characterization, full litters of mice were used in experiments and litters were partitioned into three separate age cohorts of mice, being 3-, 6-, and 12-months, to determine age-related changes and assess physiological differences in *Taz*-KO mice compared to WT littermates. Once the mice reached the appropriate age of the designated age group, the litters underwent a phenotyping test battery with testing ordered from least invasive to most invasive (**Fig. 3**). In that regard, mice first underwent indirect calorimetry for a period of 24 hours. After a 3-day interval, mice underwent glucose tolerance testing (GTT) and then 7 days later, insulin tolerance testing (ITT). Afterwards, mice were given 10 days to recuperate before being enrolled in the treadmill exercise capacity test. Three days after completion of the

treadmill test, mice were euthanized by cervical dislocation and final body weights and organ weights were measured with an analytical balance.

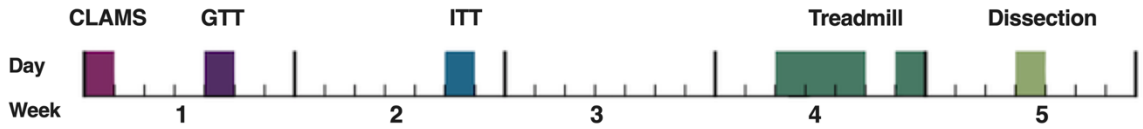

Figure 3: Sequence of the phenotyping test battery for the characterization of male *Taz*-KO mice. Cohorts of 3-, 6-, and 12-month-old mice underwent the test battery.

Chapter 4: Materials and Methods

4.1. Animal Husbandry

All animal procedures were performed with the approval of the University of Waterloo Animal Care Committee and comply with guidelines of the Canadian Council on Animal Care (AUPP#41822 and AUPP#43431). Mice were group housed with their littermates (at a maximum of 5 animals per cage) in a temperature- and humidity-controlled environment, on a 12:12-hr light/dark cycle, with free access to standard rodent chow and water. *Taz*-KO mice and their WT littermates were fed Teklad 22/5 Rodent diet from Envigo. The Tekland 22/5 diet is a fixed formula diet that provides 54% energy from carbohydrates, 29% energy from proteins, and 17% energy from fat (macronutrient composition, by weight: 40.6% carbohydrate, 22.0% crude protein, and 5.5% fat).

The *Taz*-KO mouse model (backcrossed >20-times onto a pure C57BL/6J background) was developed by Dr. Douglas Strathdee of the Cancer Research UK Beatson Institute. The generation of *Taz*-KO mice and confirmation of gene ablation have been described previously [9, 94]. Experimental mice were produced by breeding heterozygous females with wild-type male C57BL/6J mice to generate wildtype male ($Taz^{+/Y}$) and female ($Taz^{+/+}$) mice, heterozygous female mice ($Taz^{\Delta/+}$), and hemizygous null ($Taz^{\Delta/Y}$ [*Taz*-KO]) male mice. Only the male mice were studied because BTHS is a X-linked disease that primarily affects males.

Taz-KO mice and their WT littermates were evaluated cross-sectionally when they were 3-, 6-, and 12-months of age. The 3-month to 12-month age range corresponds to the beginning of adult life to the transition to middle age [95], and the additional age point of 6-months was added since increased mortality is evident in *Taz*-KO mice beginning at around 12-months of age, and therefore mice representing a 'mature' adult phase at 6-months-old was expected to facilitate closer monitoring of functional and health-related declines during aging.

4.1.1. Genotyping

Litters were weaned and ear notched for identification purposes at 4 weeks of age. The ear notches were placed in sterile 1.5 mL microfuge tubes. Genomic DNA from the ear tissue samples was obtained by the method from Green and Sambrook (2012) [96]. Mice were genotyped by polymerase chain reaction (PCR) using two sets of primers that contained the same reverse primer. The first set of primers, WT-U1 (5'- CTTGCCCACTGCTCACAAAC- 3') and WT-D1 (5'-

CAGGCACATGGTCCTGTTTC- 3'), generates the WT Taz allele, which is 383 bp product. The second set of primers, KO-U1 (5'- CCAAGTTGCTAGCCCACAAG- 3') and WT-D1 (5'- CAGGCACATGGTCCTGTTTC- 3'), generates the KO Taz allele, which is 280 bp product. All the genotyping was performed using FastStart™ PCR Master (Roche Life Science) and the Bio-Rad® T100 thermocycler under the following conditions: 95°C for 4 min; 39 cycles of 95°C for 30 sec, 56°C for 30 sec, 72°C for 1 min; and a final extension step of 72°C for 7 min. Amplicon sizes were analyzed by electrophoresis using 1% agarose gel with ethidium bromide.

4.2. Indirect Calorimetry

Mice underwent indirect calorimetry using the Comprehensive Lab Animal Monitoring System (CLAMS, Columbus Instruments, Columbus, OH, USA). In preparation for CLAMS, mice were single-housed in standard cages for 24-h during which 24-h food consumption was measured. After the 24-h acclimatization period to single-housing, mice were placed into the CLAMS apparatus. Mice were tested in individual clear sealed chambers with free access to water and standard chow, and chambers were supplied with air at 0.5 L/min and maintained at room temperature (22–23°C) with 12:12-hr light/dark cycle (light 07:00 – 19:00, dark 19:00 – 07:00). Immediately before the start of a CLAMS testing session, the gas sensors were calibrated with gas standards containing known concentrations of O_2, CO_2, and N_2. Throughout the study, rates of oxygen consumption (VO_2; ml/kg/h) and carbon dioxide production (VCO_2; ml/kg/h) in each chamber were determined at approximately 28-min intervals. The gas exchange data was used to calculate the respiratory exchange ratio (RER) (as the ratio of VCO_2 to VO_2) and energy expenditure [$(3.815 + 1.232 \times \text{RER}) \times VO_2$ (in liters)]), with energy expenditure normalized for total body weight (kg). Each chamber also contains photobeams situated in rows above the floor to monitor locomotor activity by infrared beam breaks along the *x*-(locomotion), *y*-(ambulation), and *z*-(rearing) planes. All parameters (VO_2, VCO_2, RER, energy expenditure, total locomotor activity) were measured over a total of 26 hr. The first ~2 hr served as an additional acclimatization period to the new apparatus, and were not included in CLAMS data analyses.

4.3. Treadmill

Exercise capacity is determined by an incremental exercise test on a five-lane motor-driven treadmill (Panlab; Harvard Apparatus, Barcelona, Spain). Mice were familiarized with the treadmill at a very low speed for three days before the exhaustive treadmill test to ensure they

perform appropriately when tested. Day 4 was a rest day (mice were not involved in any experimental procedure). Day 5 was the official exhaustive treadmill test. For all acclimatization and test sessions, treadmill exercises were performed in the evening (16:00 – 19:00) in a dark room with overhead red illumination, and the treadmill had a fixed slope of 5°. To encourage mice to run, they were manually prodded with a wire cleaning brush every time they approached the back of the treadmill.

4.3.1. Treadmill Acclimatization

On days 1 and 2 of acclimatization, the mice are placed on the stationary treadmill for 5 min, and then they are trained for a total of 10 mins. The mice ran at 5 cm/s for 5 mins, followed by 10 cm/s for 2 mins, and then 15 cm/s for 3 mins. On day 3 of acclimatization, the mice are placed on the static treadmill for 5 min, and then they are trained for a total of 10 mins starting at 5 cm/s for 3 mins, then 10 cm/s for 2 mins, then 15 cm/s for 2 mins, and finally 20 cm/s for 3 mins.

4.3.2. Treadmill Test

For the exhaustive treadmill test, mice were placed in the stationary treadmill for 5 min. The test started with an initial speed of 10 cm/s and was increased 3 cm/s every 2 min thereafter to a maximum speed of 70 cm/s. The mice were kept on the treadmill until reaching exhaustion which was defined as failure to run for 5 consecutive seconds when prompted with prodding by a wire brush. Running time until exhaustion was measured.

4.4. Glycemic Control Tests

Mice were first subjected to the GTT, then allowed rest for 7 days to recover from the intraperitoneal (*i.p.*) injection and blood loss, and then subjected to the ITT.

4.4.1. Glucose Tolerance Test

Glucose (20%) stock solution was freshly prepared by adding 2.0 g of D-glucose to 10 mL of sterile 0.9% saline solution. Mice were fasted for 6 hr (from 9:00 to 15:00) with access to water. Two hours before the start of GTT, mice were acclimatized to testing conditions by single-housing them in standard cages, transporting their cages to the testing room, and snipping off the last 1 mm of their tail. Body weight was measured one hour before the start of GTT to

calculate the glucose dose. At 15:00 h, baseline tail vein whole blood glucose levels were measured using Freestyle Glucose Monitoring System and test strips (Abbot Laboratories) and afterwards mice received an *i.p.* injection of 2.0-mg D-glucose per kg body weight into the lower right abdomen region using a 26 G x 5/8 needle and 1 ml syringe. Tail vein whole blood glucose levels were then collected at 15, 30, 60, 90, and 120 minutes after injection.

4.4.2. Insulin Tolerance Test

Insulin stock solution at a concentration of 0.1 U/ml was freshly prepared by adding 8.675 µl of insulin, human recombinant, zinc solution (Gibco™) to 9991 µl of sterile filtered (0.2 µm) PBS solution. Mice were fasted for 2 hr (from 13:00 to 15:00) with access to water. At the start of the 2-h fast, mice were acclimatized to testing conditions by single-housing mice in standard cages, transporting their cages to the testing room, and snipping off the last 1 mm of their tail. Body weight was measured one hour before the start of ITT to calculate the insulin dose. At 15:00 h, baseline tail vein whole blood glucose levels were measured using Freestyle Glucose Monitoring System and test strips (Abbot Laboratories) and afterwards mice received an *i.p.* injection of 0.5 U insulin per kg body weight into the lower right abdomen region using a 26 G x 5/8 needle and 1 ml syringe. Tail vein whole blood glucose levels were then collected at 15, 30, 60, 90, and 120 minutes after injection.

4.5. Necropsy

Mice were euthanized by cervical dislocation, immediately after which blood was drawn by cardiac puncture. Blood was allowed to coagulate for 60 min at room temperature, centrifuged for 10 min at 2000 x g at 4°C, after which the serum was aliquoted and snap frozen in liquid nitrogen prior to storage at −80 °C. Tissues were quickly dissected and weighed on an analytical balance in the following order: heart, pancreas, spleen, liver, adrenal glands, kidneys, perirenal WAT, testes, gonadal WAT, brain, soleus (right and left), gastrocnemius (right and left), retroperitoneal WAT, inguinal WAT, and BAT. After weighing, the tissues were snap frozen in liquid nitrogen and stored at −80 °C for future use. After organ collection, the right leg was removed, gently cleaned of all soft tissue, and the tibial bone measured using a digital caliper from the middle of the proximal articular surface to the distal-most projection of the medial malleolus to obtain tibial length.

4.6. Statistical Analysis

Comparisons between WT and *Taz*-KO mice were conducted using a two-way ANOVA to detect an interaction between genotype and age as main factors. Following a significant effect identified by two-way ANOVA, Bonferroni multiple comparison tests were used to identify: (1) significant differences in means within genotypes for cross-sectional age-related changes, and (2) significant differences between age-matched animals from different genotypes. Data are presented as mean ± standard error of the mean (SEM). Differences were considered statistically significant when $p < 0.05$. Statistical analysis and figures were generated using GraphPad Prism version 9.0.0 for Mac (GraphPad Software, San Diego, California, USA).

Chapter 5: Birth Rates, Survival, and Gross Anatomy

5.1. Introduction

The cardioskeletal myopathy is arguably the cardinal manifestation of BTHS, and the high-energy demands of cardiac and skeletal muscle underscore the importance of CL in maintaining mitochondrial functional integrity, which in turn is contingent on TAZ function [97, 98]. Interestingly, TAZ is expressed in a wide array of human tissues, with highest expression found in the pancreas, spleen, and liver [99]. Although the physiological significance of TAZ in other tissues is unknown, emerging evidence suggests that the absence of TAZ in other tissues is not innocuous. Malformed mitochondria have been observed in the kidneys and livers of BTHS patients [100], and novel roles of TAZ in maintaining normal function of the pancreas [85] and brain [101] are being established.

The *Taz*-KO mouse model will enable us to better determine which tissues and organs are affected by the absence of TAZ, which in humans can be too invasive for direct testing in some situations, and may allow insight into whether these affected organ systems impact the growth, health and survival of the mouse (and therefore likely also the human) model. A gross phenotypic profile related to growth, survival, and anatomy of the *Taz*-KO mice has not yet been reported. Establishing reference values for these physiological parameters across the lifespan of *Taz*-KO mice will allow for their use in comparative studies on the pathophysiology of BTHS and effects of interventions. It will also enable understanding of the disease across the lifespan, which is particularly important since the oldest known individual with BTHS is only entering the sixth decade of life [102], and therefore there is deficiency of information on the disease and it's natural course during older adulthood.

5.2. Objectives and Hypotheses

The objectives and hypotheses for this study were as follows:

1. **Objective:** To assess viability of male *Taz*-KO mice by determining sex and genotypic proportions of mice at birth, growth curves, survival, and natural lifespan.
   Hypotheses: Male *Taz*-KO mice will be born below the expected Mendelian ratio and will exhibit growth retardation, lower survival, and a shorter lifespan than their WT littermates.

2. **Objective:** To determine changes in anatomy caused by systemic TAZ deletion by measuring body weights, tibial lengths, and gross tissue masses.
   Hypotheses: *Taz*-KO mice will have smaller body weights compared to WT littermates at all ages examined but will have no differences in tibial lengths as BTHS adults have normal height [1] and *Taz*-KD mice have normal tibial lengths [54]. The lower body weight will be a result of lower organ and tissues weights, especially adipose depots. As an exception to diminutive organs, *Taz*-KO mice will have higher heart weights than WT mice, which will increase with age in *Taz*-KO mice due to hypertrophy and/or fibrosis. With age, skeletal muscles will decrease due to atrophy.

5.3. Experimental Approach

5.3.1. Birth Rate

Birth rate assessment was based on the genotypic distribution assessed upon weaning of mouse litters (note that no mortality was detected between birth and weaning). A total of 707 mice (males and females) were genotyped to derive the birth rate. Mice breeding and genotyping studies were conducted as described in section 4.1 of chapter 4.

5.3.2. Growth Curve

Body weights of mice were measured once a week on Sunday. Each weekly age point is the average of 10 mice per genotype, with the exceptions of weeks 4 and 42 – 52 which are the averages of 2 – 7 mice, and are still a work in progress at the time of this thesis.

5.3.3. Lifespan and Survival Curve

10 litters were selected to age out and reach their natural, humane lifespan endpoint and did not undergo the test battery. These 10 litters contained a total of 28 mice, 13 of which were *Taz*-KO mice and 15 were WT mice. The humane endpoint criterion for *Taz*-KO mice was defined as the point when hindlimb weakness became debilitating to a degree that would soon prevent access to food and water; at this point the mice were euthanized and the age was recorded as their survival point. Dates were recorded for all mice that died spontaneously during the study, and their age was recorded as their survival point.

5.3.4. Necropsy

Following completion of the test battery or reaching a condition that warranted euthanasia, mice were sacrificed by cervical dislocation. Organ and tissue weights were collected and necropsies were conducted as previously described in section 4.5 of chapter 4.

Absolute weights of adipose depots are reported. Organ weights were normalized to tibial length instead of body weight due to significant differences in body weight and composition between the genotypes, which could produce misleading comparisons. Tibial length normalization is recommended since it an index of subject size, and allows normalization between subjects irrespective of differences in body composition [103].

5.3.5. Statistical Analysis

Body weight, tibial lengths, and tissue weight comparisons between WT and *Taz*-KO mice were conducted using a two-way ANOVA to detect an interaction between genotype and age as main factors. Following a significant effect identified by two-way ANOVA, Bonferroni multiple comparison tests were used to identify: (1) significant differences in means within genotypes for cross-sectional age-related changes, and (2) significant differences between age-matched animals from different genotypes. Survival of mice is presented as Kaplan–Meier survival distributions, and significance was determined by log-rank Mantel-Cox test. When a *Taz*-KO mouse reached the humane lifespan endpoint before its WT littermates, the WT littermates were sacrificed at the same age but were entered as censored data for survival analysis. The observed distribution of offspring genotypes produced from crosses of heterozygous females with WT males was compared to expected Mendelian ratios by chi-square test.

Data are presented as mean ± standard error of the mean (SEM). Differences were considered statistically significant when $P < 0.05$. Statistical analysis and figures were generated using GraphPad Prism version 9.0.0 for Mac (GraphPad Software, San Diego, California, USA).

5.4. Results

To produce male *Taz*-KO ($Taz^{\Delta/Y}$) mice, heterozygous females ($Taz^{\Delta/+}$) were crossed with WT C57BL/6J mice as male mice lacking TAZ are sterile. Seven hundred and seven pups were produced and genotyped after weaning at 4 weeks of age, and *Taz*-KO mice were found to make up only 6.1% of total pups produced, which was significantly lower than the expected Mendelian ratio of 25%, indicating embryonic or perinatal lethality due to the absence of TAZ (**Table 1**).

Table 1: *Taz*-KO mice are born below the predicted Mendelian ratio.

Sex	Genotype	Expected number of mice	Observed number of mice
Male	WT ($Taz^{+/Y}$)	176.75 (25%)	255 (36%)
	Taz-KO ($Taz^{\Delta/Y}$)	176.75 (25%)	43 (6%)
Female	WT ($Taz^{+/+}$)	176.75 (25%)	212 (30%)
	HET ($Taz^{\Delta/+}$)	176.75 (25%)	197 (28%)

Genotypic ratio of offspring at 4 weeks of age resulting from WT male and HET female breedings. The expected number of mice was calculating according to the total number of mice born and based on the expected Mendelian 1:1:1:1 ratio, and chi-square test analysis determined that the discrepancies from the expected Mendelian ratios are significant (****$P < 0.0001$).

The lifespan of *Taz*-KO mice was significantly reduced in comparison to WT mice (**Fig. 4A**). The median lifespan was 22 months and the longest lived of the *Taz*-KO mice died at 26 months; in contrast, the median lifespan reported for WT male C57 mice is 27 – 29 months [104]. The reduced longevity of *Taz*-KO mice was not due to natural deaths, as the vast majority of *Taz*-KO mice developed hind limb weakness and poor mobility at 1.5 – 2 years of age that would prevent access to food and water unaided, and therefore had to be euthanized due to animal welfare regulations. In only one case, a *Taz*-KO mouse spontaneously died of unknown causes at 9 months of age, which was the youngest recorded age of death of a mature *Taz*-KO mice. From the onset of body weight measurement at 4 weeks of age, *Taz*-KO mice were smaller than their WT littermates and their weight remained low and unchanging in adulthood while the weight of WT mice increased gradually throughout the study period (**Fig. 4B**).

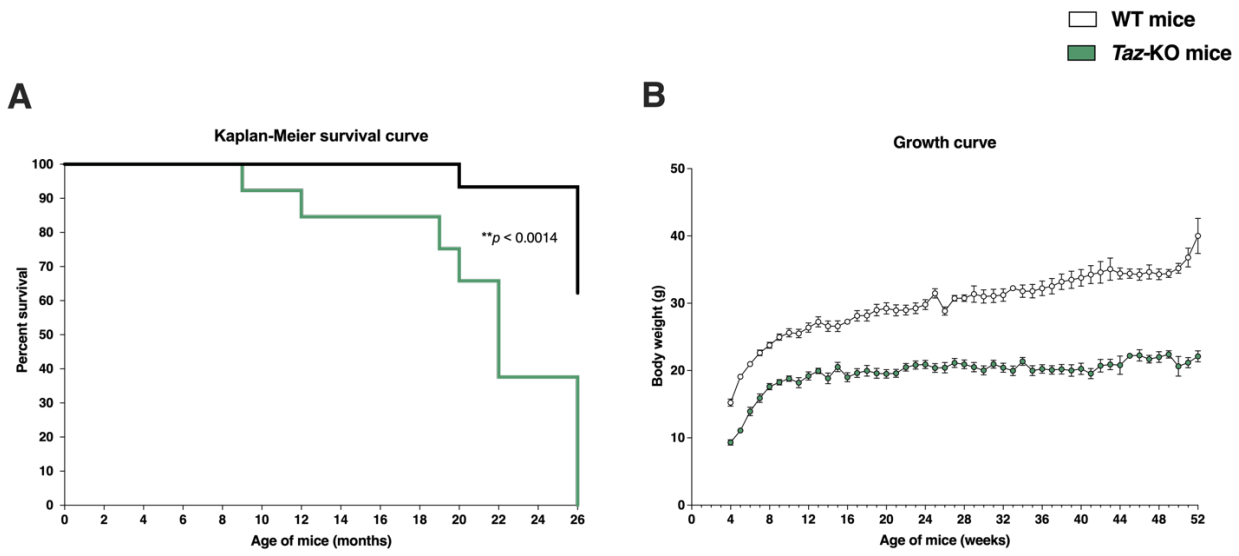

Figure 4: Survival and growth curves of *Taz*-KO mice. (**A**) Kaplan-Meier survival curves until 26 months of age of *Taz*-KO (n = 13) and WT (n = 15) mice were assessed by log-rank test. (**B**) Growth curve showing the body weight of mice from 4 to 52 weeks of age. Subject numbers: *Taz*-KO and WT, respectively, at age points: 4 weeks, n = 4 and 5; 5 – 41 weeks, n = 10 each; 42 – 52 weeks, n = 2 – 7 and 2 – 9.

Once a mouse litter completed the test battery, the mice of that litter were sacrificed and their organs and tissues were weighed. Analysis of total body weight revealed that *Taz*-KO mice were significantly smaller compared to WT mice at all three ages characterized (**Fig. 5A**), and the difference progressively increased with age due to age-associated weight gain by the WT littermates from 3-months (27.8 ± 1.9 g) to 12-months (34.5 ± 3.4 g) of age. The body weight of *Taz*-KO mice did not significantly change from 3-months (19.7 ± 2.1 g) to 12-months (21.3 ± 0.8 g) of age. This relationship results in a significant interaction between genotype and age (P < 0.05). Specifically in the *Taz*-KO mice, tibial length increased with age with significantly longer tibial bones measured in 6-month-old mice compared to 3-month-old mice and potentially indicating delayed growth. *Taz*-KO mice had significantly shorter tibial lengths compared to WT mice at all ages assessed, although this reduction in length was minor, with only a 4% difference evident in 3-month-old mice (*Taz*-KO: 17.0 ± 0.38 vs. WT: 17.8 ± 0.13 mm) and a 2% difference evident between genotypes in 12-month-old mice (*Taz*-KO: 17.6 ± 0.25 mm vs. WT: 18.1 ± 0.33 mm) (**Fig. 5B**). Importantly, this difference was tiny compared with other tissue differences between genotypes, and therefore was selected as the best measure for normalization of tissue weights. This finding also indicated that overall mouse size did not underlie the

decreased body weight observed in *Taz*-KO mice, which rather was caused by reductions in organ and tissue masses.

At the three ages characterized, *Taz*-KO mice exhibited a global reduction in organ weights, skeletal muscle depot weights, and adipose tissue weights compared to age-matched WT control mice in most, but not all cases. WT mice had larger kidney weights compared to *Taz*-KO mice, and these organs increased in weight with advancing age in WT mice, but remained stable in weight in *Taz*-KO mice (**Fig. 5G**). This relationship resulted in a significant interaction between genotype and age for kidney organ weights ($P < 0.01$). There was also a significant genotype-by-age interaction for spleen weight ($P < 0.05$), since this organ was comparable in mass between 3-month-old *Taz*-KO and WT mice; but in older mice, the spleen size of *Taz*-KO mice gradually diminished to become smaller than that of WT mice, while the spleens of WT mice did not change in weight throughout their lifespan (**Fig. 5F**). Surprisingly, *Taz*-KO mice had lower heart weights than WT mice at all three age points, negating the presence of cardiac hypertrophy when quantified by heart weight/tibial length ratio (**Fig. 5C**). The heart weight of WT mice increased significantly with age, although there was no significant genotype-by-age interaction effect of heart weight. The liver and testes did not change in weight with age in either genotype, and both organs were significantly smaller in *Taz*-KO mice regardless of age (**Fig. 5E, I**). This was particularly pronounced in the case of the testes, which in *Taz*-KO mice were less than 1/3 the mass of age-matched WT mice. Interestingly, no differences in mean organ weight of the pancreas were observed between *Taz*-KO mice and WT littermates at any age point (**Fig. 5D**). Although brain masses were significantly affected, the differences were small (**Fig. 5H**). At 3-months of age, *Taz*-KO mice had 6% smaller brains, although the difference between genotypes disappeared by 12-months of age due to a slight decline of brain weight in the WT mice. Skeletal muscle depot masses were significantly smaller (~25% lower at 3-months of age) in *Taz*-KO mice compared with WT littermate mice, but did not change significantly with age in either genotype (**Fig. 5J,K**). Overall, tissues appeared morphologically normal despite the smaller size.

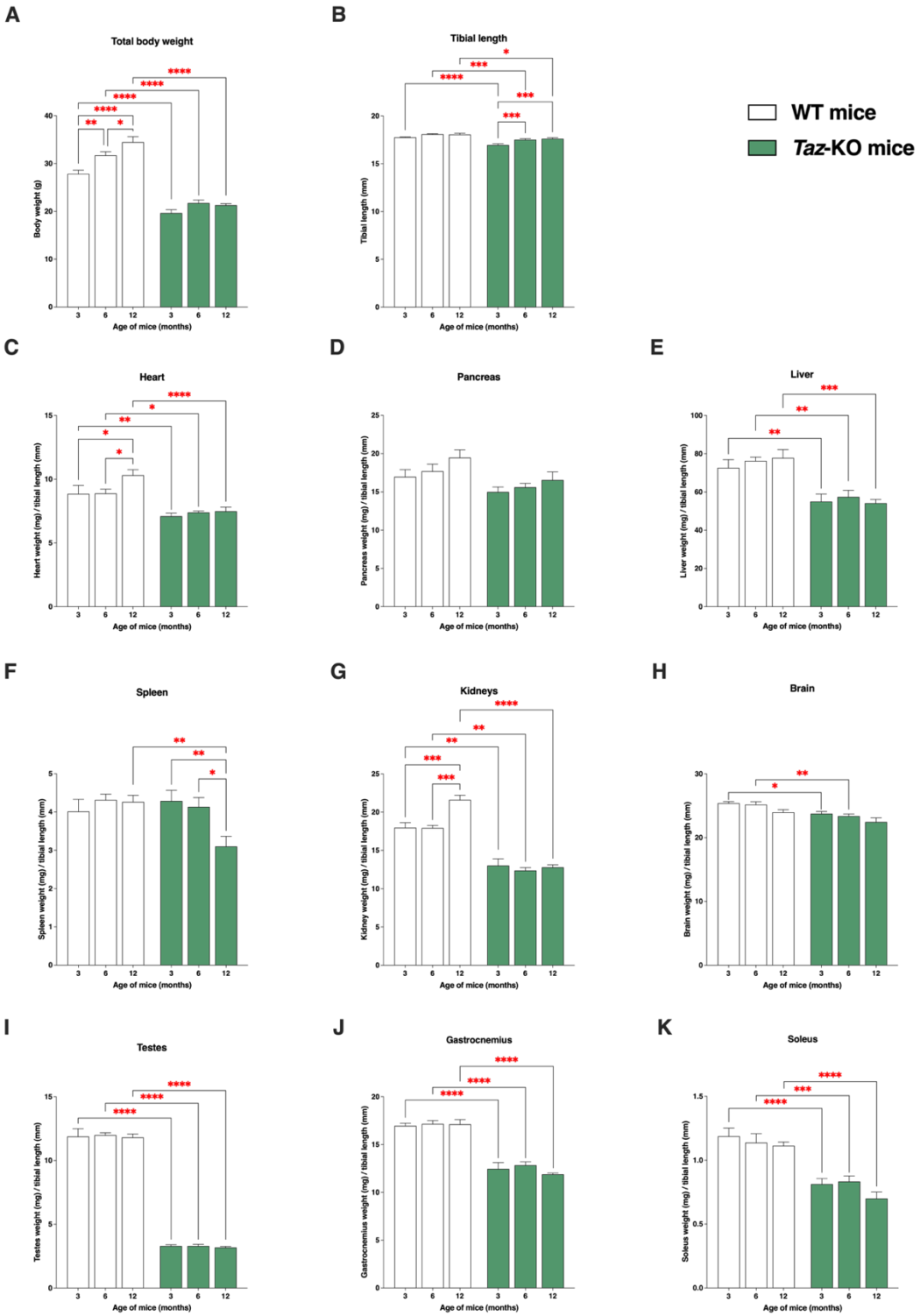

Figure 5: Total body weight, tibial lengths, and organ weights of *Taz*-KO mice. (**A, B**) Mean body weights and tibial lengths are shown. (**C – K**) Organ weights are shown normalized to tibial lengths. Subject numbers: *Taz*-KO and WT, respectively, at age points: 3 months, $n = 8$ and 8; 6 months, $n = 8$ and 9; 12 months, $n = 8$ and 6. Data are means ± SEM. Statistical analysis was performed using two-way ANOVA followed by Bonferroni multiple comparisons tests. $^{*}P<0.05$, $^{**}P<0.01$, $^{***}P<0.001$, $^{****}P<0.0001$.

Gonadal, perirenal, inguinal, and retroperitoneal white adipose tissues depots in WT mice increased in weight as the mice aged, while there was no change in these adipose depots weights in the *Taz*-KO mice with age (**Fig. 6**), and as such there was a significant genotype-by-age interaction effect for all measured WAT depots (gonadal WAT and perirenal WAT: $P < 0.0001$; inguinal WAT and retroperitoneal WAT: $P < 0.01$). A striking difference in adiposity was apparent between the two genotypes, and the absolute weights of all measured WAT depots were significantly smaller in *Taz*-KO mice at all age points, with the exception of inguinal WAT, which was not yet different between genotypes at 3-months of age. For example, the gonadal and perirenal WAT depots were 52% and 64% smaller, respectively, in 3-month *Taz*-KO mice in comparison to WT littermates. Brown adipose tissue also significantly increased in weight with age in WT mice but remained unchanged and significantly smaller in *Taz*-KO mice across the timepoints measured.

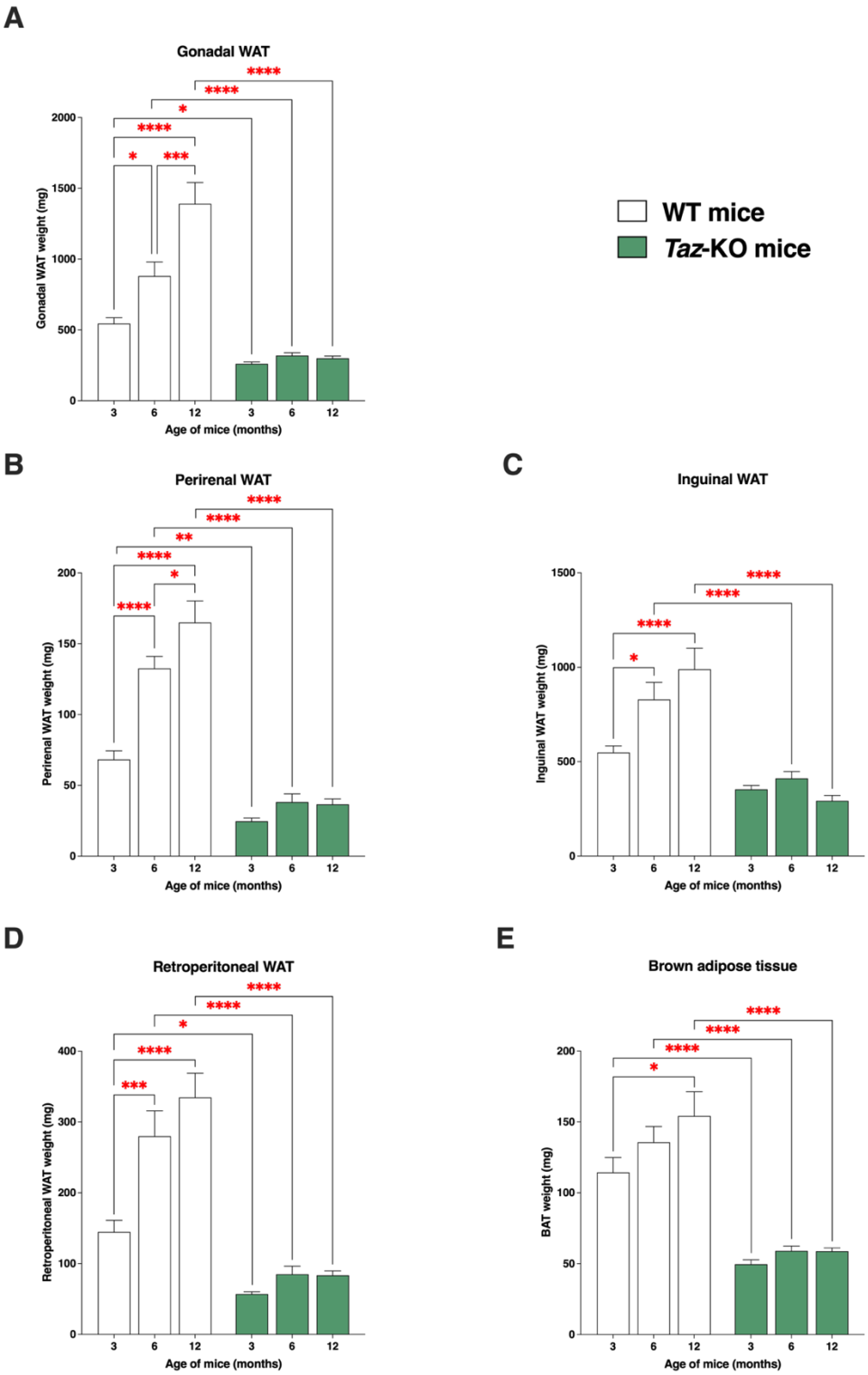

Figure 6: Adipose depots weights of *Taz*-KO mice. (**A – E**) Absolute weights of adipose depots. Subject numbers: *Taz*-KO and WT, respectively, at age points: 3 months, $n = 8$ and 8; 6 months, $n = 8$ and 9; 12 months, $n = 8$ and 6. Data are means ± SEM. Statistical analysis was performed using two-way ANOVA followed by Bonferroni multiple comparisons tests. *$P<0.05$, **$P<0.01$, ***$P<0.001$, ****$P<0.0001$.

5.5. Discussion

Systemic TAZ deletion negatively affects the viability of *Taz*-KO mice across their lifespan. The embryonic and perinatal loss of *Taz*-KO mice was clearly substantial, since only 6% of mice at 4 weeks of age were *Taz*-KO mice. In humans, BTHS is recognized as a cause of male fetal death resulting in miscarriage and stillbirth, with cardiac failure ascertained as a contributing factor to the fetal/neonatal deaths [105]. A prior report of the *Taz*-KD mouse model varied the timing of TAZ knockdown in gestation using an aggressively high Dox dose, and demonstrated that induction with Dox at the start of gestation (at E7.5 and at E10.5) lead to cardiac noncompaction and fetal lethality, whereas Dox induction later in gestation (E13.5 and E14.5) induced neither structural cardiomyopathy or fetal demise [106].

These findings suggest a critical window where TAZ-dependent mitochondrial function is required for optimal cardiogenesis. However, this concept has recently been challenged by studies on the *Taz*-KO and *Taz*-cKO mice. Our finding of the low birthrate of *Taz*-KO mice corroborates the low birthrate reported by Wang et al. (2020), although this group closely monitored the *Taz*-KO pups in the early postnatal days which lead to the discovery that *Taz*-KO mice display rapid perinatal lethality [9]. It was reported that *Taz*-KO mice were born at a rate of ~17% at post-natal day zero, which is still below the expected Mendelian ratio of 25%; however, most liveborn *Taz*-KO mice died in the neonatal period so that the birthrate diminished to ~7% based on the total number of mice alive at 4 weeks of age, which is the age that this thesis measured the birthrate.

Surprisingly, the low neonatal survival rate was not replicated in *Taz*-cKO mice, which were born at the expected Mendelian ratio (25%), and fewer that 5% of *Taz*-cKO mice displayed perinatal lethality [86], suggesting that the survival of *Taz*-KO fetuses and pups was impaired not by cardiac insufficiency, but skeletal muscle dysfunction [9]. While BTHS infants have been reported to be hypotonic, lethargic, and to have feeding issues [1], medical and dietary interventions prevent mortality from these complications in human patients [107]. Rather, cardiomyopathy is defined as the main cause of death in BTHS, which presents the greatest morbidity and mortality to patients throughout their lifespan, but particularly during fetal development and infancy [105]. Thus, the low neonatal mortality of *Taz*-cKO mouse is contrary to the human experience of BTHS. The *Taz*-KO mouse model, with systemic loss of TAZ, is therefore more true to the human condition than either the *Taz*-cKO or *Taz*-KD models, although

findings from the two other mouse models are relevant for understanding the embryonic and neonatal mortality of the *Taz*-KO mouse, with combined cardiac and skeletal muscle dysfunction together representing the major cause of lethality.

Skeletal muscle weakness again becomes a determining factor for survival towards the end of the lifespan of *Taz*-KO mice, since these mice developed progressive hindlimb weakness that required humane euthanasia at a median age of 22 months. The mice were not allowed to die a “natural death” due to ethical standards, and it is likely that their natural lifespan would be longer than 22 months if given daily assistance, although it can be concluded that they have a shortened natural lifespan in comparison to WT mice, which live to a median age of 27 to 29 months according to various studies [104].

Notably, only one mature mouse spontaneously died at 9 months of age before reaching an ethnical endpoint, although the cause of death was unknown. This tentatively implies that cardiac function is relatively well preserved in surviving *Taz*-KO mice, as also seen in *Taz*-cKO mice up to 1 year of age [86], and parallels the human condition. Longitudinal clinical studies on BTHS patients reveal that cardiac function is heterogenous across the BTHS population and variable over time in an individual patient, but generalize that cardiac function tends to stabilize and is only mildly abnormal in most subjects outside of infancy (albeit most patients are maintained on indefinite medical therapy for heart failure) [66, 108, 109]. However, the deteriorating skeletal muscle function of the *Taz*-KO mice was a consistent finding and determinant factor of mice that reached the humane lifespan endpoint.

The most prominent observed aspect of the *Taz*-KO mouse phenotype was the lower body weight and lean body composition. Interestingly, tibial lengths were only slightly smaller, by ~4% in Taz-KO mice, which reveals that these mice had a comparatively similar skeletal frame size to WT mice. Thus, differences in tissue mass must underlie the body weight differences. In agreement, the mean weight of the gastrocnemius and soleus skeletal muscles was significantly lower in *Taz*-KO mice, but the reduction was comparable to that of other major organs such as heart, liver, and kidneys, which also weighed approximately 30% less than their WT counterparts. In this regard, BTHS patients also reach normal adult heights following a delayed post-pubertal growth spurt [66], but have lower percent and absolute skeletal muscle masses, as indexed by fat-free mass measurements with body composition assessments [75, 78].

The cause of the diminutive organ size in *Taz*-KO mice and low skeletal muscle mass in BTHS is not clear. A possible origin for the BTHS growth defect is an imbalance of catabolic and

anabolic metabolism, since decreased levels of the anabolic factor insulin-like growth factor 1 (IGF-1) and elevations in the catabolic cytokine interleukin-6 (IL-6) have been found in the plasma of BTHS patients [78, 110]. Elevation of inflammatory cytokines such as IL-6 may inhibit the secretion and biological activity of IGF-1 [111]. IGF-1 is a known promotor of muscle hypertrophy [112] and mouse models of IGF-1 deficiencies frequently exhibit a smaller body size and lower organ weights [113-115]. Alternatively, the innate mitochondrial dysfunction of BTHS may precipitate an energy deficit that potentially stunts body and organ growth, since the energy cost of growth is high [116].

Contrary to my initial hypothesis, there was a lack of cardiac hypertrophy in the *Taz*-KO mouse as indexed by heart weight/tibial length ratio. Initially, this may seem to preclude a cardiac phenotype, but histological studies on hearts of *Taz*-KO mice by Wang et al. (2020) reveal left ventricular dilation and cardiac fibrosis, with concurrent cardiac dysfunction [9]. These observations are consistent with the DCM and endocardial fibroelastosis phenotypes of cardiomyopathy reported in BTHS patients [1]. However, it is interesting to note that heart weight doesn't significantly change with age in *Taz*-KO mice, and this, once again, offers preliminary evidence that although cardiac function may be compromised, it is relatively stable. In contrast, heart weight increases significantly as a function of age in WT mice, in addition to kidney weights, which may be a phenomenon related more to the progressive ectopic fat infiltration of organs with age than to a change in organ mass, *per se* [117].

The only organ that significantly changed in mass with age in the *Taz*-KO mice was the spleen, which displayed a significant reduction in weight later in the lifespan. The spleen is critical for immune system function, since it is the key site for T cell activation and B cell differentiation into plasma cells, which are the primary effector cells of the adaptive immune system [118]. This change in spleen weight is crucial, as atrophy of the spleen is expected to result in impaired immunity [119]. *Taz*-KD and *Taz*-KO mice show immunodeficient phenotypes with impaired B cell [120] and T cell [88] function, respectively. Although neutropenia is a hallmark characteristic of BTHS, defective function of other immune cell types may also be involved in the pathogenesis of infections in BTHS, and warrant further investigation since severe infections are the second most common cause of hospitalization in this patient population [66].

The testes of *Taz*-KO mice were drastically smaller, weighing ~70% less than their WT counterparts, indicating that these organs are particularly targeted as a consequence of TAZ

deficiency in the mouse model. The testicular atrophy of *Taz*-KO mice was also reported by Ren et al. (2019), who discovered a novel, extramitochondrial role for CL in germ cell meiosis, and attributed the sterility of *Taz*-KO mice to defective spermatogenesis [94]. Male sterility is also replicated in the Drosophila model of BTHS [42], suggesting that TAZ has an evolutionary role in male fertility. However, infertility has not been clearly demonstrated in BTHS patients, and some patients have had children [121], highlighting that in humans, BTHS is complicated by phenotypic variability.

The adipose depots were also drastically altered in the *Taz*-KO mice, with 40 – 60% reductions compared to WT mice at 3-months of age. Notably, this disparity only increased with age, since the *Taz*-KO mice did not exhibit increased fat mass accumulation from 3- to 12-months of age, while the WT mice did. This aspect of the mouse phenotype was in contrast to that observed in BTHS patients, who tend to have greater absolute fat mass and body fat percentages [78]. Both adolescents and adults tend to have gynoid proportions with truncal fat distribution [122], which also was not observed in mice. The reason for the greater adiposity seen in humans with BTHS may be a result of a sedentary lifestyle resulting from the skeletal and cardiac myopathies, or it may be a consequence of inhibited adipose tissue lipolysis [123] resulting from the beta-blocker regimen that greater than half of BTHS patients are on [78].

Whether the lean phenotype of the *Taz*-KO mouse is a result of triglyceride depletion of adipose stores due to excess energy wasting, or defective adipocyte differentiation and triglyceride storage was not determined by this study, but interpretation of data from BTHS patients and *Taz*-KD mice suggests the former is more likely responsible for the attenuation of adiposity. Mouse models of lipodystrophy have deficient storage of fat in adipose tissue, but fat overgrowth occurs in other body areas and organs, leading to cellular lipotoxicity and manifestations of insulin resistance, fatty liver, and hypertriglyceridemia [124]. Previous work showed that *Taz*-KD mice placed on a high-fat diet (HFD) gain less body weight than their WT littermates and are protected from insulin resistance and excess lipid accumulation in non-adipose tissues such as the skeletal muscle and liver, presumably due to hypermetabolism driven by increased hepatic fatty acid oxidation [54]. Both BTHS patients [75] and chow- and HFD-fed *Taz*-KD mice display normal plasma levels of triglycerides [54], in addition to reports of lower plasma levels of total and low-density cholesterol with similar high-density cholesterol in BTHS patients compared to healthy controls [78]. BTHS patients exhibit a three-fold increase in plasma free fatty acid (FFAs) concentration, and despite finding lower rates of lipolysis relative to

controls, Cade et al. (2019) postulate that the lipolytic rate of adipose tissue in BTHS patients is inherently elevated but counteracted and subdued by beta-blocker medication or negative feedback on lipolysis induced by increased circulating FFAs [78]. Therefore, evidence points to TAZ deficiency conferring leanness rather than lipodystrophy in the mice.

Interestingly, some organs were seemingly spared of growth deficiency in the *Taz*-KO mouse model, since there were no significant differences in the mean weight of the pancreas and only minor differences in brain weights between *Taz*-KO and WT mice. The normal brain weight in the face of other major organs weighing 30% less in *Taz*-KO mice relative to WT counterparts is interesting, because it underscores the phenomenon of minimal central nervous system involvement in BTHS [125], which is a deviation from other inherited mitochondrial disorders in which the nervous system is typically compromised due to its high energy demand [126]. This can be postulated to be due to the greater CL heterogeneity found in the brain [127], and hence lower dependency on TAZ-mediated production of L4-CL or some other form of a highly structured CL composition. Notably, reports of cognitive difficulties among patients do exist, including lower visual spatial skills and impaired mathematical ability [128], and *Taz*-KD mice studies have raised the concern of anxiety and memory issues due to the impaired performance of mice in behavioural assays [101]. Therefore, the mild but real cognitive phenotype of BTHS should be acknowledged.

Although the pancreas was trending lower in the *Taz*-KO males, the difference was not statistically significant. Cole et al. (2021) found a 170% higher MLCL/CL ratio and altered CL species in pancreatic islets from *Taz*-KD mice, concurrent with increased markers of inflammation and fibrosis, and histological visualization confirming greater pancreatic fibrosis in *Taz*-KD mice [85]. As disturbances of CL metabolism seem to be upstream of impaired organ function, pancreas abnormalities may still be present despite the apparently normal size of the pancreas in the *Taz*-KO mouse.

Chapter 6: Measures of Whole-Body Energy Metabolism, Respiration, and Voluntary Physical Activity Levels

6.1. Introduction

Energy expenditure is a major determinant of metabolic homeostasis and body composition. *Taz*-KO mice have significantly lower body weights than their WT littermates at all age points. This weight difference is accounted for by both lean tissue and fat mass differences, but the majority of the weight difference resides in a reduction in fat mass in *Taz*-KO mice as evaluated by tissue dissection. Indirect calorimetry allows for determination of total energy expenditure (TEE) from measurements of oxygen consumption and carbon dioxide production, and can also provide information on the type of metabolic substrate utilization *in vivo*. Whole-body metabolic analysis can therefore provide insight into whether *Taz*-KO mice have altered whole-body energetics, and whether altered energetics underlie the observed differences in body weight and composition between *Taz*-KO and WT mice. The comprehensive laboratory animal monitoring system (CLAMS) can also record movement in the *x*, *y*, and *z* planes, and therefore differences in voluntary activity between genotypes at specific ages, and within genotypes during aging, can also be considered.

6.2. Objectives and Hypotheses

The objectives and hypotheses for this study were as follows:

1. **Objectives:** To determine whether *Taz*-KO mice exhibit differences in whole-body energetics, respiration, metabolic fuel use and locomotor activity levels compared to WT littermates at 3-, 6-, or 12-months of age, and whether there are longitudinal differences in these parameters with aging within the WT and *Taz*-KO genotypes.
   Hypotheses: Due to the skeletal myopathy phenotype [9], *Taz*-KO mice will have decreased voluntary physical activity levels compared to WT littermates at each age-point examined. However, *Taz*-KO mice will have higher TEE at 3-months of age due to elevated basal metabolism, although differences between genotypes will become smaller with advancing age due to decreasing physical activity levels of the *Taz*-KO mice with progressive skeletal myopathy. Throughout their lifetime, *Taz*-KO mice will rely more on carbohydrate fuels compared to WT mice and thus will have increased RER, based on evidence of impaired fat metabolism in individuals with BTHS [78].

6.3. Experimental Approach

6.3.1. Indirect Calorimetry

Mice were housed individually 24 hours prior to the indirect calorimetry experiment. Mice were placed into the metabolic chambers and allowed to acclimate for 2 hours prior to the start of the calorimetry measurements. Calorimetry measurements were completed over a 24-h period during which the mice have free access to food and water. Oxygen (O_2) consumption, carbon dioxide (CO_2) production, TEE, RER, and physical activity (recorded as beam breaks in the *x*, *y*, and *z* coordinates) were measured using a 12 cage Columbus Instruments Oxymax-CLAMS apparatus (Columbus Instruments). The equations used for the calculations of total energy expenditure and RER are listed in section 4.2. of chapter 4. The metabolic measurements are expressed per kg of body weight and averaged by photoperiod.

6.3.2. Food Intake

Food intake was measured by placing pre-weighed food pellets into the home cage or metabolic chamber and then subtracting the uneaten food after the study period. Food measurements were done when the mice were single-housed in standard cages for 24-h and when mice were housed in the metabolic chambers during indirect calorimetry for 26-h.

6.3.3. Statistical Analysis

Comparisons of the averages of food intake, VO_2, VCO_2, TEE, RER, and sums of physical activity measures in all three directional dimensions between WT and *Taz*-KO mice were conducted using a two-way ANOVA to detect an interaction between genotype and age as main factors. Following a significant effect identified by two-way ANOVA, Bonferroni multiple comparison tests were used to identify: (1) significant differences in means within genotypes for cross-sectional age-related changes, and (2) significant differences between age-matched animals from different genotypes.

Data are presented as mean ± standard error of the mean (SEM). Differences were considered statistically significant when $p < 0.05$. Statistical analysis and figures were generated using GraphPad Prism version 9.0.0 for Mac (GraphPad Software, San Diego, California, USA).

6.4. Results

Indirect calorimetry was used to better understand if the lean phenotype of *Taz*-KO mice was a consequence of alterations in their total energy balance. There was no difference in absolute food

consumption between *Taz*-KO and WT mice, whether single-housed in a standard home-cage environment or in CLAMS, and food consumption remained consistent across aging in both genotypes (**Fig. 7A,C**). When adjusted for body weight, *Taz*-KO mice had significantly higher food intakes at all age points, indicating lower food efficiency, and food intake also decreased with age in both genotypes, although this was likely explained, at least in part, by normalization with increasing body weights (**Fig. 7B, D**). Therefore, lower food intake cannot account for the lean phenotype of *Taz*-KO mice.

For almost all parameters measured in the metabolic chambers, there were significant differences between *Taz*-KO and WT mice at 12-months of age. *Taz*-KO mice had higher rates of oxygen consumption and TEE compared to WT mice at 12-months of age (**Fig. 8, 10**). Across all three age-points, *Taz*-KO mice had significantly higher rates of carbon dioxide production compared to WT littermates (**Fig. 9**), which was paralleled with a higher RER (VCO_2/VO_2) in *Taz*-KO mice at 6- and 12-months of age during the dark phase (**Fig. 11F**), accordant with nocturnal feeding habits. These findings indicate that *Taz*-KO mice use a greater ratio of carbohydrates as a fuel source in contrast to WT mice (RER of 12-month *Taz*-KO mice: 0.94 ± 0.06 vs. RER of 12-month WT mice: 0.85 ± 0.06). At 3-months of age, there were no significant differences in these metabolic indices between genotypes, except for VCO_2, although these measurements decreased with age in WT mice while they remained stable in *Taz*-KO mice. Hence significant differences between genotypes tended to result at later stages of the lifespan of the mice. Of note, these age-dependent decreases in WT mice may be due, at least in part, to the increasing body weight of aged mice that is a normalization factor in respiratory and energy measurements, coupled with a marked shift toward the use of lipids due to increased fat accumulation.

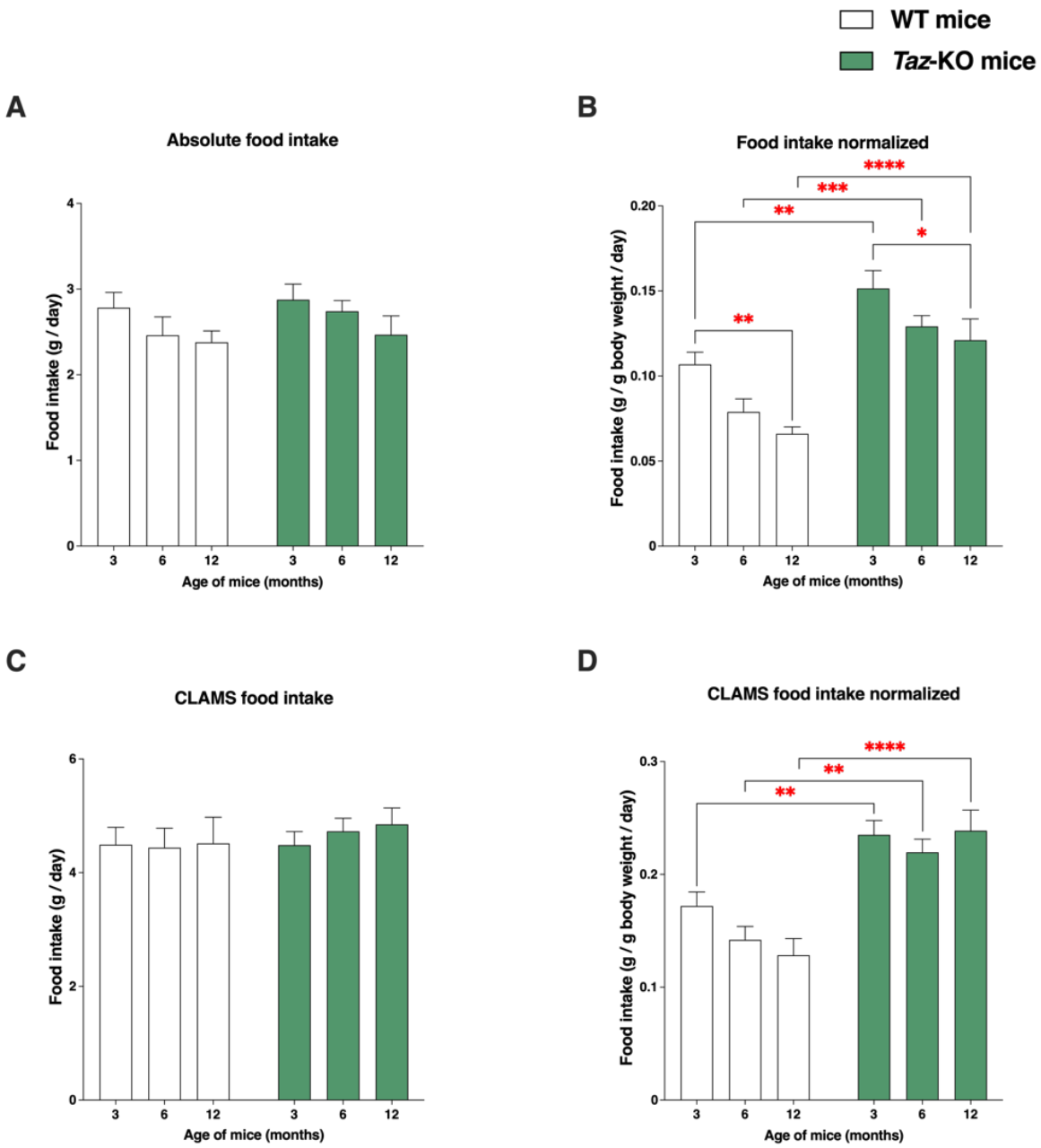

Figure 7: Daily food intake prior to and during indirect calorimetry. Absolute food intake measured when mice were housed in (**A**) standard cages and (**C**) metabolic chambers. Food intake normalized to body weight when mice were housed in (**B**) standard cages and (**D**) metabolic chambers. Subject numbers: *Taz*-KO and WT, respectively, at age points: 3 months, $n = 13$ and 11; 6 months, $n = 12$ and 10; 12 months, $n = 12$ and 14. Data are means ± SEM. Statistical analysis was performed using two-way ANOVA followed by Bonferroni multiple comparisons tests (**A – D**). *$P<0.05$, **$P<0.01$, ***$P<0.001$, ****$P<0.0001$.

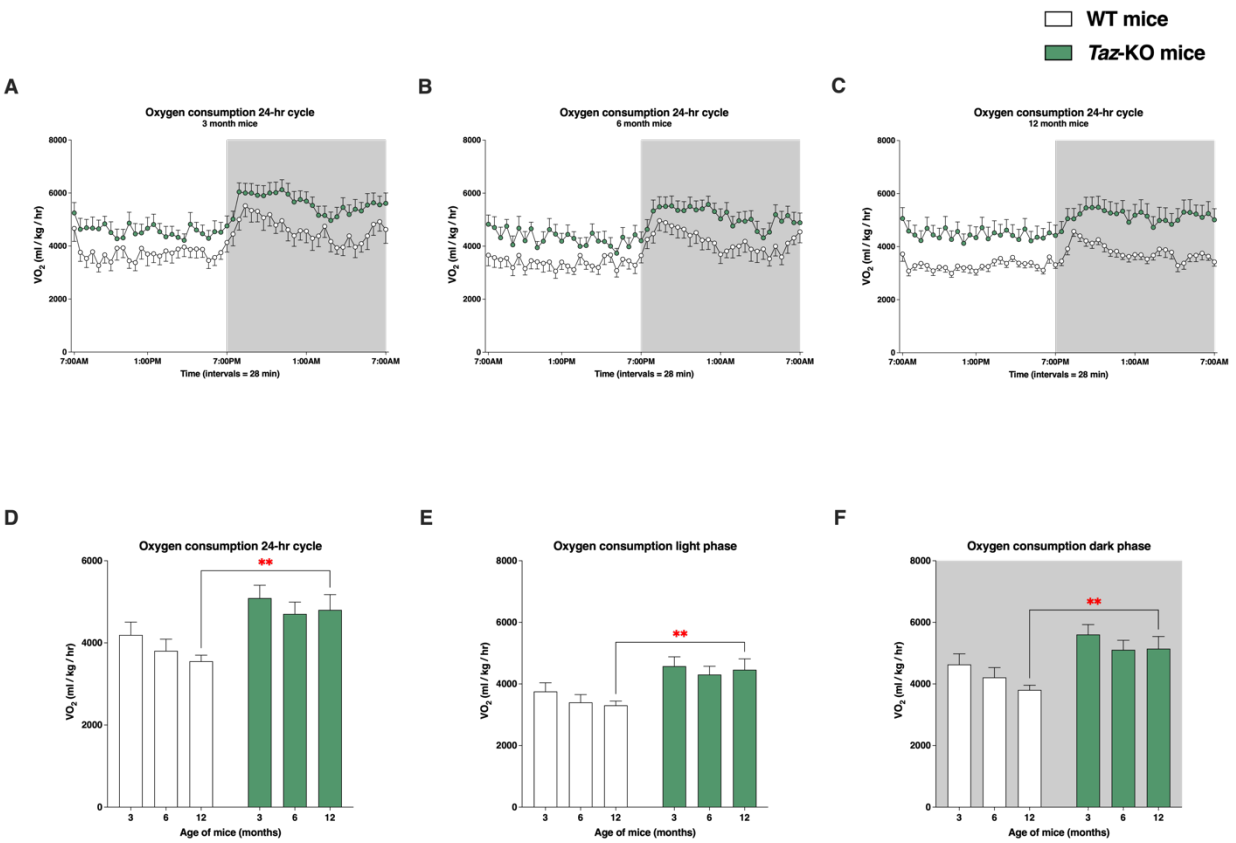

Figure 8: Oxygen consumption over 24-h in *Taz*-KO and WT mice at different ages. Oxygen consumption rates (normalized to body weight) of (**A**) 3-, (**B**) 6-, and (**C**) 12-month-old *Taz*-KO and WT mice was determined cross-sectionally by indirect calorimetry for a period of 24-h. Averages of normalized oxygen consumption rates over the (**D**) total 24-h and during the (**E**) light phase and (**F**) dark phase were analyzed using two-way ANOVA followed by Bonferroni multiple comparisons tests. Subject numbers: *Taz*-KO and WT, respectively, at age points: 3 months, n = 13 and 11; 6 months, n = 12 and 10; 12 months, n = 12 and 14. Data are means ± SEM. $^{**}P<0.01$.

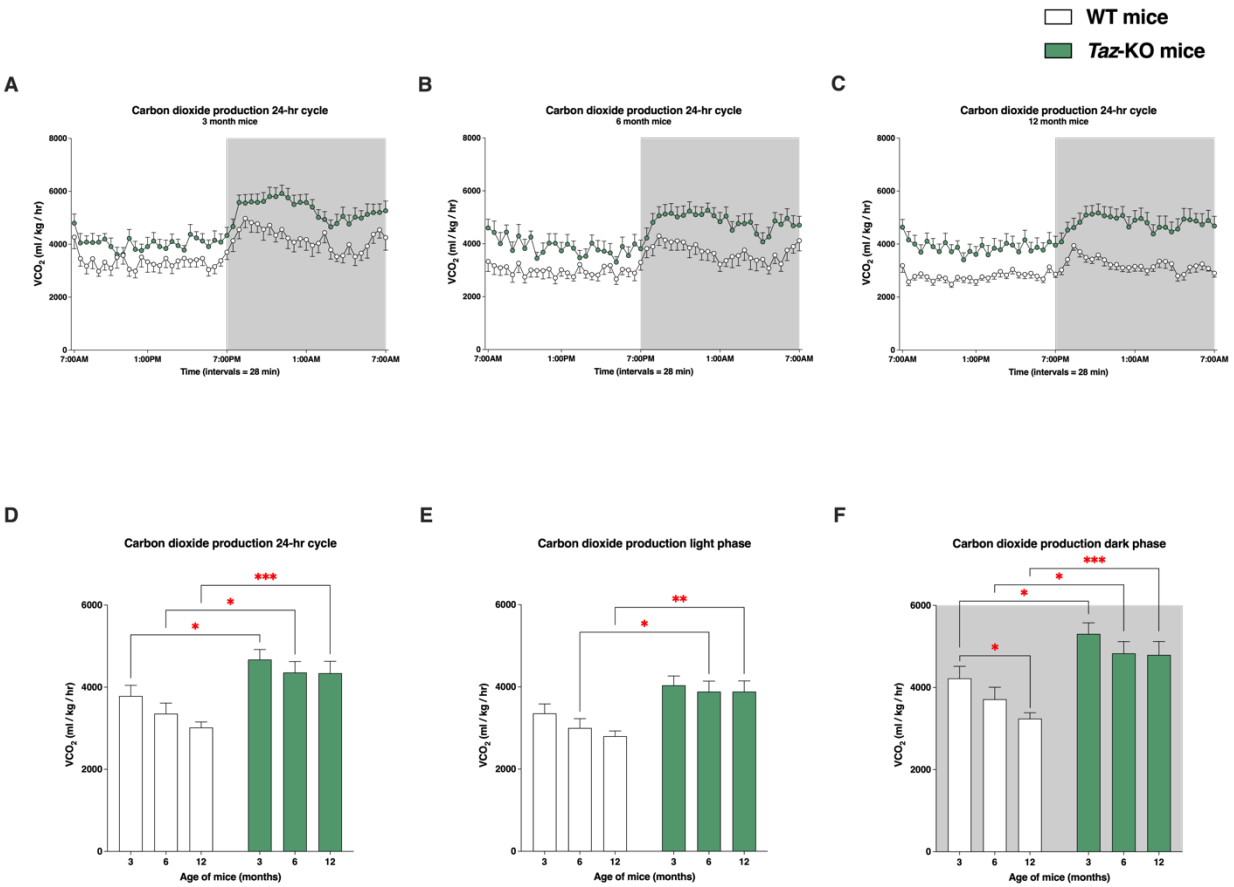

Figure 9: Carbon dioxide production over 24-h in *Taz*-KO and WT mice at different ages.
Carbon dioxide production rates (normalized to body weight) of (**A**) 3-, (**B**) 6-, and (**C**) 12-month-old *Taz*-KO and WT mice was determined cross-sectionally by indirect calorimetry for a period of 24-h. Averages of normalized carbon dioxide production rates over the (**D**) total 24-h and during the (**E**) light phase and (**F**) dark phase were analyzed using two-way ANOVA followed by Bonferroni multiple comparisons tests. Subject numbers: *Taz*-KO and WT, respectively, at age points: 3 months, $n = 13$ and 11; 6 months, $n = 12$ and 10; 12 months, $n = 12$ and 14. Data are means ± SEM. $^{*}P<0.05$, $^{**}P<0.01$, $^{***}P<0.001$.

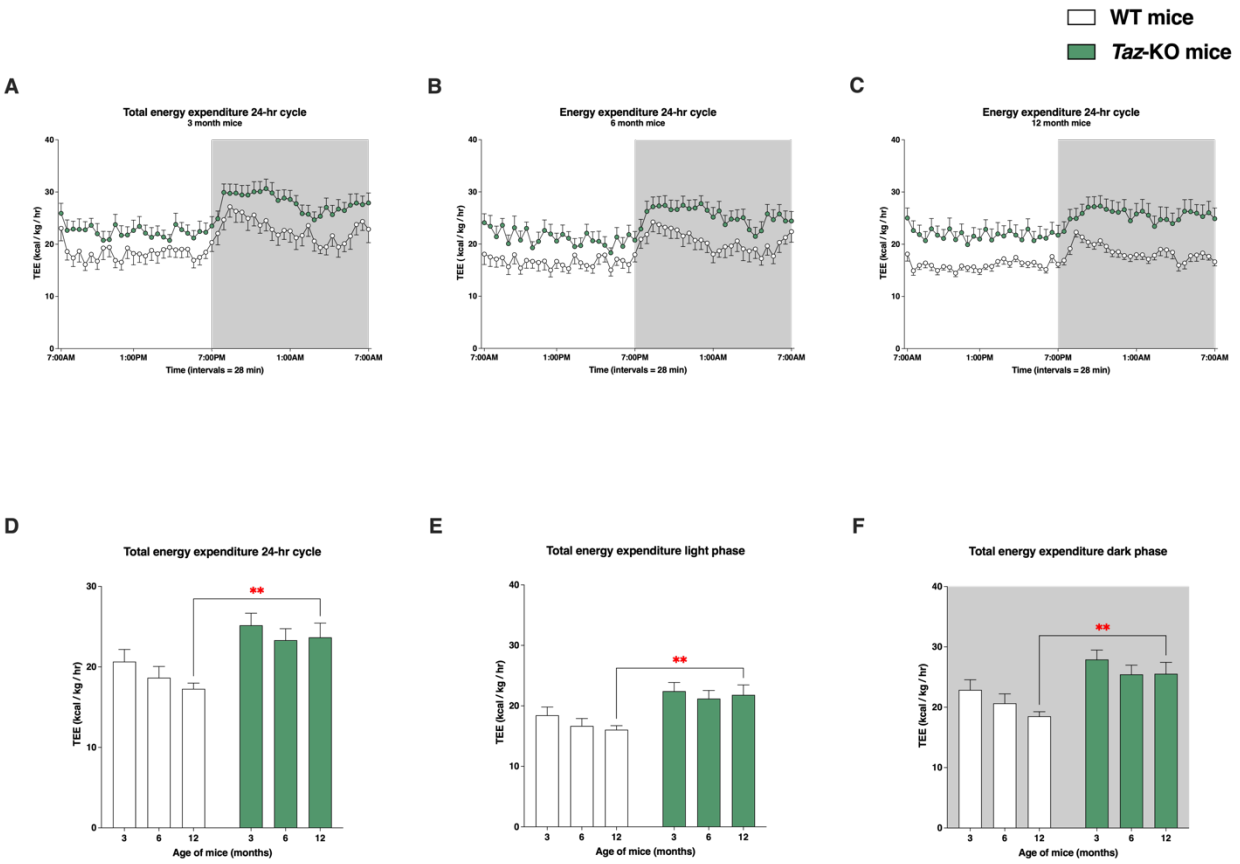

Figure 10: Total energy expenditure (TEE) over 24-h in *Taz*-KO and WT mice at different ages. TEE of (**A**) 3-, (**B**) 6-, and (**C**) 12-month-old *Taz*-KO and WT mice was determined cross-sectionally by indirect calorimetry for a period of 24 hr. Averages of TEE over the (**D**) total 24-h and during the (**E**) light phase and (**F**) dark phase were analyzed using two-way ANOVA followed by Bonferroni multiple comparisons tests. Subject numbers: *Taz*-KO and WT, respectively, at age points: 3 months, $n = 13$ and 11; 6 months, $n = 12$ and 10; 12 months, $n = 12$ and 14. Data are means ± SEM. $^{**}P<0.01$.

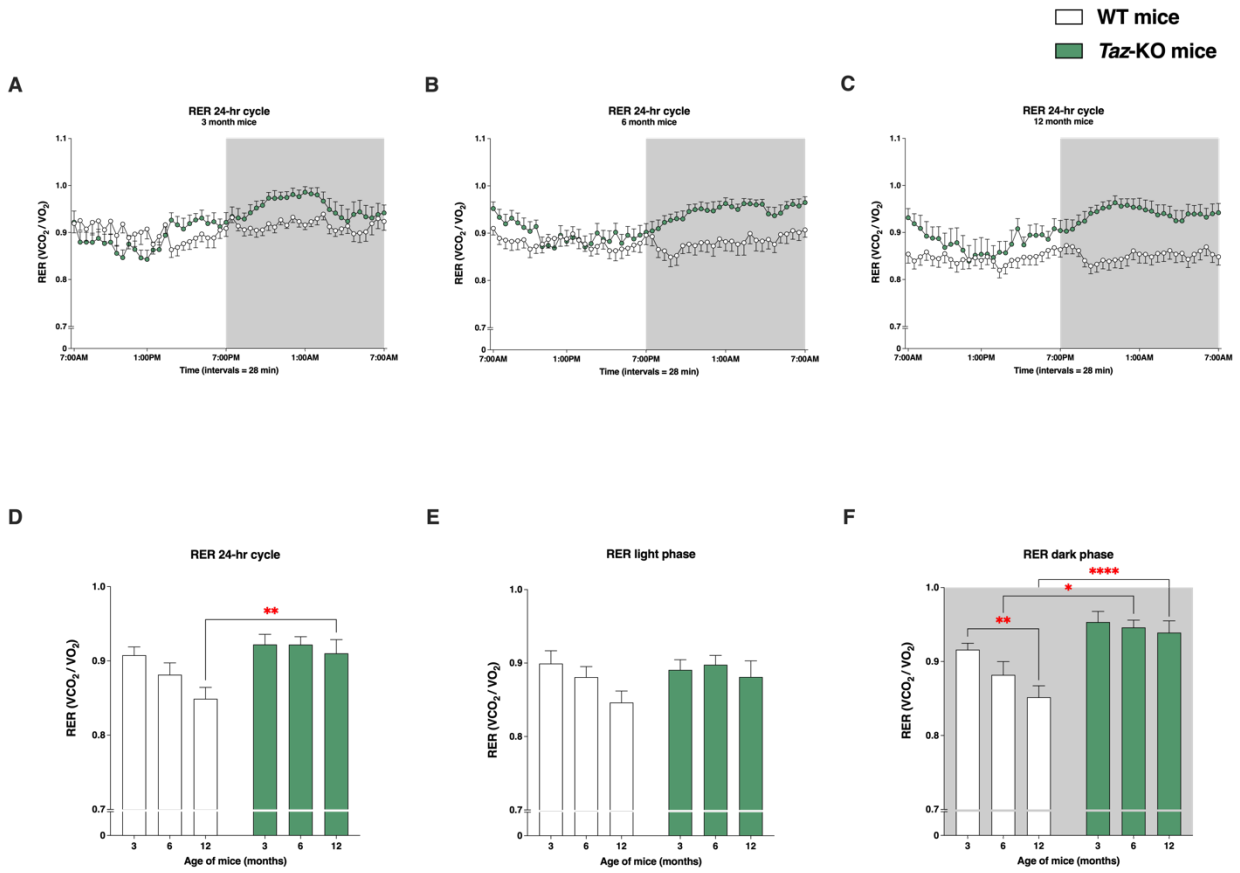

Figure 11: Respiratory exchange ratio (RER) over 24-h in *Taz*-KO and WT mice at different ages. RER of (**A**) 3-, (**B**) 6-, and (**C**) 12-month-old *Taz*-KO and WT mice was determined cross-sectionally by indirect calorimetry for a period of 24-h. Averages of RER over the (**D**) total 24-h and during the (**E**) light phase and (**F**) dark phase were analyzed using two-way ANOVA followed by Bonferroni multiple comparisons tests. Subject numbers: *Taz*-KO and WT, respectively, at age points: 3 months, $n = 13$ and 11; 6 months, $n = 12$ and 10; 12 months, $n = 12$ and 14. Data are means ± SEM. *$P<0.05$, **$P<0.01$, ***$P<0.001$, ****$P<0.0001$.

TEE partly results from energy expended with motor activity, and the CLAMS system is equipped to measure the spontaneous physical activity levels of mice while the gas exchange data is collected. Remarkably, there were no significant differences between genotypes at any age-point in ambulatory activity (**Fig. 12D – F**), which is the activity recorded when a mouse traverses the chamber. Both genotypes experience age-related declines in ambulatory activity, with a significant decrease from 3-months to 12-months of age for WT mice, but a more rapid onset of ambulatory activity decline in the *Taz*-KO mice, with significantly reduced ambulatory activity already by 6-months of age in *Taz*-KO mice compared to 3-month *Taz*-KO mice. In the rearing activity dimension, 6-month-old WT mice were significantly more active than 6-month-old *Taz*-KO mice, but there were no differences between genotypes at 3-months and 12-months, and overall no significant age-related declines (**Fig. 12G – I**). Total locomotor activity, which is

the sum of all movements of mice including repetitive behaviours such as grooming and feeding, was only different between the genotypes at 12-months of age (**Fig. 12A – C**). The locomotor activity of WT mice decreased as they aged from 3- to 12-months, with longitudinal differences most discernable during the dark phase. Specifically in the light phase, two-way ANOVA indicates significant effects of genotype ($P < 0.01$) on locomotor activity, with the effect of genotype dependent on age ($P < 0.01$). While the locomotor activity of WT mice trends towards a decrease with age, *Taz*-KO mice demonstrated significantly increased locomotor activity with age during the light period, which corresponds to the inactive (sleep) phase of mice.

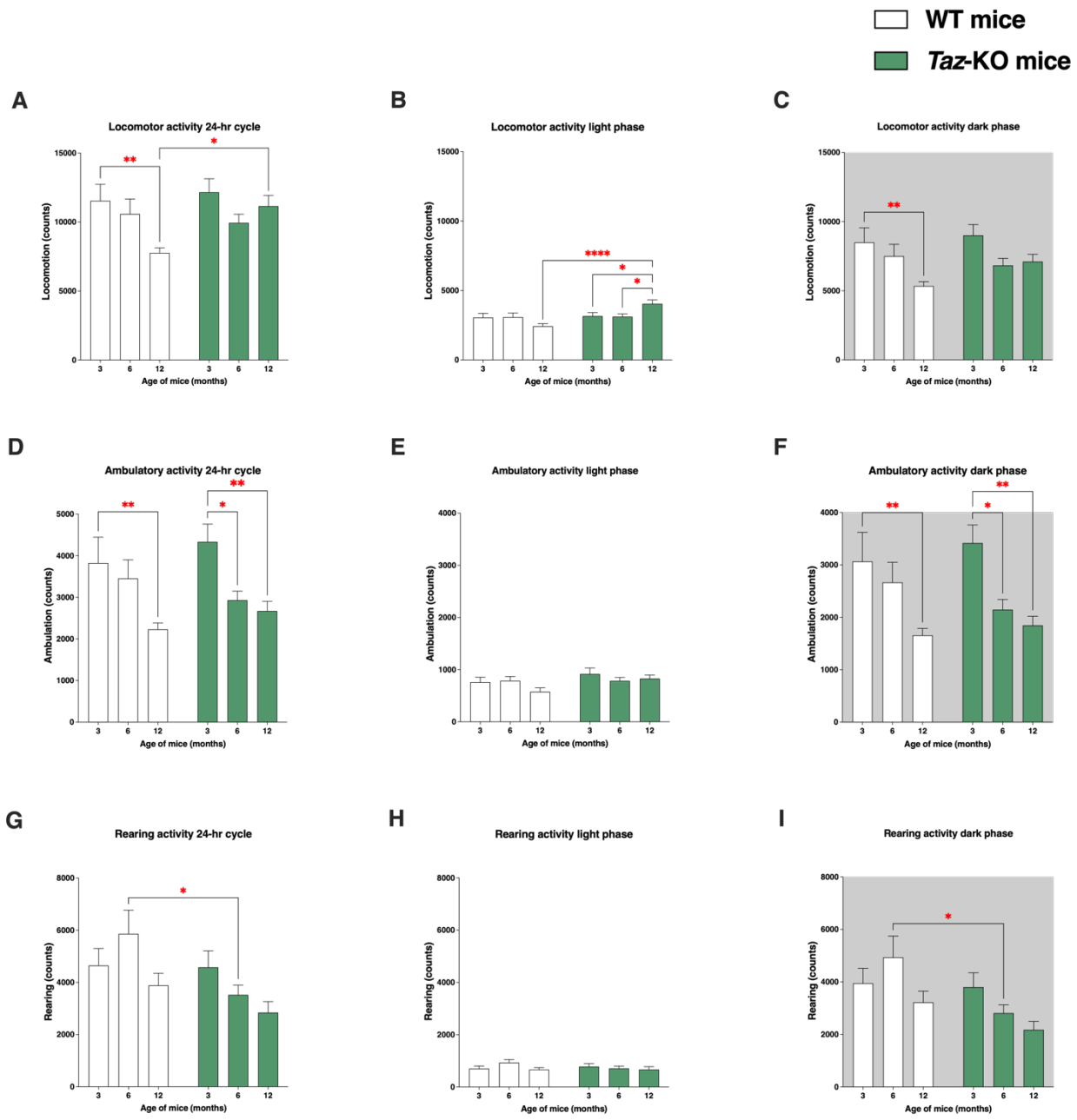

Figure 12: Sums of physical activity counts over 24-h of *Taz*-KO and WT mice at different ages. (**A – C**) Locomotion represents activity in *x* plane and encompasses small, repetitive movements such as grooming and eating. (**D – F**) Ambulation represents activity in the *y* plane such as when a mouse traverses the metabolic chamber. (**G – I**) Rearing represents activity in the *z* plane. Total activity is presented in addition to activity by photoperiod. Subject numbers: *Taz*-KO and WT, respectively, at age points: 3 months, $n = 13$ and 11; 6 months, $n = 12$ and 10; 12 months, $n = 12$ and 14. Statistical analysis was performed using two-way ANOVA followed by Bonferroni multiple comparisons tests (**A – I**). Data are means ± SEM. *$P<0.05$, **$P<0.01$, ***$P<0.001$, ****$P<0.0001$.

6.5. Discussion

Body composition is intricately tied to a balance between energy intake and expenditure; even a small imbalance between the two determinants can result in significant changes in mouse body weight and composition over a span of days or weeks [129]. Energy intake is most simply assessed by measuring food consumption. Despite their smaller size, *Taz*-KO mice consumed the same absolute amount of food as their WT littermates, and could even be considered hyperphagic compared to WT mice when chow intakes were normalized to body weight. Although intestinal caloric absorption was not measured to ensure there are no digestive issues, a previous study has found no impairments in nutrient absorption in *Taz*-KD mice [54], which implies that the source of the lean phenotype of *Taz*-KO mice lies in the other component of the energy balance equation, including increased energy expenditure.

After accounting for their smaller body weight, daily TEE was higher in 12-month-old *Taz*-KO mice than WT mice, and 3- and 6-month-old *Taz*-KO mice demonstrated a trend towards higher TEE ($P = 0.07$ and $P = 0.08$, respectively). In human subjects, BTHS patients were found to have similar resting energy expenditure to controls, when energy expenditure was normalized to lean body mass (LBM) [75]. Of important consideration, however, is the normalization factor used as a denominator in analyzing TEE. Normalizing by body weight assumes that all tissues have an equivalent metabolic demand; however, the metabolic activity in adipose tissue is lower than in most other tissues and contributes relatively little to the TEE of an organism compared with lean mass [129]. When TEE is corrected by BW, inherent contrasts in body composition between genotypes can induce an underestimation of the TEE of obese animals because a greater relative portion of their BW is composed of WAT. This may be the case with our analysis of TEE, and would suggest that differences in TEE between WT and *Taz*-KO mice are mostly driven by differences in body weight rather than differences in genotype.

We do not have the equipment on campus to measure body composition, so TEE was normalized to total body weight, which is the simplest and most widely used method [130]. There are drastic differences in total body weight between WT and *Taz*-KO mice, with *Taz*-KO mice weighing 38% less at 12-months of age, but even more drastic differences in adipose depots weights, as 12-month *Taz*-KO mice have ~75% smaller WAT depots compared to age-matched WT mice. Many studies address the issue of contrasting body composition between groups by normalizing EE with LBM, the “metabolically active” portion of body weight. In fact, a study measuring energy expenditure in *Taz*-KD mice found that *Taz*-KD mice had significantly higher

TEE when normalized to body weight compared to WT mice, however, the differences disappeared when TEE was adjusted for LBM [55]. Therefore, it is possible that the *Taz*-KO mice do not have a higher resting energy expenditure than WT mice. However, the problem is not solved by simply normalizing to LBM and completely disregarding adiposity differences. Despite exhibiting lower metabolic activity than other organs such as the heart and kidneys when measured *in vitro* [131], WAT is an active endocrine tissue *in vivo* that participates in regulating metabolic homeostasis by secreting local and systemic signals such as leptin and adiponectin [132]. Furthermore, adipose tissue constitutes a substantial portion of body weight in fatter animals and can account for an important proportion of TEE in relation to basal metabolism. Therefore, it is important to account for adiposity in the analysis of TEE. The aforementioned Goncalves et al. (2021) study acknowledged that *Taz*-KD mice may indeed have higher rates of energy expenditure, since when TEE was measured between mouse genotypes before differences in body weight and adiposity have developed (being 3-months of age), the *Taz*-KD mouse did have higher TEE corrected for total body weight [55]. Therefore, while the Cade et al. (2013) study found no differences in energy expenditure expressed per unit of LBM between BTHS patients and healthy controls [75], the results may have matched the current mouse findings if TEE of human BTHS patients was normalized to total body weight, instead of LBM.

TEE results from the energy expended in four main compartments: energy expended with motor activity, thermic effect of food (TEF), thermoregulation, and basal (resting) energy expenditure, which itself is determined by numerous factors including but not limited to body composition, mitochondrial content, and mitochondrial respiratory capacity and efficiency [130, 133]. An essential first step for identifying the basis of differences in TEE is distinction between total versus resting metabolic rates. Accounting for the comparable levels of food intake and spontaneous physical activity, the findings of the current study suggest that hyperactive basal energy expenditure may contribute to the lean phenotype of *Taz*-KO mice.

Considering that mitochondrial dysfunction is central to the etiology of BTHS, it is possible that decreased efficiency of mitochondrial OXPHOS, i.e., increased uncoupling of mitochondrial oxygen consumption and ATP production, may be compensated by increased substrate metabolism to generate the same amount of ATP [133]. On the whole-body level, this would manifest as higher levels of oxygen consumption, carbon dioxide production, and thus energy expenditure, as was observed in our study.

Cardiomyocytes derived from induced pluripotent stem cells (iPSC-CMs) from human patients with BTHS were shown to have increased proton leak across the inner membrane, resulting in elevated basal O_2 consumption [134], and mitochondrial inefficiency has been linked to higher rates of whole-body oxygen consumption in mice [133, 135]. In contrast, respirometry analysis on cardiac mitochondria from *Taz*-KD mice frequently yields comparable or lower basal oxygen consumption rates to controls [49, 57, 68], although the cardiomyopathy phenotype of *Taz*-KD mice is problematic due to its delayed manifestation. Alternatively, many *Taz*-KD mouse studies have reported elevated mitochondrial content due to compensatory biogenesis [47, 51, 136], which can also contribute to higher rates of whole-body energy expenditure. However, these interpretations are speculative as mitochondrial function and content analysis were not performed in this study.

Although the simplifying assumption was made that the other components of TEE were equal between the two mouse groups to explore the possibility of increased basal metabolism augmenting TEE, alternative hypotheses exist since increased TEF and thermoregulation may also be important factors of TEE in *Taz*-KO mice. In this framework, the increased TEE observed in *Taz*-KO mice in the present study may have resulted from greater consumption of food relative to body weight [137, 138], and since mice are housed at room temperatures below their thermoneutral zone (30°C), *Taz*-KO mice may have to activate thermogenesis to a greater degree than WT mice to maintain core body temperature due to their relative lack of insulating adipose tissue [139]. Further work is required to confirm the increased TEE of *Taz*-KO mice, ideally with the use of analysis of covariance with fat-free and fat mass included as two independent covariates [140], and to dissect the source of increased TEE by careful integration of all components of TEE.

Loss of TAZ seems to affect fuel substrate selection, with studies on human patients suggesting that fatty acid oxidation is impaired but partially compensated by increased glucose turnover [78, 79]. These metabolic derangements have been implicated in the cardioskeletal myopathy and exercise intolerance of BTHS. *Taz*-KO mice seem to recapitulate the preference for glucose as a fuel, as supported by the finding of higher RERs compared to WT mice in this study. Even at the earliest age point measured, *Taz*-KO mice have significantly higher CO_2 production in the face of similar O_2 consumption compared to WT mice. At 6- and 12-months, *Taz*-KO mice have a higher RER (the ratio of VCO_2 to VO_2) than WT mice, reflecting dominant consumption of carbohydrates over fatty acids. The metabolism of carbohydrates is more oxygen efficient

compared to lipid metabolism, in that to produce the same amount of ATP (and carbon dioxide as a by-product), lipids will require a greater relative cost of oxygen [130]. Consequently, greater production of carbon dioxide mice despite similar oxygen consumption as WT mice indicates that carbohydrates are used as the main energetic substrate in *Taz*-KO mice.

It is likely that substrate metabolism abnormalities will become exacerbated upon exercise in *Taz*-KO mice, as seen in human BTHS patients, since whole-body fatty acid oxidization is not different between patients and controls at rest [75], yet submaximal exercise conditions revealed that the ability to upregulate fatty acid oxidation was severely blunted in BTHS patients [78]. In the indirect calorimetric chambers, mice exhibit spontaneous physical activity but are not subjected to submaximal exercise. Analysis of metabolic indices during exercise of increasing intensity using indirect calorimetry in metabolic treadmill chambers may reveal more severe metabolic inflexibility in *Taz*-KO mice.

Skeletal myopathy is a prominent symptom of BTHS and many patients additionally experience chronic fatigue, exercise intolerance, pain, postural imbalance, delayed motion reaction time, and cognitive difficulties [102, 141-143]. These symptoms result in physical disability and a reduction in patient quality of life. Previous research on *Taz*-KD and *Taz*-KO mice has established that both mouse models have impaired exercise capacity when subjected to forced treadmill exercise testing that is consistent with the exercise intolerance of the human condition [9, 144, 145]. In this current study, spontaneous physical activity levels were measured in the *Taz*-KO mice since their horizontal and vertical displacements, and activities without significant displacement, such as grooming and feeding, were recorded in the metabolic chambers. Unexpectedly, levels of spontaneous physical activity were overall similar between WT and *Taz*-KO mice, contrary to my hypothesis. This finding was surprising because Thompson et al. (2016) found that BTHS patients are strongly affected by fatigue and covered less distance during a 6MWT and observed that 6MWT performance correlated with measures of reported fatigue and daily activity [8].

It is unknown why the *Taz*-KO mice do not seem to be impaired by fatigue in terms of daily activity, but this finding agrees with *Taz*-KD mouse studies, which also report either no differences or higher levels of physical activity in *Taz*-KD mice while in metabolic chambers [49, 55]. It is possible that higher levels of spontaneous physical activity in the BTHS mouse models may reflect a kind of anxiety-like behaviour, counteracting the fatigue. *Taz*-KD mice in an open-field test demonstrated signs of elevated anxiety in conjunction with normal motor functions

[101], and the increasing locomotor activity of *Taz*-KO mice with age during the light phase, when mice are typically inactive or asleep, potentially indicates age-related declines in cognition. Apart from locomotor activity, both WT and *Taz*-KO mice undergo age-related declines in physical activity with age-related limitations most apparent in the ambulation component of activity. This decline is more gradual and continuous into 12-months of age in WT mice, while the ambulatory activity of *Taz*-KO mice declines earlier in life, with a significant decrease from 3- to 6-months of age but no significant change from 6- to 12-months of age. While the decrease in physical activity in WT mice is likely related to its obese phenotype, it is more likely related to declining skeletal muscle function in the *Taz*-KO mice.

Chapter 7: Endurance Exercise Capacity

7.1. Introduction

Reports of increasing fatigue and progressive muscle weakness with older age in individuals with BTHS are concerning [7, 8, 102]. In a prior report, *Taz*-KO mice were shown to have severely reduced exercise capacity [9], although age-related changes have not been investigated yet in a BTHS-related mouse model. Use of the treadmill exhaustion test to evaluate exercise capacity in *Taz*-KO mice at various ages will provide insight into changes in cardiac and skeletal muscle performance *in vivo* over time.

7.2. Objectives and Hypotheses

The objective and hypotheses for this study were as follows:

1. **Objective:** To perform a forced treadmill exhaustion test on *Taz*-KO and WT mice at 3-, 6-, and 12-months of age to evaluate exercise endurance.
   Hypotheses: *Taz*-KO mice will have drastically lower exercise capacity compared to WT mice at all age points, and *Taz*-KO mice will exhibit steeper and/or earlier declines in exercise capacity with age.

7.3. Experimental Approach

7.3.1. Treadmill Exhaustion Test

The treadmill exhaustion test consists of mice running on a treadmill with 5° inclination with increasing speed until exhaustion. The starting speed is 10 cm/s, and every 2 minutes the speed is increased to 3 cm/s until the maximum speed of 70 cm/s is reached. To encourage mice to run, they were gently prodded with a wire cleaning brush every time they approached the back of the treadmill. Once mice failed to run for 5 consecutive seconds despite prodding, the mice were considered to have reached exhaustion, and therefore were removed from the treadmill and exhaustive running time was recorded. Prior to the official exhaustive treadmill test, mice were trained on the treadmill for three consecutive days at low speeds for 10 minutes, followed by a rest day, as described in section 4.3.1 in chapter 4.

7.3.2. Statistical Analysis

Comparisons of the averages of running time until exhaustion between WT and *Taz*-KO mice were conducted using a two-way ANOVA to detect an interaction between genotype and age as

main factors. Following a significant effect identified by two-way ANOVA, Bonferroni multiple comparison tests were used to identify: (1) significant differences in means within genotypes for cross-sectional age-related changes, and (2) significant differences between age-matched animals from different genotypes.

Data are presented as mean ± standard error of the mean (SEM). Differences were considered statistically significant when $p < 0.05$. Statistical analysis and figures were generated using GraphPad Prism version 9.0.0 for Mac (GraphPad Software, San Diego, California, USA).

7.4. Results

Exercise capacity was assessed in the *Taz*-KO mice. The *Taz*-KO mice were required to run to exhaustion on a motorized treadmill apparatus with increasing speed. At all age-points, *Taz*-KO mice exhibited a markedly reduced capacity to sustain running exercise. On average, 3-month-old *Taz*-KO mice ran 26 min 36 s until exhaustion, which was 30% less time than age-matched WT littermates, which lasted 38 min 7 s on the treadmill (**Fig. 13**).

Furthermore, *Taz*-KO mice demonstrated larger, and earlier-onset, declines in exercise capacity during aging compared to WT littermates. While the exhaustion time (34 min 3 s) of 6-month-old WT mice decreased by 11% compared to 3-month-old WT mice, the exhaustion time (14 min 52 s) of 6-month-old *Taz*-KO mice decreased by 44% compared to 3-month-old *Taz*-KO mice, exhibiting a far more severe exercise capacity deterioration with age. Exercise capacity further decreased from the ages of 6- to 12-months. The exhaustion time for 12-month-old WT mice was 29 min 30 s and for 12-month-old *Taz*-KO mice was 10 min 30 s. These numbers represent a 13% reduction in exercise capacity for WT mice and 29% reduction for *Taz*-KO mice compared to their respective genotype 6-month-old counterparts. Again, the *Taz*-KO mice exhibited a relatively greater deterioration in exercise capacity compared to WT mice, but the decrease did not reach statistical significance, presumably due to a small sample size. There was a significant interaction between genotype and age ($P < 0.01$) due to the severe declines in exercise capacity of *Taz*-KO mice.

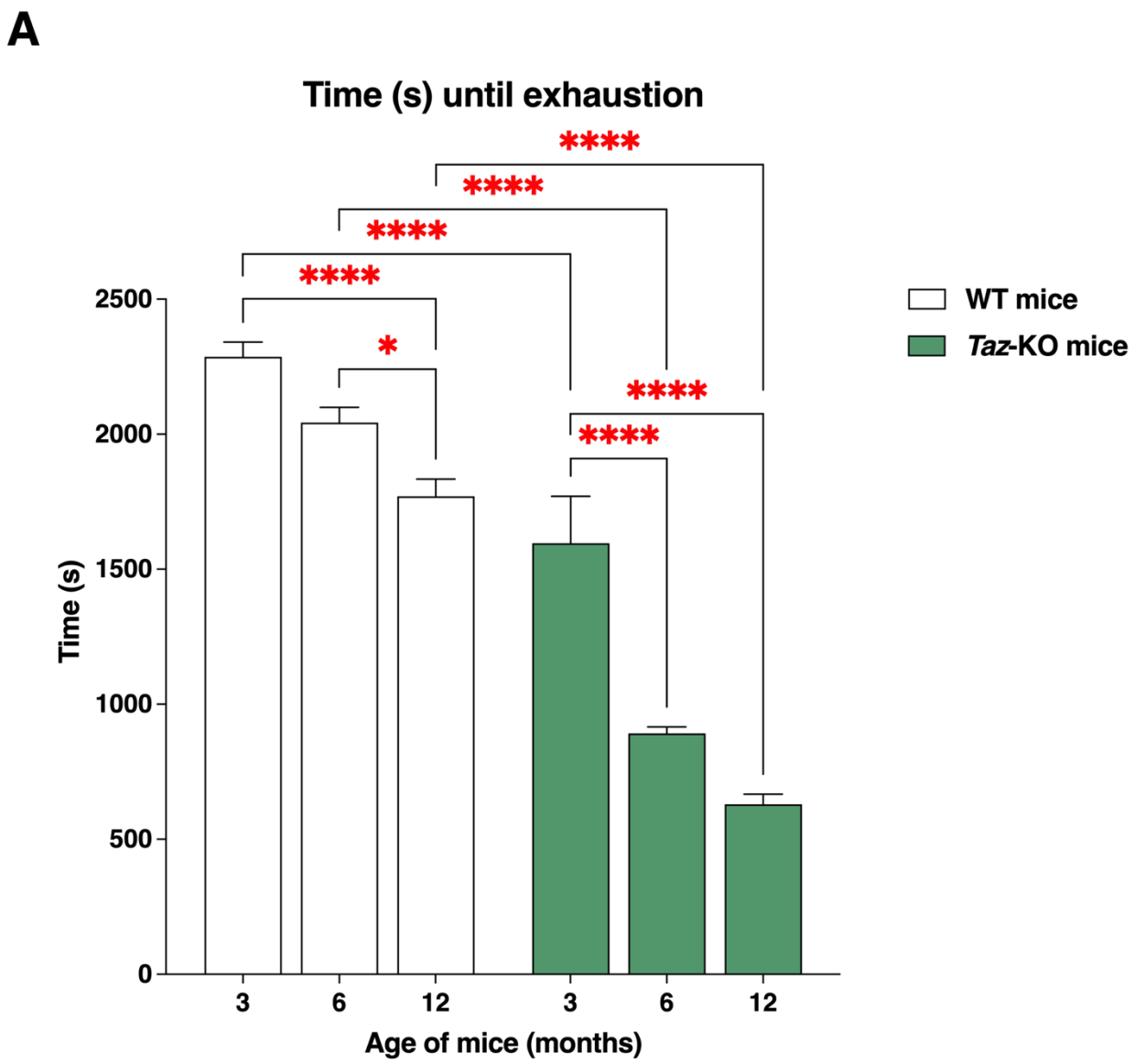

Figure 13: Declining exercise capacity in *Taz*-KO mice with age. Mice ran on the treadmill until exhaustion, at which point the maximal running time was recorded. Subject numbers: *Taz*-KO and WT, respectively, at age points: 3 months, $n = 4$ and 4; 6 months, $n = 7$ and 7; 12 months, $n = 4$ and 8. Data are means ± SEM. Statistical analysis was performed using two-way ANOVA followed by Bonferroni multiple comparisons tests. *$P<0.05$, **$P<0.01$, ***$P<0.001$, ****$P<0.0001$.

7.5. Discussion

Consistent with prior reports on the *Taz*-KD mouse model and BTHS patients, the exercise capacity of the *Taz*-KO mouse is severely reduced. This study is the first to evaluate changes in exercise capacity with age in the *Taz*-KO mice. Considering the notion that cardiac function is viewed as being relatively stable in BTHS patients [66, 108, 109] and *Taz*-cKO mice [86], work

from this study demonstrates that exercise capacity in contrast undergoes drastic and detrimental declines with age in *Taz*-KO mice.

Strenuous exercise induces more than a 100-fold increase in ATP turnover rate compared to resting conditions [146]. Initially, muscle ATP stores and phosphocreatine are used to support the increased energy requirement but are depleted within seconds. Subsequently, skeletal muscle must use oxidative metabolism to manufacture additional ATP from energy stored in nutrients [147]. Inadequate oxygen supply and impaired fuel substrate utilization will limit energy production, and both of these factors have been demonstrated to be present in BTHS.

Taz-KD mouse studies show that despite unaltered total content of myoglobin in the heart, these animals exhibit a 2-fold decrease in mitochondria-associated myoglobin, which suggests disrupted interaction between myoglobin and CL-depleted mitochondria, and ultimately impaired oxygen delivery [47]. In human BTHS patients, decreased skeletal muscle oxygen utilization, in addition to impaired cardiac contractile reserve, were also identified to contribute to exercise intolerance. During a graded exercise test, near-infrared spectroscopy measurements revealed that BTHS patients were unable to properly extract blood oxygen despite increasing saturation of blood with oxyhemoglobin [148]. Furthermore, the utilization of fatty acids as a source of energy for ATP production requires oxygen, and it has been reported that the upregulation of fatty acid oxidation is markedly blunted during exercise in BTHS patients [78].

Although impaired fat oxidation may be a consequence of low oxygen supply, it has also been shown in *Taz*-KD mouse hearts that the association of fatty acid oxidation enzymes and ETC supercomplexes are destabilized [47], disrupting the formation of “hypercomplexes” that facilitate efficient metabolic convergence and substrate channelling of fatty acid oxidation and ETC [149]. Accordingly, disruption of fatty acid oxidation and OXPHOS will induce an energy deficit and exercise intolerance. Enhanced glucose metabolism is reported to partially compensate for the fatty acid oxidation defect in BTHS [78], but inadequate oxygen supply is a limiting factor again, and glucose metabolism will consequently shift to anerobic glycolysis. Even at low levels of exercise intensity, plasma lactate concentrations [78] and RER [148] are significantly higher in BTHS patients, indicating precocious anaerobic supplementation at very low workloads.

The type of exercise test employed in the current study was one of gradually increasing speed and therefore intensity, thus requiring the mice to work progressively harder, necessitating faster muscle contraction and thus high levels of ATP. At high exercise intensities, oxygen

demand outpaces oxygen supply which diminishes fatty acid oxidation and limits carbohydrate substrate metabolism to anaerobic glycolysis [147]. In anerobic glycolysis, glucose is metabolized to 2 ATP molecules and 2 pyruvate molecules which are subsequently converted to lactate by the enzyme lactate dehydrogenase. The accumulation of lactate causes a decrease in pH levels, which is one of the inhibitory regulatory mechanisms of phosphofructokinase (PFK), the rate-determining enzyme of glycolysis [150]. Inhibition of PFK ceases glycolysis and skeletal muscles are protected from muscle acidosis, although the last remaining energy-producing pathway is now halted and muscle fatigue is induced [151]. In BTHS patients and *Taz*-KO mice, depressed cardiac output and impaired oxygen uptake in muscles will activate anaerobic glycolysis at lower exercise intensities and contribute to the limited exercise capacity during the forced treadmill exercise capacity test [47, 148].

Interestingly, while anaerobic glycolysis induces metabolic acidosis and yields less energy, which will limit exercise [147], lactate accumulation is no longer considered the primary cause of skeletal muscle fatigue and instead inorganic phosphate accumulation, with a subsequent effect on Ca^{2+} signaling, is increasingly recognized as playing a causative role in the extreme muscle fatigue [152], which is also evident in BTHS. Ca^{2+} release from the sarcoplasmic reticulum (SR) into the cytosol initiates skeletal muscle contraction. Concurrently, the increased cytosolic Ca^{2+} upregulates mitochondrial OXPHOS to match the increased skeletal muscle contractile ATP demands, by entering mitochondria through the mitochondrial calcium uniporter (MCU). Impaired calcium homeostasis in BTHS has been implicated by findings of MCU loss in B-lymphoblasts and cardiac tissue of BTHS patients [153], higher Ca^{2+} leak from the SR in BTHS iPSC-CMs [87], and impaired SERCA activity (which catalyzes the transport of Ca^{2+} back into the SR) in the cardiomyocytes of *Taz*-KD mice [154]. To my knowledge, no investigations into intracellular Ca^{2+} regulatory mechanisms have been conducted in the skeletal muscle of the mouse models of BTHS, but it will be important to determine whether abnormal Ca^{2+} handling may explain aspects of BTHS pathophysiology such as the disabling muscle fatigue, considering that Ca^{2+} is a critical regulator of muscle contraction.

Aging is a complex process that leads to gradual and irreversible decline in physiological functions of the organism. The mitochondrial dysfunction of BTHS limits exercise capacity through a variety of potential mechanisms; these limitations seem to be additive to the aging effect on exercise capacity. A statistically significant interaction resulted whereby age influenced the effect of genotype, in which the effect of aging seems to be amplified in the *Taz*-KO mouse as

more severe deteriorations in exercise capacity were observed. The decline in exercise capacity was progressive, but there was a slower decline later in the lifespan, since there was a greater percent reduction in exercise capacity from 3-months to 6-months of age (i.e., over a 3-month period) than from 6-months to 12-months of age (i.e., over a 6-month period). Of note, mice do undergo more accelerated maturation compared to humans earlier in their life (maturing 45 times faster than humans from 1 – 6 months of age) than later in their life (maturing 25 times faster than humans after 6 months of age) [155]. Regardless, aging may not be uniform across different cells, tissues, and organs [156]. The *Taz*-KO mouse model should be utilized in future studies to dissect whether changes in skeletal muscle or cardiac function drive the reductions in exercise capacity with age.

Chapter 8: Glucose Homeostasis

8.1. Introduction

Alterations of mitochondrial function have long been recognized in the pathogenesis of insulin resistance and diabetes [157]. Although mitochondrial dysfunction and altered substrate utilization has been demonstrated at multiple levels in BTHS, it remains to be established whether TAZ deficiency in a mammalian model precipitates disruptions in whole-body glucose metabolism. Due to minimal invasiveness and ease-of-use, GTTs and ITTs are first-line experiments to assess glucose homeostasis [158].

8.2. Objectives and Hypotheses

The objectives and hypotheses for this study were as follows:

1. **Objectives:** To evaluate disposal of a bolus administration of glucose during GTT and glucose clearance in response to a bolus administration of insulin during ITT in *Taz*-KO mice and WT littermates at 3-, 6-, and 12-months of age.
   Hypotheses: *Taz*-KO mice will have greater glucose clearance during GTT compared to WT mice since individuals with BTHS demonstrated increased glucose reliance [75, 78]. Since insulin sensitivity is preserved in *Taz*-KD mice [85], and therefore *Taz*-KO mice will demonstrate a similar response to ITT as WT mice across their lifespan.

8.3. Experimental Approach

8.3.1 Glycemic Control Testing

Mice were first subjected to the GTT, then allowed rest for 7 days to recover from the intraperitoneal injection and blood loss, and then subjected to the ITT, as described in sections 4.4 in chapter 4. GTTs and ITTs were performed after a 6-h and 2-h fast, respectively. For GTT, mice were given an *i.p.* glucose dose of 2.0 mg/kg body weight. For ITT, mice were given an *i.p.* insulin dose of 0.5 U/kg body weight. Blood glucose concentrations were measured in tail vein whole blood using the Freestyle Glucose Monitoring System and test strips (Abbot Laboratories) before glucose application (time 0) and at 15, 30, 60, 90 and 120 minutes after injection.

8.3.2. Statistical Analysis

Differences in serial measurements of blood glucose levels during the GTT and ITT between *Taz*-KO and WT genotypes at the same age were analyzed using a repeated-measures two-way ANOVA with genotype and time after injection as grouping factors, followed by Bonferroni multiple comparisons tests to identify the timepoints during GTT and ITT that blood glucose levels differed between genotypes.

For GTT of blood glucose concentrations over time, the area under the curve (AUC) above basal glucose concentration was calculated using the trapezoid rule for each mouse individually and averaged for age and genotype. For ITT of blood glucose concentrations over time, the inverse AUC (iAUC) under basal glucose concentration was calculated using the trapezoid rule for each mouse individually and averaged for age and genotype. Averages of GTT AUCs and ITT iAUCs were conducted using a two-way ANOVA to detect an interaction between genotype and age as main factors. Following a significant effect identified by two-way ANOVA, Bonferroni multiple comparison tests were used to identify: (1) significant differences in means within genotypes for cross-sectional age-related changes, and (2) significant differences between age-matched animals from different genotypes.

Data are presented as mean ± standard error of the mean (SEM). Differences were considered statistically significant when $p < 0.05$. Statistical analysis and figures were generated using GraphPad Prism version 9.0.0 for Mac (GraphPad Software, San Diego, California, USA).

8.4. Results

The fasting blood glucose of *Taz*-KO and WT mice showed no differences at any age (**Fig. 14, 15**). When subjected to *i.p.* GTT, glucose tolerance was equivalent between young (i.e., 3-month-old) Taz-KO and WT mice. Across ages, WT mice showed gradually worsening glucose clearance in response to GTT, with significant differences between 3-month-old WT mice and 6- and 12-month-old WT mice due to higher blood glucose AUCs in the older WT mice. Meanwhile, the glucose tolerance of *Taz*-KO mice remained stable with age. Ultimately, the divergence of glucose clearance trends between WT and *Taz*-KO mice with age yielded a significant genotype-by-age interaction ($^{**}P < 0.01$) and significant discrepancies in glucose homeostasis, as shown in **Fig. 14D**, in which 6- and 12-month-old WT mice were glucose intolerant compared to age-matched *Taz*-KO mice.

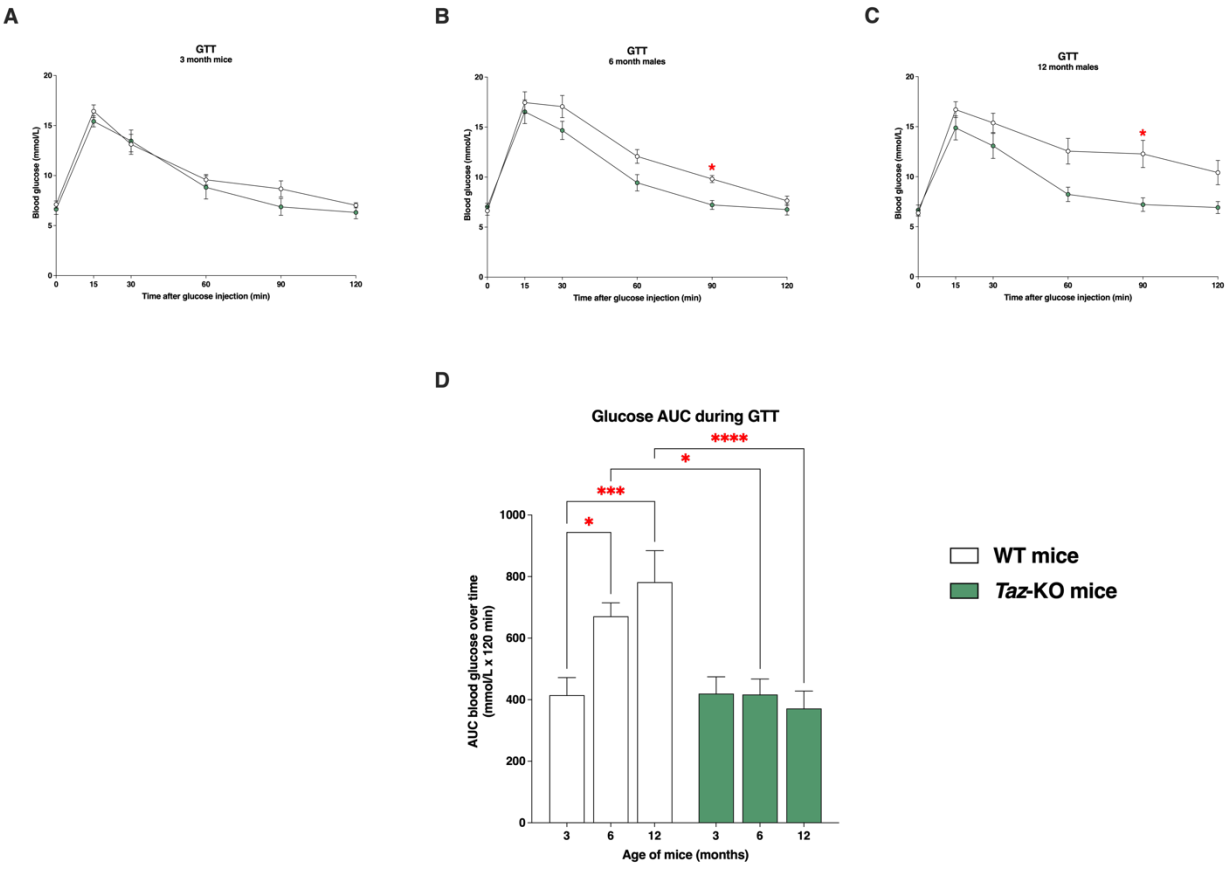

Figure 14: *Taz*-KO mice are protected from age-related decreases in glucose tolerance. Glucose tolerance test performed in mice with a glucose dose of 2 mg/kg body weight. Blood glucose levels over time in (**A**) 3-, (**B**) 6-, and (**C**) 12-month-old mice during GTT. Significant differences in glycemia across timepoints during GTT were assessed by repeated-measured two-way ANOVA followed by Bonferroni multiple comparison tests. *P<0.05. (**D**) Corresponding AUC of GTT in WT and Taz-KO mice performed at 3-, 6-, and 12-months of age. Subject numbers: *Taz*-KO and WT, respectively, at age points: 3 months, n = 9 and 10; 6 months, n = 10 and 10; 12 months, n = 10 and 10. Data are means ± SEM. Statistical analysis was performed using two-way ANOVA followed by Bonferroni multiple comparisons tests. *P<0.05, **P<0.01, ***P<0.001, ****P<0.0001.

The insulin sensitivity did not change significantly with age in WT mice, and thus the age-related changes in glucose handling capability may be insulin-independent. However, the insulin sensitivity did trend towards a decrease in the WT mice while the *Taz*-KO mice were protected against major age-related changes, so that at 12-months of age, WT mice were significantly more insulin insensitive in comparison to *Taz*-KO mice (**Fig. 15D**). Altogether, these data suggest that *Taz*-KO mice exhibit protection against the impairments of glucose homeostasis induced by advancing age and/or adiposity, despite presumed mitochondrial dysfunction.

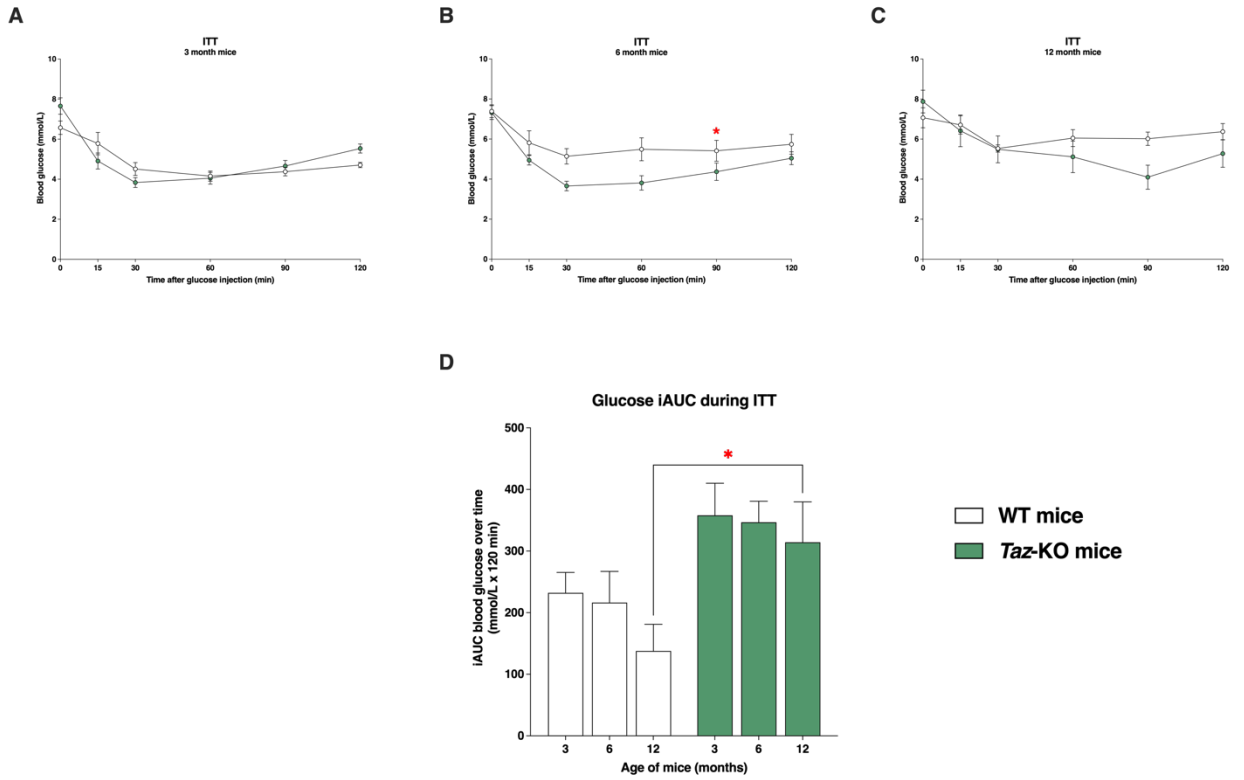

Figure 15: Retained insulin sensitivity through aging in *Taz*-KO mice. Insulin tolerance test performed in mice with an insulin dose of 0.5 U/kg body weight. Blood glucose levels over time in (**A**) 3-, (**B**) 6-, and (**C**) 12-month-old mice during ITT. Significant differences in glycemia across timepoints during ITT were assessed by repeated-measured two-way ANOVA followed by Bonferroni multiple comparisons tests. (**D**) Corresponding inverse AUC of ITT in WT and *Taz*-KO mice performed at 3-, 6-, and 12-months of age. Subject numbers: *Taz*-KO and WT, respectively, at age points: 3 months, $n = 12$ and 12; 6 months, $n = 8$ and 9; 12 months, $n = 11$ and 8. Data are means ± SEM. Statistical analysis was performed using two-way ANOVA followed by Bonferroni multiple comparisons tests. $^*P<0.05$.

8.5. Discussion

This study demonstrated that *Taz*-KO mice exhibit no differences in glucose tolerance compared to control mice when assessed at 3-months of age. As the mice aged, the glucose tolerance of WT mice diminished, presumably due to progressive age-related increases in adiposity, while the glucose tolerance of *Taz*-KO mice remained unchanged. Despite the divergent aging trend, it could not be concluded that *Taz*-KO mice have an enhanced ability to clear glucose from the peripheral circulation as originally hypothesized. Previously, Cole et al. (2016) reported that *Taz*-KD mice showed ~25% lower fasting plasma insulin levels at all timepoints during GTT with consequent hyperglycemia [54]. Cole et al. (2021) recently elucidated the hyperglycemia of *Taz*-KD mice to be due to impaired insulin secretion during basal (low-glucose conditions). While the pancreatic islets respond comparatively to glucose and demonstrate an equivalent fold-increase in glucose-stimulated insulin secretion, the low starting levels of plasma insulin cannot be

overcome by an equivalent secretion, which results in a downward shift in plasma insulin levels, and ultimately reduced glucose clearance from the blood [85]. During GTT, the disposal of a glucose load is determined by insulin secretion, insulin action, and glucose effectiveness [159]. Therefore, if the impaired basal insulin secretion of the *Taz*-KD mouse is translatable to the *Taz*-KO mouse, it is plausible that *Taz*-KO mice do not exhibit hyperglycemia during GTT due to a counterbalancing increase in insulin action. However, this is speculative as plasma insulin levels were not measured during the GTT of this study, and the role of glucose effectiveness can also not be discredited without further investigation.

Measurements of ITT did not demonstrate enhanced insulin sensitivity in the *Taz*-KO mice, although the ITT is more broadly meant for detecting insulin resistance rather than insulin sensitivity [158]. In that regard, *Taz*-KO mice did not exhibit insulin resistance or changes in insulin responsiveness at any age point, while the response to insulin gradually declined with increasing age in WT mice so that by 12-months of age, WT mice were insulin resistant in comparison to *Taz*-KO mice. The issue of different body composition between genotypes is potentially relevant in this study, just as it was for the indirect calorimetry studies, since the dosage of glucose and insulin for the GTT and ITT, respectively, were administered based on total body weight of mice. In GTT, lean mass (muscle, brain, and liver) is the principal site of glucose disposal [160]. As the body weight increased with age in the WT mice due to increases in adiposity, the 12-month-old WT mice were administered a ~32% higher glucose dose compared to 3-month-old WT mice, despite no major changes in the weights of skeletal muscle, brain, and liver as determined by necropsy, which potentially introduces a bias that could erroneously indicate worsening glucose intolerance. While insulin stimulates glucose uptake in both skeletal muscle and adipose tissue, skeletal muscle is considered the primary user of systemic glucose in an insulin-dependent manner, disposing up to 80% of the glucose load [161]. On the other hand, an ~27% higher insulin dose was administered to the 12-month-old WT mice, which may be masking decreased insulin sensitivity, and may be an explanation for why there weren't significant differences in insulin responsiveness between 3-month-old WT and 12-month-old WT mice. However, obesity is an established risk factor for insulin resistance and glucose intolerance, and the age-associated obesity of the WT mice makes it plausible that they are in the process of developing metabolic syndrome, which is a reported age-related complication in male C57BL/6J mice [162]. At 3-months of age, the difference in both total body weight and LBM (determined by organ weights) between *Taz*-KO mice and controls is ~30%, therefore the comparisons in

glucose tolerance and insulin resistance are robust at this age-point and primarily reflect the influence of genotype. It is interesting to note that *Taz*-KO mice are spared from age-related adiposity and its associated metabolic complications due to their lean phenotype.

A hyperinsulinemic-euglycemic clamp is the “gold standard” for gaining detailed insight into insulin sensitivity and glucose utilization. If the *Taz*-KO mice do need a greater glucose infusion rate to maintain euglycemia in the presence of constant insulin infusion, this would indicate increased insulin sensitivity and would align with findings in human studies, since BTHS patients exhibited a greater glucose disposal rate (normalized to FFM) during a hyperinsulinemic-euglycemic clamp [75].

If increased insulin sensitivity is present, it may be reflective of alternative substrate metabolism remodeling, in which there is greater reliance on glucose metabolism due to impaired fatty acid oxidation. Evidence of disruptions in intermediary mitochondrial metabolism are found in both *Taz*-KD mice and BTHS patients. The cardiac mitochondria of *Taz*-KD mice have reduced levels of Coenzyme A [83], a cofactor needed to activate fatty acids for beta-oxidation, and as discussed previously, reduced physical association of fatty acid oxidation enzymes and respiratory supercomplexes [47], disrupting the efficient channeling of fatty acid oxidation substrates into OXPHOS.

The first metabolic analysis of cardiac tissue from BTHS patients was recently published, which discovered lower expression of the enzyme that catalyzes the initial step of mitochondrial beta-oxidation of long-chain fatty acids, very long chain acyl CoA dehydrogenase (VLCAD), and altered acyl-CoA profile as a distinct metabolic signature of BTHS cardiomyopathy distinguishing this disorder from idiopathic pediatric cardiomyopathy [163]. These findings collectively suggest derangements in mitochondrial fatty acid oxidation, upstream and potentially additive to primary defects at the respiratory chain. Therefore, it can be postulated that if energy production from fatty acids is compromised, there may be increased reliance on glucose metabolism as an energy source, and this would induce enhanced insulin sensitivity due to compensatory metabolic remodeling in cardiac and skeletal muscles.

Interestingly, the liver of BTHS patients exhibited reduced responsiveness to insulin, as hepatic glucose production was suppressed to a lesser extent during the hyperinsulinemic-euglycemic clamp and was higher at baseline than controls before the insulin infusion [75]. Insulin acts on the liver to inhibit gluconeogenesis and fatty acid oxidation [164], although inhibition of these processes may be detrimental in BTHS. Cole et al. (2016) suggested, based on

Taz-KD mouse studies, that if fatty acid oxidation is hindered in cardiac and skeletal muscles, extrahepatic tissues may be shielded from excess fatty acids by the liver functioning as a fatty acid "sink" with increased hepatic fatty acid oxidation [54]. Even when *Taz*-KD mice were challenged with a HFD, they were protected against obesity and ensuing metabolic complications, and resistance to HFD-induced toxicity was attributed to the oxidation of excess fats in the hepatic mitochondria.

Although increased fatty acid oxidation in the liver may impart protection against fat mass accumulation and insulin resistance, the protective capabilities of the liver may eventually be overwhelmed. While overt liver dysfunction is not recognized as a clinical feature of BTHS, liver transaminases were elevated in 19 of 35 (54%) patients tested, and of the four patients that underwent a follow-up liver ultrasound, fatty liver was found in all four patients [165]. This is an important consideration for future research studies. In particular, it highlights that hyperinsulinemic-euglycemic clamping performed with [3-^{3}H]glucose to measure endogenous glucose production in combination with the use of radiolabel ^{14}C-2-deoxyglucose to estimate glucose disposal in different tissues, may reveal important details of the complex metabolic phenotype of *Taz*-KO mice.

Chapter 9: Integrated Discussion and Conclusion

The overarching objective of this thesis was to determine the preclinical validity of the *Taz*-KO mouse as a model for BTHS through functional and physiological characterization, and to identify therapeutic targets. The findings of this thesis are broad but integrate to reveal the bioenergetic profile of the *Taz*-KO mouse. *Taz*-KO mice have increased TEE, as measured by indirect calorimetry, which is interpreted to be driven by increased basal metabolic rate. The increased TEE counteracts and supersedes the sufficient food intake observed in the mice, and thus is a mediator of the low adiposity phenotype of the *Taz*-KO mouse that was revealed through analysis of tissue weights at necropsy.

Tests like GTT and ITT confirm that *Taz*-KO mice are protected from the onset from age-related pathologies such as glucose intolerance and insulin resistance due to their lean phenotype. Glucose intolerance and insulin resistance belong to a list of metabolic disturbances that constitute the disorder metabolic syndrome, which tends to accompany increases in adiposity which were observed in the aging WT mice, but not in aging *Taz*-KO mice.

Increased basal metabolism and substrate oxidation are hypothesized to compensate for the loss of mitochondrial efficiency due to impaired OXPHOS. Uncoupling of oxidation from energy (ATP) production would result in the requirement that a greater amount of substrate is metabolized to generate an equivalent amount of ATP compared to healthy controls. However, the impaired OXPHOS of mitochondria induces an energy deficit in times of increased energy demand such as exercise, and mitochondrial energy production is insufficient to support the working heart and skeletal muscles, profoundly compromising exercise capacity, as was seen in the treadmill endurance test.

The global organ size reduction of *Taz*-KO mice is also a noticeable defect caused by TAZ deficiency and may also be a consequence of a systemic energy deficit. In general, therefore, it seems that the phenotype of *Taz*-KO mice is a result of a systemic bioenergetic deficit, presumably due, at least in part, to dysfunction of the OXPHOS system as a product of disturbed CL remodeling, which is inherent to BTHS.

The validity of a disease model is contingent on the degree of resemblance of the mouse model to the human condition it is intended to model; ideally there will be matches in as many domains as possible, including aetiology, pathophysiology, symptomatology, and response to therapeutic interventions [90]. Since the findings of increased TEE and prevention of age-related

metabolic syndrome are highly relevant to the low adiposity of the *Taz*-KO mouse, it is intriguing that low adiposity is not replicated in BTHS patients, since adult patients have increased absolute fat mass and percent body fat compared to age- and height-matched controls [78]. This could be interpreted to indicate that increased TEE is not a feature of BTHS in humans. As discussed in chapter 5, the increased fat mass in BTHS patients may be drug-induced weight gain due to beta-blocker therapy, which exerts sympathetic antagonism action that works against weight loss [123], or a result of a sedentary lifestyle, which is widespread in North America and even more prevalent among people with chronic diseases and/or disabilities [166].

Another potential incongruity between the *Taz*-KO mouse and BTHS patients was the finding that *Taz*-KO mice had the same levels of spontaneous physical activity as WT mice during indirect calorimetry. This was unexpected, since it gives the impression that the *Taz*-KO mice are not hindered by fatigue. Of note, the fatigue experienced by BTHS patients is reported to be out of proportion to their heart disease and skeletal muscle weakness [167], and it is important to remember that fatigue is not just a physical phenomenon, but is also psychological. Measurement of spontaneous activity is just one definition of fatigue, since fatigue is a multidimensional behaviour, which may be better assessed by sleep disturbances, negative social interactions, altered performance in learned helplessness or anxiety tests, and deficits in attention and memory [168]. The *Taz*-KO mice might conform to the definition of fatigue in terms of a physical phenomenon with a different test, such as video home-cage monitoring to measure daily activity, which has the ability to detect chronic fatigue without interfering with the normal, voluntary activity of mice [169].

Nonetheless, the exercise capacity of *Taz*-KO mice was drastically reduced which indeed does confirm that the mice have severe physical limitations due to cardioskeletal myopathy, replicating the hallmark exercise intolerance of BTHS patients. The increased RER and VCO_2 production of *Taz*-KO mice, evidence of a shift towards higher glucose metabolism, is comparable to the greater reliance on glucose metabolism for energy in BTHS patients [78]. Another similarity between *Taz*-KO mice in the current work and BTHS patients is the reduced lean mass despite comparable size of skeletal frames [78] and high rates of fetal and perinatal lethality [105].

Glucose intolerance and insulin resistance are not reported features of BTHS, and therefore it is worthwhile to note that the *Taz*-KO mouse shares the same profile of present and absent symptoms. With baseline similarities established, the *Taz*-KO mouse may have predictive

value for the course of BTHS, since the natural history of the disease past the fifth decade is unknown, and therefore the aging patient population is facing lifestages that have not yet been clinically examined or described. The shortened lifespan and steeply declining exercise capacity of the *Taz*-KO mouse suggest that skeletal muscle weakness is progressive. Although there were no age-related reductions in the weight of the gastrocnemius and soleus skeletal muscles in the *Taz*-KO mouse, muscle function is lost more rapidly than muscle mass in aging humans, with this discrepancy is probably due to a loss of muscle quality [170]. An analogous deterioration of muscle quality, preceding loss of muscle mass, is likely to be occurring and additive to the effect of aging in the *Taz*-KO mouse, and may be anticipated in the aging process of BTHS patients who report worsening fatigue over time [102]. Furthermore, there was age-related atrophy of the spleen in the *Taz*-KO mouse, which highlights an important area of investigation due to the relevance of the spleen to immune function, which is also compromised in BTHS patients, but as-of-yet poorly characterized in aging.

Therapeutic targets of gene replacement therapy based on gene delivery by recombinant adeno-associated virus in a recent trial with *Taz*-KO mice were the restoration of cardiac and skeletal muscle function, and treatment was able to prevent and reverse cardiomyopathy and mildly improve endurance exercise capacity [9]. Cardiomyopathy is central to BTHS, but unfortunately the University of Waterloo does not have echocardiography equipment needed to evaluate *in vivo* heart function. However, an equally valuable therapeutic target that can be assessed on campus is exercise capacity via treadmill, which is reflective of both cardiac and skeletal muscle function.

While this thesis demonstrated that *Taz*-KO mice have an impaired exercise capacity via a treadmill test to exhaustion, it is proposed that two separate, modified treadmill protocols should be employed in any future studies to assess improvements in response to interventions. The first would be to exercise mice to the point of fatigue, rather than exhaustion, and as such the criterion for ending the treadmill test would shift from mice remaining at the wire brush for 5 consecutive seconds, to mice remaining in a designated “fatigue zone” at the rear of the treadmill lane that encompasses one body length-distance from the wire brush for 5 consecutive seconds [171]. This protocol represents a high-throughput assay that has greater sensitivity to detect improvements of intervention that may not be transformative (i.e., change overall exercise capacity), but therapeutic by delaying onset of physical fatigue. From the patient perspective,

fatigue and muscle weakness are the most impactful symptoms that both children and adults with BTHS wish to improve [167].

The second proposed protocol would be exhaustive treadmill testing using an indirect calorimetry treadmill to measure the peak rate of oxygen consumption (VO_{2peak}) during exercise in mice for cardiometabolic characterization and monitoring. VO_{2peak} in mice is analogous to maximum rate of oxygen consumption (VO_{2max}) during exercise in humans [172], which is an index of aerobic fitness and corresponds to both oxygen delivery, mediated by the cardiovascular system, and oxygen utilization, determined largely by skeletal muscle oxidative capacity [173]. VO_{2max} is an important physiological parameter that is a strong predictor of all-cause and disease-specific mortality [174]. Therefore, an intervention that improves the VO_{2peak} of *Taz*-KO mice has a promising chance of yielding meaningful improvement of the health and wellness of BTHS patients.

Limitations of this thesis must be considered. As already discussed in chapters 5 and 8, the inability to account for body composition differences for the normalization of metabolic parameters and glucose and insulin doses may influence the outcome of results from indirect calorimetry, GTT, and ITT studies. Furthermore, extrapolation of metabolic findings from the mouse to humans may be complicated due to the fact that i) the metabolism of patients may be altered as more than half of patients are taking beta-blocker medication, which decreases sympathetic nervous system activation and thus potentially inhibits lipolysis [123] and decreases insulin sensitivity, thereby negatively affecting glucose metabolism [175], and ii) the metabolism of mice may be altered as mice are housed in conditions of mild to moderate cold stress, and thus must use thermogenesis, spending a considerable amount of energy to maintain core body temperature [176]. It is unfortunate that this thesis was unable to accommodate the study of senescent *Taz*-KO mice, which would require mice to be the minimum age of 18 months. Due to the time constraints of a Master's thesis and breeding difficulty relating to low yields of male *Taz*-KO mice, the maximum age investigated was 12 months, which corresponds to middle-age for mice, but it would have been valuable for the purposes of predicting the course of the BTHS disease to enlist the mice in the phenotypic test battery when senescent changes would be present in all biomarkers [95]. The final limitation of this thesis that I will mention is that the findings are broad, with little mechanistic insight. However, they do provide direction for future studies, and a basis for evaluating the functional benefit of novel therapeutics, which was the major aim of this thesis.

A thorough characterization of the metabolic phenotype of *Taz*-KO will require further investigation. Future studies should decipher tissue-specific mitochondrial function using mitochondrial respirometry analysis to confirm that the elevated whole-body energy expenditure of *Taz*-KO mice is mitochondrial in origin. Basal respiration of cardiac and skeletal muscle mitochondria may be reduced due to combined defects of beta-oxidation and OXPHOS. The colocalization of these two bioenergetic pathways at the IMM renders them susceptible to disruption by L4-CL loss, the key architectural phospholipid of the IMM that is generated by the activity of TAZ in cardiac and skeletal tissue.

Conversely, mitochondrial respiration in the liver may be preserved or increased which may control for the excessive flux of fatty acids from skeletal or cardiac muscle, serving an adaptive purpose by preventing lipotoxic accumulation of triglycerides in extrahepatic tissues. Thus, the interplay between heart, skeletal muscle, liver, and adipose tissue in the regulation of glucose and fatty acid metabolism should be mapped in the *Taz*-KO mouse. It would be of interest to examine whether cardiac and skeletal muscle glucose oxidation is upregulated to compensate for the impaired fatty acid oxidation, while fatty acid oxidation may be elevated in the liver. Hyperinsulinemic-euglycemic clamp studies can be used to determine whether *Taz*-KO mice have increased insulin sensitivity, and thereby greater glucose disposal in insulin-dependent tissues, and whether hepatic gluconeogenesis is upregulated in basal conditions and coordinately downregulated in response to insulin.

Liver-produced glucose and ketone bodies may supply energetic fuel to cardiac and skeletal muscle [177]. Under normal physiological conditions, fatty acids are a crucial source of energy for the heart and skeletal muscle [178, 179]. Metabolic remodeling in BTHS, particularly a shift away from the use of fatty acids as an oxidative fuel to higher glucose metabolism may be maladaptive as glucose metabolism produces less than half the amount of ATP molecules than fatty acid metabolism per gram of substrate oxidized [180], which may precipitate an energy deficit, predisposing the heart and skeletal muscle to functional impairment [78]. Therefore, multiple layers of metabolic pathways will need to be clarified to determine whether systemic metabolic alterations contribute to the disease pathogenesis of BTHS.

It is reasonable to hypothesizes that the metabolic pathways that originate at the IMM will be directly disturbed by TAZ deficiency, which implicates beta-oxidation and OXPHOS. The two pathways are functionally linked by mitochondrial trifunctional protein, which catalyzes three of the four steps of beta-oxidation and is physically associated with the supercomplexes of

OXPHOS to support flux of reducing equivalents generated from beta-oxidation to the ETC [6]. Thus, the utilization of carbohydrate and fat oxidation for energy production is potentially compromised due to their colocalization to the IMM in BTHS. Glycolysis occurs in the cytoplasm of the cell, and thus may be immune to CL disturbances and upregulated to supplement energy needs due to impaired aerobic metabolism. Further work is required to determine the activation of anaerobic glycolysis and role of metabolic inefficiency in BTHS, especially since BTHS patients have higher basal glucose utilization compared to controls [7]. The increased glucose utilization may be enforced by a greater reliance on anerobic glycolysis, circumventing mitochondrial oxidative metabolism of glucose. Skeletal muscle fiber type has been examined through non-invasive 31P-nuclear magnetic resonance spectroscopy in patients with BTHS, which revealed a higher content of Type 2 (fast-twitch) and a smaller fraction of Type 1 (slow-twitch) oxidative fibers, reflecting muscle metabolism remodeling that could result from impaired fat oxidation [8]. Reflecting this, RER is higher in BTHS patients at submaximal exercise, indicating anaerobic energy supplementation at very low workloads [9].

In conclusion, this thesis contributed to characterizing the phenotype of the *Taz*-KO mouse model of BTHS across three age points, and found commonalities while confirming a lack of significant differences with the human condition. Therefore, this mouse model provides a particularly important resource for investigations into the pathophysiology and treatment of BTHS.

References

1. Clarke, S.L., et al., *Barth syndrome.* Orphanet J Rare Dis, 2013. **8**: p. 23.
2. Vreken, P., et al., *Defective remodeling of cardiolipin and phosphatidylglycerol in Barth syndrome.* Biochem Biophys Res Commun, 2000. **279**(2): p. 378-82.
3. Rigaud, C., et al., *Natural history of Barth syndrome: a national cohort study of 22 patients.* Orphanet J Rare Dis, 2013. **8**: p. 70.
4. Huhta, J.C., H.H. Pomerance, and E.G. Barness, *Clinicopathologic conference: Barth Syndrome.* Fetal Pediatr Pathol, 2005. **24**(4-5): p. 239-54.
5. Barth P G, S.H.R., Berden J A, Van der Klei-Van Moorsel J M, Luyt-Houwen I E, Van 't Veer-Korthof E T, Van der Harten J J, Sobotka-Plojhar M A., *An X-linked mitochondrial disease affecting cardiac muscle, skeletal muscle and neutrophil leucocytes.* J Neurol Sci., 1983. **62**(1-3): p. 327-55.
6. Mazar, I., et al., *Understanding the life experience of Barth syndrome from the perspective of adults: a qualitative one-on-one interview study.* Orphanet J Rare Dis, 2019. **14**(1): p. 243.
7. Ronvelia, D., et al., *Intrafamilial variability for novel TAZ gene mutation: Barth syndrome with dilated cardiomyopathy and heart failure in an infant and left ventricular noncompaction in his great-uncle.* Mol Genet Metab, 2012. **107**(3): p. 428-32.
8. Thompson, W.R., et al., *New targets for monitoring and therapy in Barth syndrome.* Genet Med, 2016. **18**(10): p. 1001-10.
9. Wang, S., et al., *AAV Gene Therapy Prevents and Reverses Heart Failure in a Murine Knockout Model of Barth Syndrome.* Circ Res, 2020. **126**(8): p. 1024-1039.
10. Barth, P.G., et al., *X-linked cardioskeletal myopathy and neutropenia (Barth syndrome): an update.* Am J Med Genet A, 2004. **126A**(4): p. 349-54.
11. Spencer C T, B.R.M., Day J, Gonzalez I L, Colan S D, Reid Thompson W, Berthy J, Redfearn S P, Byrne B J., *Cardiac and clinical phenotype in Barth syndrome.* Pediatrics., 2006. **118**(2): p. 337-46.
12. Miller, P.C., et al., *A Bayesian Analysis to Determine the Prevalence of Barth Syndrome in the Pediatric Population.* J Pediatr, 2020. **217**: p. 139-144.
13. Storch, E.A., et al., *Psychosocial Functioning in Youth with Barth Syndrome.* Child Health Care, 2009. **38**(2): p. 137-156.
14. Houtkooper, R.H. and F.M. Vaz, *Cardiolipin, the heart of mitochondrial metabolism.* Cell Mol Life Sci, 2008. **65**(16): p. 2493-506.
15. Sparagna, G.C., et al., *Loss of cardiac tetralinoleoyl cardiolipin in human and experimental heart failure.* J Lipid Res, 2007. **48**(7): p. 1559-70.
16. Guan, Z.Z., et al., *Content and fatty acid composition of cardiolipin in the brain of patients with Alzheimer's disease.* Neurochem Int, 1994. **25**(3): p. 295-300.
17. Koshkin, V. and M.L. Greenberg, *Cardiolipin prevents rate-dependent uncoupling and provides osmotic stability in yeast mitochondria.* Biochem J, 2002. **364**(Pt 1): p. 317-22.
18. Zhang, M., E. Mileykovskaya, and W. Dowhan, *Gluing the respiratory chain together. Cardiolipin is required for supercomplex formation in the inner mitochondrial membrane.* J Biol Chem, 2002. **277**(46): p. 43553-6.
19. Dudek, J., M. Hartmann, and P. Rehling, *The role of mitochondrial cardiolipin in heart function and its implication in cardiac disease.* Biochim Biophys Acta Mol Basis Dis, 2019. **1865**(4): p. 810-821.

20. Schlame, M., *Cardiolipin remodeling and the function of tafazzin.* Biochim Biophys Acta, 2013. **1831**(3): p. 582-8.
21. Gonzalvez, F. and E. Gottlieb, *Cardiolipin: setting the beat of apoptosis.* Apoptosis, 2007. **12**(5): p. 877-85.
22. Schlame, M., *Cardiolipin synthesis for the assembly of bacterial and mitochondrial membranes.* J Lipid Res, 2008. **49**(8): p. 1607-20.
23. Saric, A., et al., *Barth Syndrome: From Mitochondrial Dysfunctions Associated with Aberrant Production of Reactive Oxygen Species to Pluripotent Stem Cell Studies.* Front Genet, 2015. **6**: p. 359.
24. Ikon, N. and R.O. Ryan, *Cardiolipin and mitochondrial cristae organization.* Biochim Biophys Acta Biomembr, 2017. **1859**(6): p. 1156-1163.
25. Mejia, E.M., L.K. Cole, and G.M. Hatch, *Cardiolipin metabolism and the role it plays in heart failure and mitochondrial supercomplex formation.* Cardiovasc Hematol Disord Drug Targets, 2014. **14**(2): p. 98-106.
26. Schlame, M., et al., *Molecular symmetry in mitochondrial cardiolipins.* Chem Phys Lipids, 2005. **138**(1-2): p. 38-49.
27. van Werkhoven, M.A., et al., *Monolysocardiolipin in cultured fibroblasts is a sensitive and specific marker for Barth Syndrome.* J Lipid Res, 2006. **47**(10): p. 2346-51.
28. Agarwal, P., et al., *Phosphokinome Analysis of Barth Syndrome Lymphoblasts Identify Novel Targets in the Pathophysiology of the Disease.* Int J Mol Sci, 2018. **19**(7).
29. Lou, W., et al., *Loss of tafazzin results in decreased myoblast differentiation in C2C12 cells: A myoblast model of Barth syndrome and cardiolipin deficiency.* Biochim Biophys Acta Mol Cell Biol Lipids, 2018. **1863**(8): p. 857-865.
30. Kulik, W., et al., *Bloodspot assay using HPLC-tandem mass spectrometry for detection of Barth syndrome.* Clin Chem, 2008. **54**(2): p. 371-8.
31. Houtkooper, R.H., et al., *Cardiolipin and monolysocardiolipin analysis in fibroblasts, lymphocytes, and tissues using high-performance liquid chromatography-mass spectrometry as a diagnostic test for Barth syndrome.* Anal Biochem, 2009. **387**(2): p. 230-7.
32. Monteiro, J.P., P.J. Oliveira, and A.S. Jurado, *Mitochondrial membrane lipid remodeling in pathophysiology: a new target for diet and therapeutic interventions.* Prog Lipid Res, 2013. **52**(4): p. 513-28.
33. Mejia, E.M. and G.M. Hatch, *Mitochondrial phospholipids: role in mitochondrial function.* Journal of Bioenergetics and Biomembranes, 2016. **48**(2): p. 99-112.
34. Schlame, M., et al., *The physical state of lipid substrates provides transacylation specificity for tafazzin.* Nature Chemical Biology, 2012. **8**(10): p. 862-869.
35. Acehan, D., et al., *Comparison of lymphoblast mitochondria from normal subjects and patients with Barth syndrome using electron microscopic tomography.* Laboratory Investigation, 2007. **87**(1): p. 40-48.
36. Xu, Y., et al., *A Drosophila model of Barth syndrome.* Proceedings of the National Academy of Sciences of the United States of America, 2006. **103**(31): p. 11584-11588.
37. Yadav, P.K. and R. Rajasekharan, *Misregulation of a DDHD Domain-containing Lipase Causes Mitochondrial Dysfunction in Yeast.* J Biol Chem, 2016. **291**(35): p. 18562-81.
38. Falabella, M., et al., *Cardiolipin, Mitochondria, and Neurological Disease.* Trends Endocrinol Metab, 2021. **32**(4): p. 224-237.
39. Khuchua, Z., et al., *A zebrafish model of human Barth syndrome reveals the essential role of tafazzin in cardiac development and function.* Circ Res, 2006. **99**(2): p. 201-8.

40. Ye, C., et al., *Deletion of the cardiolipin-specific phospholipase Cld1 rescues growth and life span defects in the tafazzin mutant: implications for Barth syndrome.* J Biol Chem, 2014. **289**(6): p. 3114-25.
41. Baile, M.G., et al., *Unremodeled and remodeled cardiolipin are functionally indistinguishable in yeast.* J Biol Chem, 2014. **289**(3): p. 1768-78.
42. Malhotra, A., et al., *Role of calcium-independent phospholipase A2 in the pathogenesis of Barth syndrome.* Proc Natl Acad Sci U S A, 2009. **106**(7): p. 2337-41.
43. Acehan, D., et al., *Cardiac and skeletal muscle defects in a mouse model of human Barth syndrome.* J Biol Chem, 2011. **286**(2): p. 899-908.
44. Soustek, M.S., et al., *Characterization of a transgenic short hairpin RNA-induced murine model of Tafazzin deficiency.* Hum Gene Ther, 2011. **22**(7): p. 865-71.
45. Powers, C., et al., *Diminished Exercise Capacity and Mitochondrial bc1 Complex Deficiency in Tafazzin-Knockdown Mice.* Front Physiol, 2013. **4**: p. 74.
46. Adès L C, G.A.K., Wilson M J, LathamM, Partington M W, Mulley J C, Nelson J, Lui K, Sillence D O., *Barth syndrome: clinical features and confirmation of gene localisation to distal Xq28.* Am J Med Genet., 1993. **45**(3): p. 327-34.
47. Huang, Y., et al., *The PPAR pan-agonist bezafibrate ameliorates cardiomyopathy in a mouse model of Barth syndrome.* Orphanet J Rare Dis, 2017. **12**(1): p. 49.
48. Ikon, N., et al., *Evaluation of cardiolipin nanodisks as lipid replacement therapy for Barth syndrome.* J Biomed Res, 2018. **32**(2): p. 107-112.
49. Johnson, J.M., et al., *Targeted overexpression of catalase to mitochondria does not prevent cardioskeletal myopathy in Barth syndrome.* J Mol Cell Cardiol, 2018. **121**: p. 94-102.
50. Schafer, C., et al., *The Effects of PPAR Stimulation on Cardiac Metabolic Pathways in Barth Syndrome Mice.* Front Pharmacol, 2018. **9**: p. 318.
51. Suzuki-Hatano, S., et al., *AAV-Mediated TAZ Gene Replacement Restores Mitochondrial and Cardioskeletal Function in Barth Syndrome.* Hum Gene Ther, 2019. **30**(2): p. 139-154.
52. Ren, M., et al., *A critical appraisal of the tafazzin knockdown mouse model of Barth syndrome: what have we learned about pathogenesis and potential treatments?* Am J Physiol Heart Circ Physiol, 2019. **317**(6): p. H1183-H1193.
53. Cadalbert, L.C., et al., *Mouse Tafazzin Is Required for Male Germ Cell Meiosis and Spermatogenesis.* PLoS One, 2015. **10**(6): p. e0131066.
54. Cole, L.K., et al., *Impaired Cardiolipin Biosynthesis Prevents Hepatic Steatosis and Diet-Induced Obesity.* Diabetes, 2016. **65**(11): p. 3289-3300.
55. Goncalves, R.L.S., et al., *Cardiolipin deficiency in Barth syndrome is not associated with increased superoxide/H(2) O(2) production in heart and skeletal muscle mitochondria.* FEBS Lett, 2021. **595**(3): p. 415-432.
56. Whited, K., et al., *Seven functional classes of Barth syndrome mutation.* Hum Mol Genet, 2013. **22**(3): p. 483-92.
57. Dudek, J., et al., *Cardiac-specific succinate dehydrogenase deficiency in Barth syndrome.* EMBO Mol Med, 2016. **8**(2): p. 139-54.
58. Szczepanek, K., et al., *Acquired deficiency of tafazzin in the adult heart: Impact on mitochondrial function and response to cardiac injury.* Biochim Biophys Acta, 2016. **1861**(4): p. 294-300.
59. Luger, A.L., et al., *Doxycycline Impairs Mitochondrial Function and Protects Human Glioma Cells from Hypoxia-Induced Cell Death: Implications of Using Tet-Inducible Systems.* Int J Mol Sci, 2018. **19**(5).
60. Wust, R.C.I., et al., *The Antibiotic Doxycycline Impairs Cardiac Mitochondrial and Contractile Function.* Int J Mol Sci, 2021. **22**(8).

61. Kang, S.L., et al., *Clinical Characteristics and Outcomes of Cardiomyopathy in Barth Syndrome: The UK Experience.* Pediatr Cardiol, 2016. **37**(1): p. 167-76.
62. Bleyl, S.B., et al., *Neonatal, lethal noncompaction of the left ventricular myocardium is allelic with Barth syndrome.* Am J Hum Genet, 1997. **61**(4): p. 868-72.
63. Spencer, C.T., et al., *Ventricular arrhythmia in the X-linked cardiomyopathy Barth syndrome.* Pediatr Cardiol, 2005. **26**(5): p. 632-7.
64. Bissler, J.J., et al., *Infantile dilated X-linked cardiomyopathy, G4.5 mutations, altered lipids, and ultrastructural malformations of mitochondria in heart, liver, and skeletal muscle.* Lab Invest, 2002. **82**(3): p. 335-44.
65. Mangat, J., et al., *Successful cardiac transplantation in Barth syndrome--single-centre experience of four patients.* Pediatr Transplant, 2007. **11**(3): p. 327-31.
66. Roberts, A.E., et al., *The Barth Syndrome Registry: distinguishing disease characteristics and growth data from a longitudinal study.* Am J Med Genet A, 2012. **158a**(11): p. 2726-32.
67. Soustek, M.S., et al., *Endurance training ameliorates complex 3 deficiency in a mouse model of Barth syndrome.* J Inherit Metab Dis, 2015. **38**(5): p. 915-22.
68. Kim, J., et al., *Cardiac mitochondrial structure and function in tafazzin-knockdown mice.* Mitochondrion, 2018. **43**: p. 53-62.
69. Spencer, C.T., et al., *Impaired cardiac reserve and severely diminished skeletal muscle O(2) utilization mediate exercise intolerance in Barth syndrome.* Am J Physiol Heart Circ Physiol, 2011. **301**(5): p. H2122-9.
70. Bittel, A.J., et al., *Reduced Muscle Strength in Barth Syndrome May Be Improved by Resistance Exercise Training: A Pilot Study.* JIMD Rep, 2018. **41**: p. 63-72.
71. Barth, P.G., et al., *X-linked cardioskeletal myopathy and neutropenia (Barth syndrome) (MIM 302060).* J Inherit Metab Dis, 1999. **22**(4): p. 555-67.
72. Neustein, H.B., et al., *An X-linked recessive cardiomyopathy with abnormal mitochondria.* Pediatrics, 1979. **64**(1): p. 24-9.
73. Kelley, R.I., et al., *X-linked dilated cardiomyopathy with neutropenia, growth retardation, and 3-methylglutaconic aciduria.* J Pediatr, 1991. **119**(5): p. 738-47.
74. Takeda, A., et al., *Barth syndrome diagnosed in the subclinical stage of heart failure based on the presence of lipid storage myopathy and isolated noncompaction of the ventricular myocardium.* Eur J Pediatr, 2011. **170**(11): p. 1481-4.
75. Cade, W.T., et al., *Substrate metabolism during basal and hyperinsulinemic conditions in adolescents and young-adults with Barth syndrome.* J Inherit Metab Dis, 2013. **36**(1): p. 91-101.
76. Bashir, A., et al., *Impaired cardiac and skeletal muscle bioenergetics in children, adolescents, and young adults with Barth syndrome.* Physiol Rep, 2017. **5**(3).
77. Cade, W.T., et al., *Peak oxygen uptake (VO2peak) across childhood, adolescence and young adulthood in Barth syndrome: Data from cross-sectional and longitudinal studies.* PLoS One, 2018. **13**(5): p. e0197776.
78. Cade, W.T., et al., *Blunted fat oxidation upon submaximal exercise is partially compensated by enhanced glucose metabolism in children, adolescents, and young adults with Barth syndrome.* J Inherit Metab Dis, 2019. **42**(3): p. 480-493.
79. Cade, W.T., et al., *Myocardial glucose and fatty acid metabolism is altered and associated with lower cardiac function in young adults with Barth syndrome.* J Nucl Cardiol, 2021. **28**(4): p. 1649-1659.
80. Vernon, H.J., et al., *Clinical laboratory studies in Barth Syndrome.* Mol Genet Metab, 2014. **112**(2): p. 143-7.

81. Goncalves, R.L.S., et al., *Cardiolipin deficiency in Barth syndrome is not associated with increased superoxide/H2 O2 production in heart and skeletal muscle mitochondria.* FEBS Lett, 2021. **595**(3): p. 415-432.
82. Kiebish, M.A., et al., *Dysfunctional cardiac mitochondrial bioenergetic, lipidomic, and signaling in a murine model of Barth syndrome.* J Lipid Res, 2013. **54**(5): p. 1312-25.
83. Le, C.H., et al., *Tafazzin deficiency impairs CoA-dependent oxidative metabolism in cardiac mitochondria.* J Biol Chem, 2020. **295**(35): p. 12485-12497.
84. Greenwell, A.A., et al., *Barth syndrome-related cardiomyopathy is associated with a reduction in myocardial glucose oxidation.* Am J Physiol Heart Circ Physiol, 2021. **320**(6): p. H2255-H2269.
85. Cole, L.K., et al., *Tafazzin Deficiency Reduces Basal Insulin Secretion and Mitochondrial Function in Pancreatic Islets From Male Mice.* Endocrinology, 2021. **162**(7).
86. Zhu, S., et al., *Cardiolipin Remodeling Defects Impair Mitochondrial Architecture and Function in a Murine Model of Barth Syndrome Cardiomyopathy.* Circulation: Heart Failure, 2021. **14**(6): p. e008289.
87. Liu, X., et al., *Increased Reactive Oxygen Species-Mediated Ca^{2+}/Calmodulin-Dependent Protein Kinase II Activation Contributes to Calcium Handling Abnormalities and Impaired Contraction in Barth Syndrome.* Circulation, 2021. **143**(19): p. 1894-1911.
88. Corrado, M., et al., *Dynamic Cardiolipin Synthesis Is Required for CD8(+) T Cell Immunity.* Cell metabolism, 2020. **32**(6): p. 981-995.e7.
89. Sohn, J., et al., *A new murine model of Barth Syndrome neutropenia links TAFAZZIN deficiency to increased ER stress induced apoptosis.* Blood Advances, 2022.
90. Varga, O.E., et al., *Validating animal models for preclinical research: a scientific and ethical discussion.* Altern Lab Anim, 2010. **38**(3): p. 245-8.
91. Perrin, S., *Preclinical research: Make mouse studies work.* Nature, 2014. **507**(7493): p. 423-425.
92. Denayer, T., T. Stöhr, and M. Van Roy, *Animal models in translational medicine: Validation and prediction.* New Horizons in Translational Medicine, 2014. **2**(1): p. 5-11.
93. Van Norman, G.A., *Limitations of Animal Studies for Predicting Toxicity in Clinical Trials: Is it Time to Rethink Our Current Approach?* JACC: Basic to Translational Science, 2019. **4**(7): p. 845-854.
94. Ren, M., et al., *Extramitochondrial cardiolipin suggests a novel function of mitochondria in spermatogenesis.* Journal of Cell Biology, 2019. **218**(5): p. 1491-1502.
95. Dutta, S. and P. Sengupta, *Men and mice: Relating their ages.* Life Sci, 2016. **152**: p. 244-8.
96. Green, M.R. and J. Sambrook, *Molecular Cloning: A Laboratory Manual.* . 2012, New York: Cold Spring Harbor Laboratory Press.
97. Schlame, M., et al., *Deficiency of tetralinoleoyl-cardiolipin in Barth syndrome.* Ann Neurol, 2002. **51**(5): p. 634-7.
98. Bione, S., et al., *A novel X-linked gene, G4.5. is responsible for Barth syndrome.* Nat Genet, 1996. **12**(4): p. 385-9.
99. Houtkooper, R.H., et al., *The enigmatic role of tafazzin in cardiolipin metabolism.* Biochim Biophys Acta, 2009. **1788**(10): p. 2003-14.
100. Bissler, J.J., et al., *Infantile Dilated X-Linked Cardiomyopathy, G4.5 Mutations, Altered Lipids, and Ultrastructural Malformations of Mitochondria in Heart, Liver, and Skeletal Muscle.* Laboratory Investigation, 2002. **82**(3): p. 335-344.
101. Cole, L.K., et al., *Aberrant cardiolipin metabolism is associated with cognitive deficiency and hippocampal alteration in tafazzin knockdown mice.* Biochim Biophys Acta Mol Basis Dis, 2018. **1864**(10): p. 3353-3367.

102. Mazar, I., et al., *Understanding the life experience of Barth syndrome from the perspective of adults: a qualitative one-on-one interview study.* Orphanet Journal of Rare Diseases, 2019. **14**(1): p. 243.
103. Yin, F.C., et al., *Use of tibial length to quantify cardiac hypertrophy: application in the aging rat.* Am J Physiol, 1982. **243**(6): p. H941-7.
104. Ladiges, W., et al., *Lifespan extension in genetically modified mice.* Aging Cell, 2009. **8**(4): p. 346-52.
105. Steward, C.G., et al., *Barth syndrome: an X-linked cause of fetal cardiomyopathy and stillbirth.* Prenatal diagnosis, 2010. **30**(10): p. 970-976.
106. Phoon, C.K., et al., *Tafazzin knockdown in mice leads to a developmental cardiomyopathy with early diastolic dysfunction preceding myocardial noncompaction.* J Am Heart Assoc, 2012. **1**(2).
107. Reynolds, S., *Successful management of Barth syndrome: a systematic review highlighting the importance of a flexible and multidisciplinary approach.* Journal of multidisciplinary healthcare, 2015. **8**: p. 345-358.
108. Rigaud, C., et al., *Natural history of Barth syndrome: a national cohort study of 22 patients.* Orphanet Journal of Rare Diseases, 2013. **8**(1): p. 70.
109. Chowdhury, S., et al., *Longitudinal Observational Study of Cardiac Outcome Risk Factor Prediction in Children, Adolescents, and Adults with Barth Syndrome.* Pediatr Cardiol, 2022.
110. Wilson, L.D., et al., *Higher IL-6 and IL6:IGF Ratio in Patients with Barth Syndrome.* J Inflamm (Lond), 2012. **9**(1): p. 25.
111. Al-Shanti, N. and C.E. Stewart, *Inhibitory effects of IL-6 on IGF-1 activity in skeletal myoblasts could be mediated by the activation of SOCS-3.* J Cell Biochem, 2012. **113**(3): p. 923-33.
112. Yakar, S. and O. Isaksson, *Regulation of skeletal growth and mineral acquisition by the GH/IGF-1 axis: Lessons from mouse models.* Growth Horm IGF Res, 2016. **28**: p. 26-42.
113. Stratikopoulos, E., et al., *The hormonal action of IGF1 in postnatal mouse growth.* Proc Natl Acad Sci U S A, 2008. **105**(49): p. 19378-83.
114. Lorenzini, A., et al., *Mice producing reduced levels of insulin-like growth factor type 1 display an increase in maximum, but not mean, life span.* J Gerontol A Biol Sci Med Sci, 2014. **69**(4): p. 410-9.
115. Yakar, S. and M.L. Adamo, *Insulin-like growth factor 1 physiology: lessons from mouse models.* Endocrinol Metab Clin North Am, 2012. **41**(2): p. 231-47, v.
116. McClave, S.A. and H.L. Snider, *Dissecting the energy needs of the body.* Curr Opin Clin Nutr Metab Care, 2001. **4**(2): p. 143-7.
117. Lessard-Beaudoin, M., et al., *Characterization of age-associated changes in peripheral organ and brain region weights in C57BL/6 mice.* Exp Gerontol, 2015. **63**: p. 27-34.
118. Bronte, V. and M.J. Pittet, *The spleen in local and systemic regulation of immunity.* Immunity, 2013. **39**(5): p. 806-818.
119. Turner, V.M. and N.A. Mabbott, *Influence of ageing on the microarchitecture of the spleen and lymph nodes.* Biogerontology, 2017. **18**(5): p. 723-738.
120. Zegallai, H.M., et al., *Tafazzin deficiency impairs mitochondrial metabolism and function of lipopolysaccharide activated B lymphocytes in mice.* Faseb j, 2021. **35**(12): p. e22023.
121. Cadalbert, L.C., et al., *Mouse Tafazzin Is Required for Male Germ Cell Meiosis and Spermatogenesis.* PloS one, 2015. **10**(6): p. e0131066-e0131066.
122. Hastings, R., et al., *Dysmorphology of Barth syndrome.* Clin Dysmorphol, 2009. **18**(4): p. 185-7.
123. Cleroux, J., et al., *Effects of beta 1- vs. beta 1 + beta 2-blockade on exercise endurance and muscle metabolism in humans.* J Appl Physiol (1985), 1989. **66**(2): p. 548-54.

124. Reitman, M.L., *Metabolic lessons from genetically lean mice.* Annu Rev Nutr, 2002. **22**: p. 459-82.
125. Christodoulou, J., et al., *Barth syndrome: clinical observations and genetic linkage studies.* Am J Med Genet, 1994. **50**(3): p. 255-64.
126. Finsterer, J., *Central nervous system manifestations of mitochondrial disorders.* Acta Neurol Scand, 2006. **114**(4): p. 217-38.
127. Cheng, H., et al., *Shotgun lipidomics reveals the temporally dependent, highly diversified cardiolipin profile in the mammalian brain: temporally coordinated postnatal diversification of cardiolipin molecular species with neuronal remodeling.* Biochemistry, 2008. **47**(21): p. 5869-80.
128. Mazzocco, M.M., A.E. Henry, and R.I. Kelly, *Barth syndrome is associated with a cognitive phenotype.* J Dev Behav Pediatr, 2007. **28**(1): p. 22-30.
129. Tschöp, M.H., et al., *A guide to analysis of mouse energy metabolism.* Nature Methods, 2012. **9**(1): p. 57-63.
130. Even, P.C. and N.A. Nadkarni, *Indirect calorimetry in laboratory mice and rats: principles, practical considerations, interpretation and perspectives.* Am J Physiol Regul Integr Comp Physiol, 2012. **303**(5): p. R459-76.
131. Elia, M., *Organ and Tissue Contribution to Metabolic Rate*, in *Energy Metabolism: Tissue Determinants and Cellular Corollaries*, J.M.T. Kinney, H. N., Editor. 1992, Raven Press: New York. p. 61 - 79.
132. Kaiyala, K.J., et al., *Identification of body fat mass as a major determinant of metabolic rate in mice.* Diabetes, 2010. **59**(7): p. 1657-66.
133. van den Berg, S.A., et al., *High levels of whole-body energy expenditure are associated with a lower coupling of skeletal muscle mitochondria in C57Bl/6 mice.* Metabolism, 2010. **59**(11): p. 1612-8.
134. Wang, G., et al., *Modeling the mitochondrial cardiomyopathy of Barth syndrome with induced pluripotent stem cell and heart-on-chip technologies.* Nat Med, 2014. **20**(6): p. 616-23.
135. Speakman, J.R., et al., *Uncoupled and surviving: individual mice with high metabolism have greater mitochondrial uncoupling and live longer.* Aging Cell, 2004. **3**(3): p. 87-95.
136. Acehan, D., et al., *Cardiac and skeletal muscle defects in a mouse model of human Barth syndrome.* The Journal of biological chemistry, 2011. **286**(2): p. 899-908.
137. Yamazaki, T., et al., *A novel method for measuring diet-induced thermogenesis in mice.* MethodsX, 2019. **6**: p. 1950-1956.
138. Calcagno, M., et al., *The Thermic Effect of Food: A Review.* J Am Coll Nutr, 2019. **38**(6): p. 547-551.
139. Cannon, B. and J. Nedergaard, *Nonshivering thermogenesis and its adequate measurement in metabolic studies.* J Exp Biol, 2011. **214**(Pt 2): p. 242-53.
140. Arch, J.R., et al., *Some mathematical and technical issues in the measurement and interpretation of open-circuit indirect calorimetry in small animals.* Int J Obes (Lond), 2006. **30**(9): p. 1322-31.
141. Hornby, B., et al., *Functional exercise capacity, strength, balance and motion reaction time in Barth syndrome.* Orphanet Journal of Rare Diseases, 2019. **14**(1): p. 37.
142. Taylor, D., et al., *Characterization of pain in patients with Barth syndrome.* Children's Health Care, 2016. **45**(2): p. 192-203.
143. Bashir, A., et al., *Impaired cardiac and skeletal muscle bioenergetics in children, adolescents, and young adults with Barth syndrome.* Physiological reports, 2017. **5**(3): p. e13130.
144. Powers, C., et al., *Diminished Exercise Capacity and Mitochondrial bc1 Complex Deficiency in Tafazzin-Knockdown Mice.* Frontiers in physiology, 2013. **4**: p. 74-74.

145. Schafer, C., et al., *The Effects of PPAR Stimulation on Cardiac Metabolic Pathways in Barth Syndrome Mice.* Frontiers in Pharmacology, 2018. **9**.
146. Gaitanos, G.C., et al., *Human muscle metabolism during intermittent maximal exercise.* J Appl Physiol (1985), 1993. **75**(2): p. 712-9.
147. Hargreaves, M. and L.L. Spriet, *Skeletal muscle energy metabolism during exercise.* Nature Metabolism, 2020. **2**(9): p. 817-828.
148. Spencer, C.T., et al., *Impaired cardiac reserve and severely diminished skeletal muscle O_2 utilization mediate exercise intolerance in Barth syndrome.* Am J Physiol Heart Circ Physiol, 2011. **301**(5): p. H2122-9.
149. Wang, Y., et al., *Evidence for physical association of mitochondrial fatty acid oxidation and oxidative phosphorylation complexes.* J Biol Chem, 2010. **285**(39): p. 29834-41.
150. Dobson, G.P., E. Yamamoto, and P.W. Hochachka, *Phosphofructokinase control in muscle: nature and reversal of pH-dependent ATP inhibition.* American Journal of Physiology-Regulatory, Integrative and Comparative Physiology, 1986. **250**(1): p. R71-R76.
151. Wan, J.-j., et al., *Muscle fatigue: general understanding and treatment.* Experimental & Molecular Medicine, 2017. **49**(10): p. e384-e384.
152. Westerblad, H., D.G. Allen, and J. Lännergren, *Muscle Fatigue: Lactic Acid or Inorganic Phosphate the Major Cause?* Physiology, 2002. **17**(1): p. 17-21.
153. Ghosh, S., et al., *An essential role for cardiolipin in the stability and function of the mitochondrial calcium uniporter.* Proceedings of the National Academy of Sciences, 2020. **117**(28): p. 16383-16390.
154. Braun, J.L., et al., *SERCA2a tyrosine nitration coincides with impairments in maximal SERCA activity in left ventricles from tafazzin-deficient mice.* Physiol Rep, 2019. **7**(16): p. e14215.
155. Flurkey, K., J. M. Currer, and D.E. Harrison, *Chapter 20 - Mouse Models in Aging Research*, in *The Mouse in Biomedical Research (Second Edition)*, J.G. Fox, et al., Editors. 2007, Academic Press: Burlington. p. 637-672.
156. Rando, T.A. and T. Wyss-Coray, *Asynchronous, contagious and digital aging.* Nature Aging, 2021. **1**(1): p. 29-35.
157. Kim, J.-a., Y. Wei, and J.R. Sowers, *Role of Mitochondrial Dysfunction in Insulin Resistance.* Circulation Research, 2008. **102**(4): p. 401-414.
158. Alquier, T. and V. Poitout, *Considerations and guidelines for mouse metabolic phenotyping in diabetes research.* Diabetologia, 2018. **61**(3): p. 526-538.
159. Ayala, J.E., et al., *Standard operating procedures for describing and performing metabolic tests of glucose homeostasis in mice.* Dis Model Mech, 2010. **3**(9-10): p. 525-34.
160. Honka, M.-J., et al., *Insulin-stimulated glucose uptake in skeletal muscle, adipose tissue and liver: a positron emission tomography study.* European journal of endocrinology, 2018. **178**(5): p. 523-531.
161. DeFronzo, R.A. and D. Tripathy, *Skeletal muscle insulin resistance is the primary defect in type 2 diabetes.* Diabetes care, 2009. **32 Suppl 2**(Suppl 2): p. S157-S163.
162. Reynolds, T.H., et al., *The impact of age and sex on body composition and glucose sensitivity in C57BL/6J mice.* Physiological reports, 2019. **7**(3): p. e13995-e13995.
163. Chatfield, K.C., et al., *Long-chain fatty acid oxidation and respiratory complex I deficiencies distinguish Barth Syndrome from idiopathic pediatric cardiomyopathy.* J Inherit Metab Dis, 2022. **45**(1): p. 111-124.
164. Meshkani, R. and K. Adeli, *Hepatic insulin resistance, metabolic syndrome and cardiovascular disease.* Clin Biochem, 2009. **42**(13-14): p. 1331-46.
165. Taylor, C., et al., *Clinical presentation and natural history of Barth Syndrome: An overview.* J Inherit Metab Dis, 2022. **45**(1): p. 7-16.

166. Carroll, D.D., et al., *Vital signs: disability and physical activity--United States, 2009-2012.* MMWR Morb Mortal Wkly Rep, 2014. **63**(18): p. 407-13.
167. Gwaltney, C., et al., *Development and content validity of the Barth Syndrome Symptom Assessment (BTHS-SA) for adolescents and adults.* Orphanet J Rare Dis, 2021. **16**(1): p. 264.
168. Harrington, M.E., *Neurobiological studies of fatigue.* Prog Neurobiol, 2012. **99**(2): p. 93-105.
169. Wolff, B.S., S.A. Raheem, and L.N. Saligan, *Comparing passive measures of fatigue-like behavior in mice.* Scientific Reports, 2018. **8**(1): p. 14238.
170. McGregor, R.A., D. Cameron-Smith, and S.D. Poppitt, *It is not just muscle mass: a review of muscle quality, composition and metabolism during ageing as determinants of muscle function and mobility in later life.* Longevity & healthspan, 2014. **3**(1): p. 9-9.
171. Dougherty, J.P., D.A. Springer, and M.C. Gershengorn, *The Treadmill Fatigue Test: A Simple, High-throughput Assay of Fatigue-like Behavior for the Mouse.* J Vis Exp, 2016(111).
172. Ayachi, M., et al., *Validation of a Ramp Running Protocol for Determination of the True VO2max in Mice.* Front Physiol, 2016. **7**: p. 372.
173. Strasser, B. and M. Burtscher, *Survival of the fittest: VO(2)max, a key predictor of longevity?* Front Biosci (Landmark Ed), 2018. **23**(8): p. 1505-1516.
174. Harber, M.P., et al., *Impact of Cardiorespiratory Fitness on All-Cause and Disease-Specific Mortality: Advances Since 2009.* Prog Cardiovasc Dis, 2017. **60**(1): p. 11-20.
175. Fonseca, V.A., *Effects of beta-blockers on glucose and lipid metabolism.* Curr Med Res Opin, 2010. **26**(3): p. 615-29.
176. Neff, E.P., *A point on thermoneutrality for mice.* Lab Animal, 2020. **49**(6): p. 169-169.
177. Rui, L., *Energy metabolism in the liver.* Comprehensive Physiology, 2014. **4**(1): p. 177-197.
178. Tran, D.H. and Z.V. Wang, *Glucose Metabolism in Cardiac Hypertrophy and Heart Failure.* J Am Heart Assoc, 2019. **8**(12): p. e012673.
179. Hood, D.A., et al., *Coordination of metabolic plasticity in skeletal muscle.* J Exp Biol, 2006. **209**(Pt 12): p. 2265-75.
180. Darvey, I.G., *How does the ratio of ATP yield from the complete oxidation of palmitic acid to that of glucose compare with the relative energy contents of fat and carbohydrate?* Biochemical Education, 1998. **26**(1): p. 22-23.